University of Karlsruhe (TH)
Institute of High-Frequency and Quantum Electronics (IHQ)

Head of Institute
Prof. Dr. Jürg Leuthold

Master Thesis Nr. 785

of Mr Jordi Abril Aguilera

DPSK regeneration: phase and amplitude noise suppression based on Kerr medium

Start: 01.04.2008
End: 24.10.2008

Supervisors: Dr. Stilianos Sygletos

Prof. Dr. Jürg Leuthold

Institute of High-Frequency and Quantum Electronics (IHQ)

I hereby declare that I have done my master thesis independently, without the use of any inadmissible foreign aids. All used literature sources are given in the references.

Karlsruhe, 24th October, 2008

Jordi Abril Aguilera

Abstract

The scope of this thesis is to identify and propose new schemes for Deferential Phase Shift Keying (DPSK) regeneration. DPSK modulation format presents increased robustness against ASE noise, which makes it strong candidate for use in long haul transmission systems. To achieve reasonable DPSK regeneration suppression of both the amplitude and phase noise is required. Three types of all-optical regenerators that make use of a Kerr medium, which can be a highly nonlinear fiber are analyzed. The first scheme is based on a modified nonlinear optical loop mirror (NOLM), with a subsequent addition of a bidirectional attenuator (DA-NOLM). The bidirectional attenuator allows to counterbalance the generation of the phase noise generated by the Gordon Mollenauer effect inside the Kerr medium. The second type of optical regenerator is based on the Self Phase Modulation (SPM) effect and offset filtering. Finally a novel scheme derived from the concepts of two former setups is presented and compared to the previous proposed. The operational conditions for optimum noise rejection are identified for each one of them. Through numerical simulations and detailed benchmarink we identify that our proposal outperforms all the schemes that have been presented previously in literature.

Contents

List of Figures

List of tables

Abbreviations

DPSK	Differential phase shift keying
RZ	Return to zero
SPM	Self phase modulation
XPM	Cross phase modulation
NRZ	No return to zero
HNLF	Highly nonlinear fiber
NOLM	Nonlinear Optical Loop Mirror
2R	Reamplifying and reshaping
DWDM	Dense Wavelength Division Multiplexing
OOK	On-off keying
FDM	Frequency Division Multiplexing
DD	Direct detection
DGD	Differential group delay
CW	Continuous wave
Tx	Transmitter
Rx	Receiver
AMI	Alternate Mark Inversion
DB	Duobinary
DI	Delay interferometer
OSNR	Optical noise to noise ratio
MZI	Mach-Zehnder Interferomter
BW	Band width
DA-NOLM	Directional attenuator Nonlinear optical loop mirror
FWM	Four wave mixing
ASK	Amplitude shift keying
MMF	Multimode fiber
SMF	Singlemode fiber
DFL	Distributed feedback lasers
LD	Laser diodes
FSK	Frequency shift keying

1 Introduction

1.1 Motivation

Nowadays a great part of the research in optical transmission systems is focused on increasing the system reach and robustness. All-optical signal regeneration is a promising technique to achieve this transparent extension. Optical regeneration requires reshaping of the signal in the optical domain. This is normally achieved with the use of nonlinear optical materials. Optical fiber is a promising nonlinear material especially for ultra-high-speed operation. Although long lengths of fiber (typically longer than a few hundred meters) are currently needed for obtaining sufficient nonlinearity, future developments of highly nonlinear fibers will make the system more compact and practical

At the same time differential phase-shift keying (DPSK) has become the format of choice for long-haul optical transmission systems, due to the 3-dB improvement in receiver sensitivity compared to on-off keying (OOK) and enhanced tolerance to dispersion and nonlinear effects, particularly intra channel four-wave mixing. However, using the DPSK format, amplitude and phase noise is expected to degrade the transmission performance. These degradations are attributed either to the propagation of nonlinear distortions or to the accumulation of the ASE noise. Hence, it is needed to investigate and develop schemes that not only regenerate the amplitude but also the phase, to make them feasible. Various methods have been developed for regenerating the impaired signal.

Basically, all-optical signal regenerators are based on three kinds of fiber nonlinearities, self-phase modulation (SPM), cross-phase modulation (XPM), four-wave mixing (FWM) to regenerate the quality of the signal. Over the last decade, there have been numerous experimental demonstrations of 2R optical schemes, mainly designed to work with On-Off keying amplitude modulated signals, and lately more focused on DPSK. Thus, there are great chances either to improve existing schemes or study new ideas.

1.2 Objective of the thesis

Regarding the capabilities of DPSK signal in long-haul transmissions, the principal aim of this thesis is to discover a method to improve the quality of the signal in order to achieve longer distances between the transmitter and the receiver.

A signal after being transmitted is unavoidably degraded by several factors such as spontaneous noise emission, fiber dispersion, nonlinearities, and many other minor effects, which directly results in a loss of quality in the signal. In order to deal with all these

problems, first we will analyze some solutions already proposed in the literature; and in particular we will focus on the systems based on fiber nonlinearities as a method to regenerate the signal.

We will focus on regenerating a 40-Gb/s DPSK signal. Note that white noise will be added before the signal goes through the regenerator, and then by measuring the signal after the setup we will have a qualitative idea of the noise suppression.

According to the main goal, regenerating the signal, there are two basic issues to face; firstly the amplitude jitter, and secondly cancelling the phase fluctuations, since in DPSK formats, phase is as important as the power amplitude. Considering this, a novel scheme will be finally presented and examined in depth in order to explore its regenerative properties. The scheme will be optimized by means of fiber and filter parameters, and consequently evaluated. Therefore, a performance comparison between all of them will prove whether our proposal is worthwhile or not.

Concerning all these issues, the thesis is structured as follows. Chapter 2 describes the background concepts appearing in the subsequent presented setups. It is split into two sections: modulation formats and optical fibers. Chapter 3 explains the different scheme designs; it is basically divided into three chapters, one for each type of regenerator, giving special attention to the principle used to achieve both amplitude and phase noise suppression. Chapter 4 focuses on the thesis' main contribution through an overall comparison of all the measured parameters. Chapter 5 gives a summary of the thesis work.

2 Theoretical Background

In order to understand the behavior of each component, a theoretical review will give us a description of the corresponding physical laws that govern its performance. Firstly, a description of different modulation techniques is given, explaining their pros and cons, and thus, to be able to understand what is a DPSK format, why it is used, and why it is more suitable for our requirements.

Next, an introductory explanation of fiber basic concepts will familiarize us with optical fiber issues. As the regenerator is based on Kerr medium effect, the SPM section will be analyzed in greater depth. Nevertheless, a general review of all linear and non-linear effects will give us a complete idea of what physical processes are developed.

2.1 Modulation formats

A brief review of transmitter types, modulation keying schemes, and modulation formats will acquaint us with optical communication basics; giving special attention to DPSK modulation process and transmission.

2.1.1 Optical transmission

- An **optical transmitter** converts an electrical signal into an optical signal and couples the signal into an optical fiber. The transmitter comprises the laser diode, the optical modules and the electrical circuit that are needed for operation.

- The **optical receiver** on the other hand converts the optical signal received at the output end of the optical fiber back into the original electrical signal. It consists of a coupler, a photo detector, and a demodulator. Often the received signal is in the form of optical pulses representing 1 and 0 bits and is converted directly into an electric current. Such a scheme is referred to as intensity modulation with direct detection (IM/DD), other receivers are optimized for phase and frequency shifted signals. Such coherent detection schemes require homo- and heterodyne detectors.

Principally, there are three types of transmitters; Firstly, the most compact and cheapest Tx are directly modulated lasers, in which is permanently applied an offset current to the laser diode, therefore the laser is beneath threshold, i.e. not yet lasing. A pulse code modulated (PCM) electrical (digital) signal is then added and brings the laser above threshold so that lasing sets in. The directly modulated laser is the cheapest and most commonly used transmitter. Recent advances have made possible directly modulated lasers at bit rates up to 10 Gb/s and in research up to 40 Gb/s. However, directly modulated lasers typically have

poor quality. The poor quality is due to strong modulations of electrical carriers within the laser that lead to severe distortions on the signal amplitude and phase.

Secondly, A Tx with external modulation in which a constant current is applied to the laser cavity so that lasing with constant power (i.e. *cw* or *continuous wave* operation) and a narrow spectral laser line is achieved. The laser signal is then guided into a modulator, which encodes the electrical PCM data signal onto the optical signal. The idea of separating laser and modulator is to use two almost ideal devices and combine them into a Tx with high signal quality. And indeed, the signal quality obtained with externally modulated lasers exceeds by far the performance of directly modulated lasers. They are used in medium, long-haul and ultra-long-haul net-works up to 10 Gb/s and in medium haul networks up to 40 Gb/s.

And thirdly, the highest quality signals are obtained, when the cw signal from the laser is first guided into a pulse-carver modulator and only then a signal is encoded on top of the carved signal. The pulse carver imprints a particular pattern onto the cw laser before the optical data are put on top of it, Fig. 2-1(c). These kind of transmitters are almost uniquely used for ultra-long haul or/and high-speed (40 Gb/s and higher) communication systems.

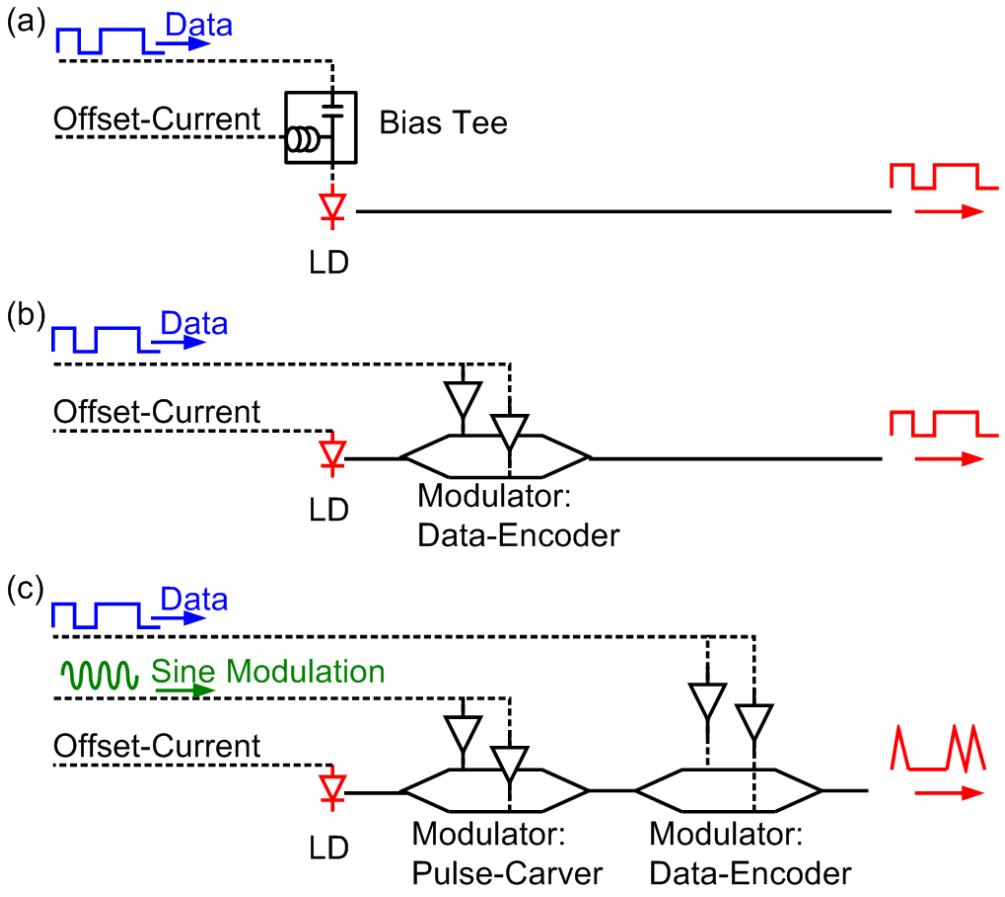

Figure 2-1: Transmitter Schemes used in optical communications. (a) Directly modulated Laser, (b) Transmitter with external modulator, (c) Transmitter with pulse carver and external modulator

2.1.2 Digital Modulation

By modulation format we mean a process of converting a particular input data into a string of bits according to a given level changing rule. Among the digital modulation schemes there can be distinguished two schemes, binary modulation and multilevel (M-ary) modulation. We will focus on the first one since all the signals that will be used are included in this group [1]
As an example one might think of converting a sequence of "1s" and "0s", into "marks" and "spaces", using a pattern of signals with amplitude and without amplitude. And indeed, that is a frequently used scheme. However, there are many reasons for introducing more complex formats that follow complicated combinations of AKS and PSKs. Reasons for choosing a particular format are

- Cheaper modulator and receiver exists for a particular format
- Better spectral efficiency
- Better behavior under long-haul transmissions
- Better sensitivity in the receiver so better signal quality
- Easier data clock recovery

As it happens with analog waveform modulation schemes, there are four basic binary waveform modulations, illustrated in Fig. 2-2.

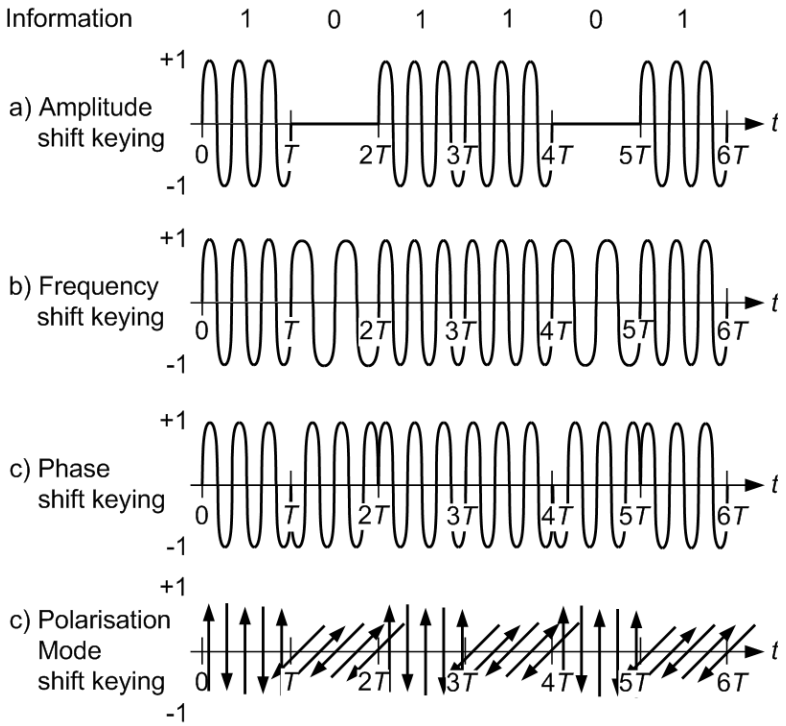

Figure 2-2: The four types of waveform keying with binary coding

An overview of the most frequently used modulations formats will be described, and the ones used in the experimental simulations of this thesis will be discussed in depth at the end of this section.

ASK modulation formats

Some of the most important unipolar binary ASK coding types can be described as follows:

- **Nonreturn-to-zero (NRZ):**
  "0": a "space" or low signal level
  "1": a "mark" or high signal level
  A string of consecutive 1s or 0s is reflected by no signal level change.
- **Return-to-zero (RZ)**: same as NRZ, but marks occupy only a certain percentage part of the bit slot.
- **Manchester coding or Phase Encoding:**
  "0": A mark within the first part of the bit-slot, a space in the second.
  "1": A space within the first part of the bit-slot, a mark in the second. The average signal power is the same for both 0s and 1s
- **Differential Manchester Coding:**
  "0": A level transition in the first part of the bit slot.
  "1": A level transition in the second part of the bit slot.
- **Coded Mark Inversion (CMI):** is a Non-Return-to-Zero (NRZ) line code, in which
  "0": is encoded as zero-to-one transition at the pulse's center and
  "1": one is encoded as constant level for entire pulse time. The one's constant level is inverted each pulse.
- **Miller Coding:**
  "0": No transition
  "1": A transition at mid-point of the bit slot from either level

PSK modulation formats

Phase Shift Keying modulation bit streams are generated by, as its name suggests, modulating the phase, while the amplitude and the frequency of the optical carrier are kept constant. For binary PSK formats, the phase takes two values, commonly chosen to be 0 and π. An advantage of the PSK format is that the intensity is constant for all bits and bit patterns and thus no nonlinear effects that constantly change with intensity do appear. However, there is some inconvenient on using PSK formats.

• PSK formats require coherent detectors: A conventional detector would only be sensitive to the intensity. However, the intensity of a PSK format does not change. Therefore, one needs phase sensitive detection schemes called coherent detectors which require a reference carrier to compare the incoming signal with. Depending on the relative phase of the reference carrier and the signal, a space or a mark is generated. This reference carrier is usually called "local oscillator" and is simply a laser source in the case of optical communications. Unfortunately, this local oscillator adds to the costs and complexity, so usually one tries to avoid these kinds of schemes.

• Compared to RF world, optical signals have an extremely short wavelength. This causes considerable stability issues. For instance, in RF a signal has a typical wavelength of several hundred of meters to several tens of millimeters, in the field of opticas however, the average wave-length is approximately 1.5 μm. Now, if a transmission over 100 km is considered, a small refractive index change would shift the phase of the incoming signal by π and thus invert the meaning of space and marks with respect to the local oscillator. In short, PSK requires that the phase of the optical carrier remain stable so that phase information can be extracted at the receiver without ambiguity. This is difficult in optical communications because of the short wavelength.

• Optical signals have a polarization. In order to make the coherent detector work properly, both the PSK signal and the local oscillator need to have the same polarization. However, after 100s of kilometers of transmission, the state of polarization is usually no longer known.

Yet, all these limitations can be loose by using a modified form of PSK. This variation is Differential PSK.

- **Differential phase-shift keying (DPSK)**: In the case of DPSK, information is coded by using the phase difference between two neighboring bits. For instance, if φ_k represents the phase of the k^{th} bit, the phase difference $\Delta\varphi = \varphi_k - \varphi_{k-1}$ is changed by π or 0, depending on whether the k^{th} bit is to be a 1 or a 0.
- π/2-**Differential phase-shift keying (DPSK)**

  "0": relative phase shift of -π/2 (clockwise)

  "1": relative phase shift of π/2 (counter-clockwise)

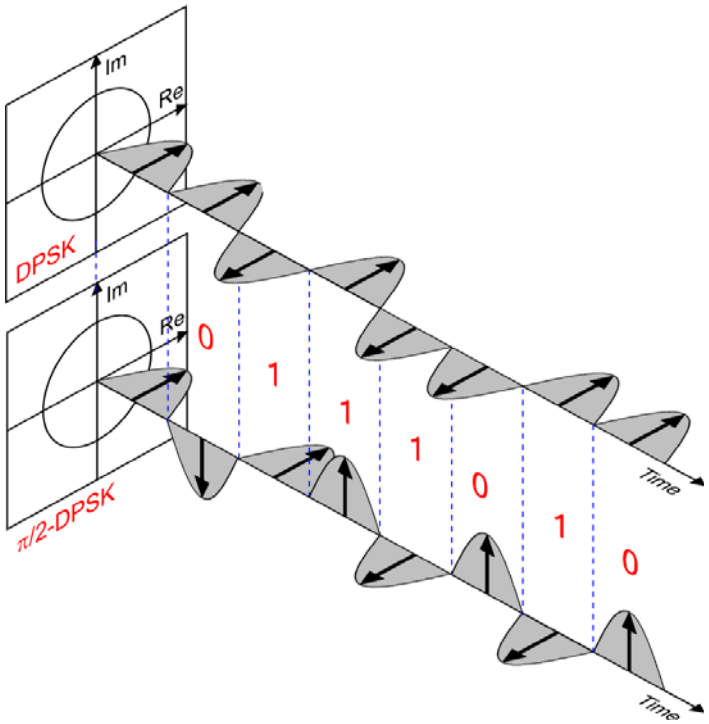

Figure 2-3: Schematic representation of the amplitude and phase evolution of DPSK (upper) and π/2-DPSK (lower). Return-to-zero (RZ) pulses are used in this example. [2]

Mention that several modulation formats which are a combination of both PSK and ASK. Some of the most common used bipolar binary PSK-ASK coding schemes are displayed in Fig. 2-4.

The VSB coding scheme is added although it is not really a bipolar modulation format. All of the modulation formats may be considered OOK schemes with a specific phase pattern encoded onto the marks. These formats may be considered a combination of conventional ASK (or OOK) with a PSK scheme. The reason for making this additional effort is almost any time either for increasing the spectral density or for improving the receiver sensitivity. Some of the most relevant modulation formats are:

- **Carrier-suppressed return-to-zero (CSRZ):** This is the conventional RZ format with an additional phase modulation. If all even bit-slots have positive amplitude, then all odd bit slots have the negative amplitude (i.e. a π phase shift offset separates even and odd bit slots.)
- **Duobinary:**
  "0": low signal level
  "1": high signal level, without sign change if there is an even number of "0s" since last "1" bit, with sign change for odd quantity of "0s" since last "1".
- **Alternate Mark Inversion (AMI)**
  "0": low signal level
  "1": high signal level, with every subsequent mark alternating phase by 180 degrees.
- **Vestigial Sideband Filtered Signal (VSB)** An optical VSB signal is usually generated with an input on-off keying (OOK) signal, either return-to-zero (RZ) or non-return-to-zero (NRZ), followed by a narrow optical filter with its passband purposely detuned from the centre frequency of the input signal. Mathematically a VSB is encoded as:
  "0": low signal level
  "1": high signal level, with progressive 90o degree phase shift added onto every bit slot.

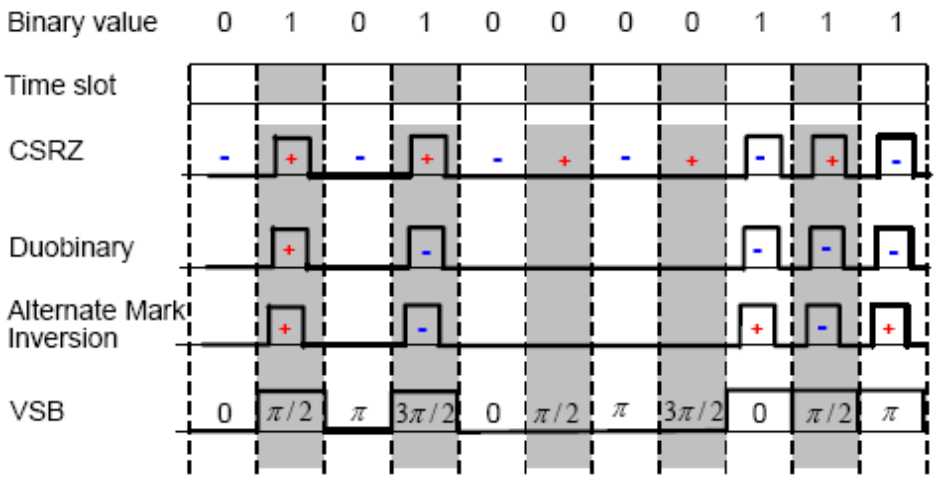

Figure 2-4: Frequently used binary bipolar schemes

FSK modulation formats

In the case of FSK modulation formats the information is encoded onto the optical carrier by shifting the carrier frequency itself. For a binary digital signal, takes two values, $\omega_o - \Delta\omega_o$, depending on whether a 1 or 0 bit is being transmitted. The shift $2\Delta f = 2\Delta\omega/(2\pi)$ is called the *tone spacing*, as it represents the frequency spacing between 1 and 0 bits. The optical field for FSK format can be written as

$$f(t) = \frac{1}{2} A \left(e^{(j(\omega \pm \Delta\omega)t + \varphi)} + e^{(-j(\omega \pm \Delta\omega)t + \varphi)} \right) \tag{2.1}$$

where the "+" and "-" signs correspond to 1 and 0 bits.

The total bandwidth of an FSK signal is approximately $2\Delta f + 2R_s$.

- The case 2Δf-Union-$2R_s$ is called the **wide-deviation** or **wideband FSK** and the bandwidth is independent of the bit rate.
- The case 2Δf-Intersection-$2R_s$ is called the **narrow-deviation** or **narrowband FSK.**

Practical implementations of FSK formats make use of:

- Directly modulating laser diodes (LD) or distributed feedback lasers (DFBs). Typical frequency shifts of 0.1-1 GHz/mA change of input currents are obtained. As a side effect the FSK goes along with a small ASK, because reducing the current reduces the output power.
- Alternatively, modulation of the phase can be used to shift frequency as well. As a matter of fact the chirp imposed onto a signal is given by (2.2)

$$\Delta f = \frac{1}{2\pi} \frac{\Delta\varphi}{\Delta t} \tag{2.2}$$

(This relation directly follows from $\varphi=\omega t$ when taking the derivative $\Delta\varphi/\Delta t$).
Thus, ideally a linear phase change is required to obtain a constant frequency shift. In order to obtain these frequency offsets the carrier phase has to vary continuously from bit to bit. Such direct modulation FSK schemes are often referred to as **continuous-phase FSK (CFSK).** A very important CFSK case is , i.e. the tone spacing is half the signal bandwidth. This case is called **Minimum-Shift Keying (MSK)**.

As a consequence of Eq. (2.2) there is often a little difference between FSK and PSK, since phase modulation and frequency shift are almost the same.
As an example for a FSK format we discuss the MSK format

• **Minimum Shift-Keying format (MSK):**

"0": relative frequency shift of $\Delta f = -R_s/4$

"1":relative frequency shift of $\Delta f = R_s/4$

in addition, in a real MSK the intensity does not change.

Note: It can be shown, that the MSK is identical to the π/2-Differential phase-shift keying. This is true as long as the intensity does not change and the phase modulation takes place continuously (the former is part of the MSK definition and the latter is a condition for getting a constant frequency shift).

Proof: The MSK condition for "0" is: $\Delta f = -R_s/4$

However from Eq. (2.2) we know that $\Delta f = 1/(2\pi)\cdot\Delta\varphi/\Delta t$, with $\Delta t = 1Rs$

The comparison of the two equations leads us $\Delta\varphi = -\pi/2$.

Thus, MSK and π/2-Differential phase-shift keying are indeed identical.

The same can be shown for the MSK "1" and π/2-Differential phase-shift "1".

The MSK example actually shows that there is often little if no difference between a FSK and PSK scheme.

2.1.2.1 DPSK. Generation and analysis

Since DPSK format is used as input signal, a more in depth description is done. Explaining the processes that take part to perform the transmission (transmitter, receiver), and the advantages one can achieve in front of other formats.

As mentioned before, binary differential phase shift keying encodes information on a binary phase change between adjacent bits; a logical "1" is encoded onto a π phase change, whereas a logical "0" is represented by the absence of a phase change. Like OOK, DPSK can be implemented in RZ and NRZ format [3].

- Transmitter

Two techniques for DPSK generation are commonly used. Both techniques use a continuously oscillating laser followed by one or two external modulators. A first modulator to encode phase-shift keying and a eventually a sinusoidal driven second modulator (pulse carver) to carve pulses out of the phase-modulated signal, thus generating RZ-DPSK.

In the first technique data encoding is performed with an external straight-line phase modulator (PM), Fig. 2.5(a). A PM only modulates the phase of the optical field, resulting in a constant-envelope optical signal. Since phase modulation does not occur instantaneously, a PM inevitably introduces chirp across bit transitions. The inset shows the resulting optical power waveform. (The seemingly limited pahse amplitude depth of the RZ-DPSK pulses is a measurement artifact, caused by detecting a 40-Gb/s signal using a 32-GHz-bandwidth photodiode).

In the second technique a MZI modulator is used for phase modulation, the modulator is biased at its transmission null in push-pull operation mode, and is driven at twice the switching voltage required for OOK modulation, Fig.2.5.

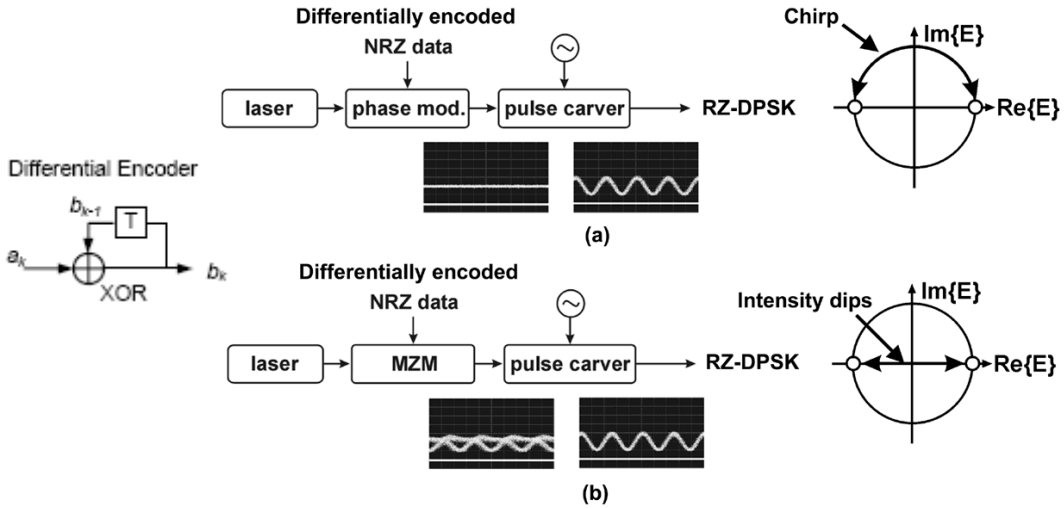

Figure 2-5: **PSK transmitters. (a) Implementation with phase modulator. (b) Implementation with Mach-Zehnder modulator**

The two techniques provide different results. This is because the two techniques use different transition paths for going from one state to the other, Fig.2.5. If a straight-line phase modulator (PM) is used, Fig.2.5(a), the speed of the phase transitions is limited by the combined bandwidth of driver amplifier and phase modulator, while the intensity of the phase-modulated light is constant. Instantaneous π phase jumps are realized at the expense of some residual intensity modulation of the phase modulated, Fig.2.5 (b).

Figure 2.6 shows spectra and eye diagrams for NRZ-DPSK and RZ-DPSK, generated by a MZI as a phase modulator. There can be observed a carrier-free nature of the spectra, as a matter of fact the NRZ spectrum without the carrier is the DPSK spectrum.
As well as DB and AMI, the DPSK owes the carrier free spectrum to the balance of -|E| and +|E| amplitude levels. Note the absence of a "0" bit rails in the eye diagrams, which is characteristic for phase-coded formats. The deep amplitude dips between two bits in the NRZ-DPSK eye represent the residual amplitude modulations of the MZI caused by the finite NRZ drive signal bandwidth.

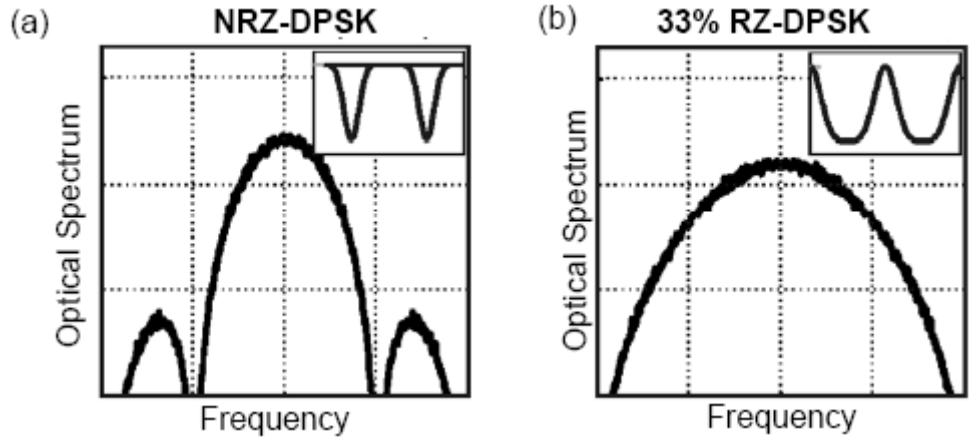

Figure 2-6: DPSK spectra and eye diagrams of (a) NRZ-DPSK and (b) RZ-DPSK

- Receiver

A typical balanced DPSK receiver is shown in Fig.2.7. The optical signal is first passed through a Mach-Zehnder delay-interferometer (DI), whose differential delay is equal to the bit period.

This optical preprocessing is necessary in direct-detection receivers to accomplish demodulation, since hotodetection is inherently insensitive to the optical phase; a detector only converts the optical signal power into an electrical signal. In a direct-detection DPSK receiver, the DI lets two adjacent bits interfere with each other on its output ports. This interference leads to the presence (absence) of power at a DI output port if two adjacent bits interfere constructively (destructively) with each other.

Thus, the preceding bit in a DPSK-encoded bit stream acts as the phase reference for demodulating the current bit. (Note that in the case of coherent detection, this phase reference can be provided by a local laser within the receiver, which beats with the received signal to produce constructive and destructive interference.)

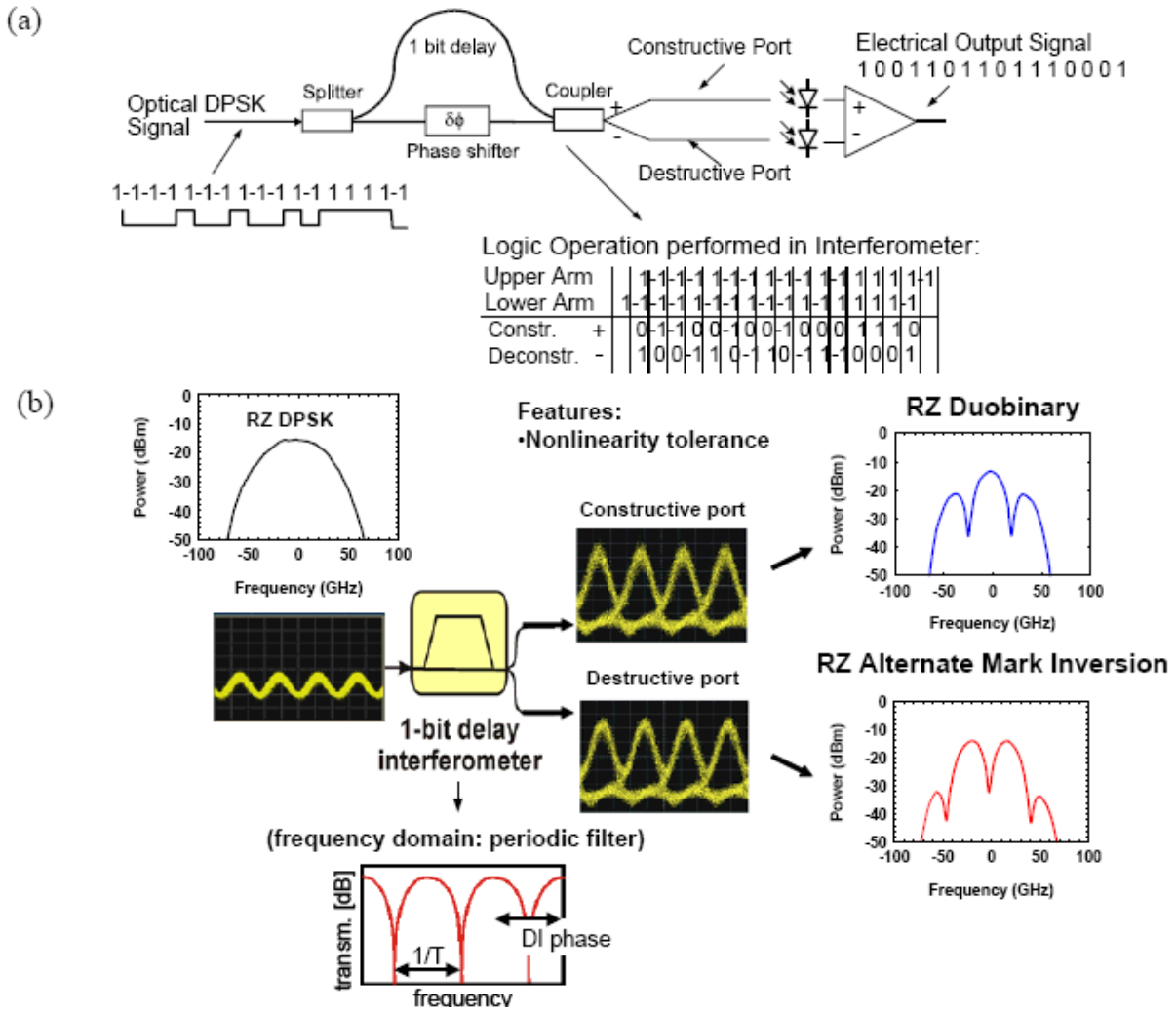

Figure 2-7: (a) Setup of balanced receiver for DPSK (b) Conversion of DPSK into a duobinary and AMI OOK format for detection and associated spectra and eye diagrams.

Ideally, one of the DI output ports is adjusted for destructive interference in the absence of phase modulation ("destructive port"), while the other output port then automatically exhibits constructive interference due to energy conservation ("constructive port"). For the same reason, the two DI output ports will carry identical, but logically inverted data streams under DPSK modulation.

Careful analysis of the optically demodulated signals at the DI output reveals that the constructive port carries duobinary modulation, whereas the destructive port carries alternate-mark inversion (AMI). Today, technical difficulties in implementing stable delay interferometers have been overcome, and DIs have been demonstrated both in fiber-based and in planar-lightwave-circuit (PLC) technologies. Fine-tuning of the differential delay to match the laser center frequency and achieve good interference quality is typically achieved using a heating element on one of the interferometer arms. Also, polarization-dependent phase shifts within the DI have to be avoided.
Identical path lengths between the output coupler of the DI and the point of subtraction within the balanced receiver can be achieved using variable optical delay units or photonic integration of the detectors with the DI. Alternatively, separate detection of both output ports in combination with joint digital signal processing can be applied.

The main advantage from using DPSK instead of OOK comes from a 3-dB sensitivity improvement at the receiver, provided that balanced detection is employed. For the same average optical power, the symbol distance in DPSK (expressed in terms of the optical field) is increased by $\sqrt{2}$. Therefore, only half the average optical power should be needed for DPSK as compared to OOK to achieve the same symbol distance, Fig. 2.8. Note, however, that this - benefit of DPSK can only be extracted using balanced detection, i.e when detecting both symbols.

Using an RZ-DPSK signal and a balanced-photodiode detection scheme, a record sensitivity of 38 photons/bit at 42.7 Gb/s has been demonstrated. This is reasonably close to the theoretical quantum limit that has been predicted to be 20 photons/bit for DPSK and a BER of $1 \cdot 10^{-9}$. (The OOK quantum limit is at 38 photons/bit for a BER of $1 \cdot 10^{-9}$ [4]). This enhanced sensitivity directly translates into increased transmission distance.

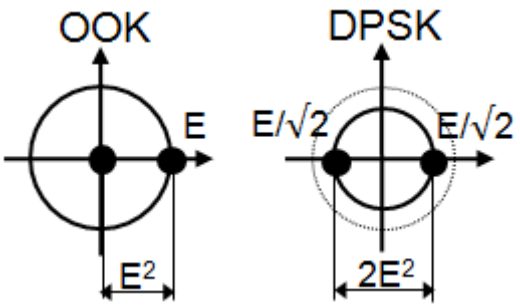

Figure 2-8: Constellation diagram for (a) on-off keying and (b) DPSK

2.2 Optical Fibers

In a very basic definition, optical fibers are thin filaments of glass through which light beams are transmitted. A fiber is made of an inner core and a cladding that surrounds it. The cladding has an index of refraction higher than the one of the core so as to totally reflect the light internally in the fiber. The cladding is coated to protect it from damage, Fig.2.9.

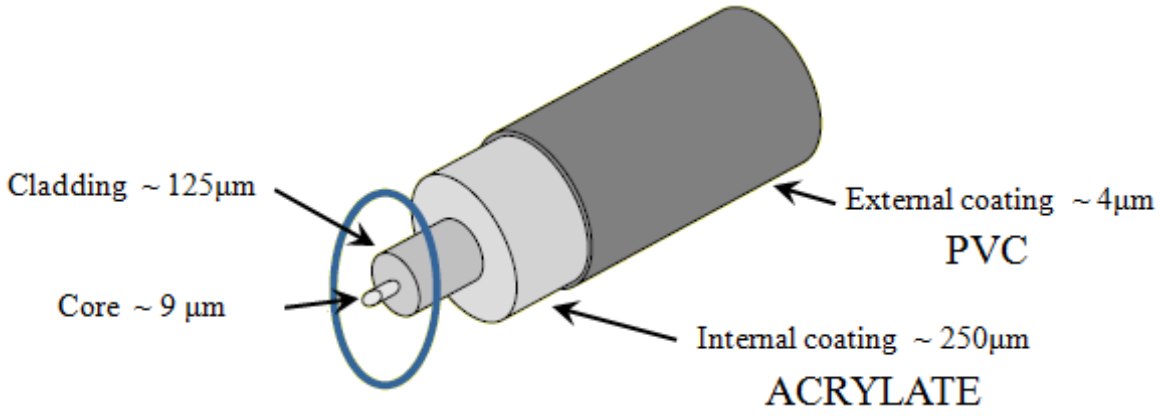

Figure 2-9: Different parts of an optical fiber

Light is kept in the "core" of the optical fiber by total internal reflection. This causes the fiber to act as a waveguide. Fibers which support many propagation paths or transverse modes are called multimode fibers (MMF). Fibers which support only a single mode are called single mode fibers (SMF). Multimode fibers generally have a large-diameter core, and are used for short-distance communication links or for applications where high power must be transmitted. Single mode fibers are used for most communication links longer than 200 meters.

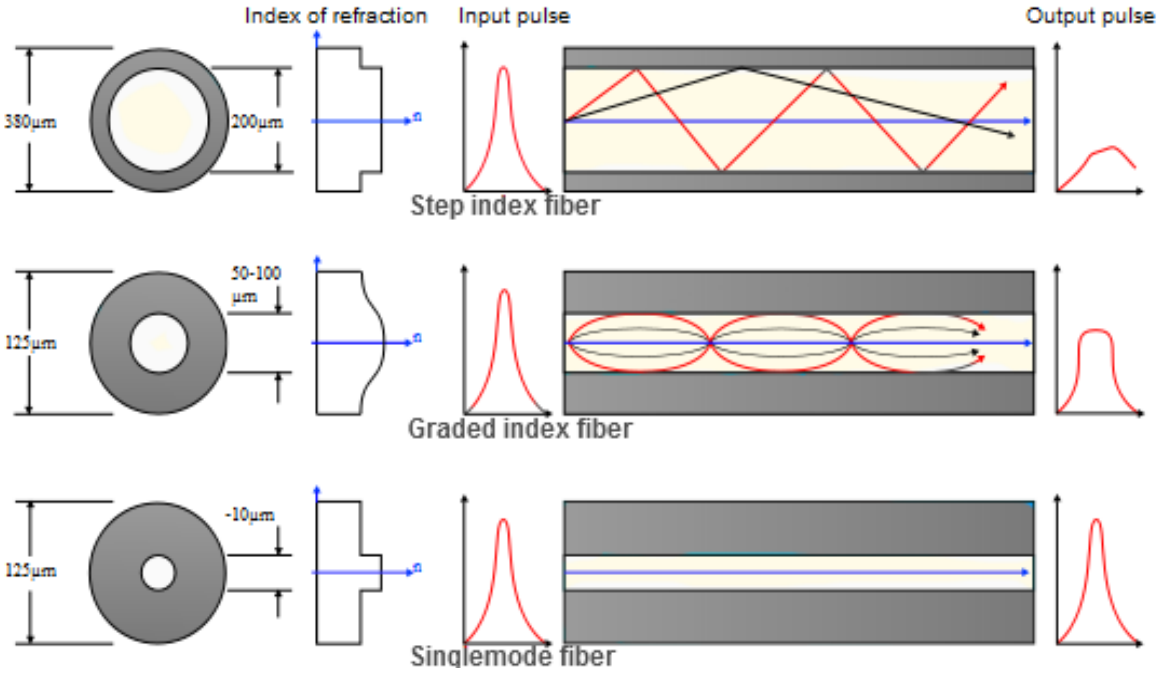

Figure 2-10: Types of optical fiber

The propagation of optical fields in optical fibers can be described by Maxwell's equations [5]:

$$\nabla \times E = -\frac{\partial B}{\partial t}$$
$$\nabla \times H = \frac{\partial D}{\partial t}$$
$$\nabla \cdot D = 0$$
$$\nabla \cdot B = 0$$

E: Electric field vector
H: Magnetic field vector
D: Electric flux density
B: Magnetic flux density

(2.3)

The flux densities D and B are caused by the propagation of E and H inside the medium and are related to them though the constitutive relations.

$$D=\varepsilon E+P$$
$$B=\mu_0+M$$

ε_0: vacuum permittivity
μ_0: vacuum permeability
P: Induced electric polarization
M: Induced magnetic polarization

(2.4)

Using the Maxwell's equations considering that the optical fibers are nonmagnetic mediums (M=0) without free charges, one can obtain the wave equation that describes the light propagation in optical fibers

$$\nabla^2 E - \frac{1}{c^2}\frac{\partial^2 E}{\partial t^2} = -\mu_0 \frac{\partial^2 P}{\partial t^2} \tag{2.5}$$

where P (induced electric polarization of the medium) consists of two parts,

$$P(r,t)=P_L(r,t)+P_{NL}(r,t)$$

P_L: Linear polarization part
P_{NL}: Nonlinear polarization part
r: Position vector
t: Time

(2.6)

The last relation needed to describe properly the light propagation in optical fibers is one which relates the electric field and the induced electric polarization. Assuming that the nonlinear response of the optical fibers is instantaneous, it can be related to the electric field by the following relation (the last relation we need to describe properly is the light propagation in optical fibers).

$$P=\varepsilon_0\left(\chi^{(1)}\cdot E+\chi^{(2)}:EE+\chi^{(3)}\vdots EEE\right) \tag{2.7}$$

The term $\chi^{(1)}$ is the linear susceptibility of the medium describing the linear part (P_L) of polarization. The nonlinear part (P_{NL}) is determined by the tensors $\chi^{(3)}$ and $\chi^{(2)}$.

Considering x-polarized light propagation in z direction, the electric field of the signal is given by

$$E=\hat{x}F(x,y)\frac{1}{2}A(z,t)e^{(j\omega_0 t-j\beta(\omega)z)}+c.c \tag{2.8}$$

where c.c means complex conjugate, F(x, y) is the modal distribution of the fundamental fiber mode, A(z, t) is the field amplitude, ω_0 the carrier frequency and $\beta(\omega)$ is the wave number explained in more detail in section 2.2.2.

From the equation (2.6), the scalar propagation equation can be derived by applying the slowly varying envelope and rotating wave approximations giving a partial differential equation known as the nonlinear Schrödinger equation:

$$\frac{\partial}{\partial z}A=-\frac{\alpha}{2}A-\beta_1\frac{\partial A}{\partial t}-\frac{j}{2}\beta_2\frac{\partial^2 A}{\partial t^2}+\frac{1}{6}\beta_3\frac{\partial^3 A}{\partial t^3}+j\gamma|A|^2A \tag{2.9}$$

Equation (2.9) describes the propagation of an optical pulse in single-mode fibers. It includes the effects of fiber loss through α (section 2.2.1), of chromatic dispersion through β_1,β_2 and β_3 (section 2.2.2); in particular, the pulse envelope moves at the group velocity $v_g=1/\beta_1$ while group-velocity dispersion (GVD) is taking into account by β_2 and β_3. The remaining parameter is γ which is the nonlinear coefficient of the fiber.

From the nonlinear Schrödinger (NLS) equation (2.9) that governs the propagation of optical pulses inside single mode fibers, a simplification can be made by considering pulses >5 ps.

$$j\frac{\partial}{\partial z}A=-\frac{j\alpha}{2}A+\frac{\beta_2}{2}\frac{\partial^2 A}{\partial T^2}-\gamma|A|^2A \tag{2.10}$$

where A is the slowly varying amplitude of the pulse envelope and
T is measured in a frame of reference moving at the group velocity ($T = t- z/v_g$)

Depending on the initial width T_0 and the peak power P_0 of the incident pulse, either dispersive or nonlinear effects may dominate along the fiber. It is useful to introduce two length scales, known as the dispersion length L_D and the nonlinear length L_{NL}.
Depending on the relative magnitudes of L_D, L_{NL}, and the fiber length L, the pulses can evolve differently.

Normalizing the time to input pulse width To, and the amplitude to $U(z,\tau)$

$$\tau=\frac{T}{T_0}=\frac{t-z/v_g}{T_0} \qquad (A,\tau)=\sqrt{P_0}e^{-\frac{\alpha z}{2}}U(z,\tau) \tag{2.11}$$

the equation (2.10) satisfies

$$j\frac{\partial U}{\partial z}A = \frac{sign(\beta_2)}{2L_D}\frac{\partial^2 U}{\partial \tau^2} - \frac{e^{-\alpha z}}{L_{NL}}|U|^2 U \tag{2.12}$$

where $sgn(\beta_2) = \pm 1$ depending on the sign of the GVD parameter β_2 and

$$L_{NL} = \frac{1}{\gamma P_0} \qquad L_D = \frac{T_0^2}{|\beta_2|} \tag{2.13}$$

When fiber length *L* is such as

- $L << L_{NL}$ and $L << L_D$, neither dispersive nor nonlinear effects play a significant role during pulse propagation.
- $L << L_{NL}$ but $L \sim L_D$, the last term in Eq. (2.12) is negligible compared to the other two, so that the pulse evolution is then governed by GVD, and the nonlinear effects play a relatively minor role
- $L << L_D$ but $L \sim L_{NL}$, the dispersion term in Eq. (2.12) is negligible compared to the nonlinear term, so that the pulse evolution in the fiber is governed by SPM that leads to spectral broadening of the pulse
- *L* is longer or comparable to both L_D and L_{NL}, dispersion and nonlinearity act together as the pulse propagates along the fiber. The interplay of the GVD and SPM effects can lead to a qualitatively different behavior compared with that expected from GVD or SPM alone.

For all the schemes and simulations, dispersion effects will not be considered, in order to reduce the simulation parameters, therefore the complexity. For further studies, taking into account all this parameters could show some improvements.

2.2.1 Attenuation

The optical mean power evolution of a signal while it is propagating through an optical fiber is given by [6].

$$\frac{dP}{dz} = -\alpha_T P \tag{2.14}$$

where α_T represents the total constant attenuation of the optical fiber and P is the optical mean power of the signal in the fiber. If P_{in} is the optical mean power introduced at the input of a fiber of length L, then the optical mean power at its output can be calculated as follows

$$P_{in} = P_{out} e^{-\alpha_T L} \tag{2.15}$$

Usually, the attenuation constant α is expressed in dB/km:

$$\alpha\ (\text{dB/Km}) = -\frac{10}{L}\log 10\left(\frac{P_{in}}{P_{out}}\right) = 4.343\alpha_T \tag{2.16}$$

The attenuation presented by the optical fiber is dependent on the wavelength of the propagating signal. A typical loss spectrum of an optical fiber is presented in Fig. 2-11.

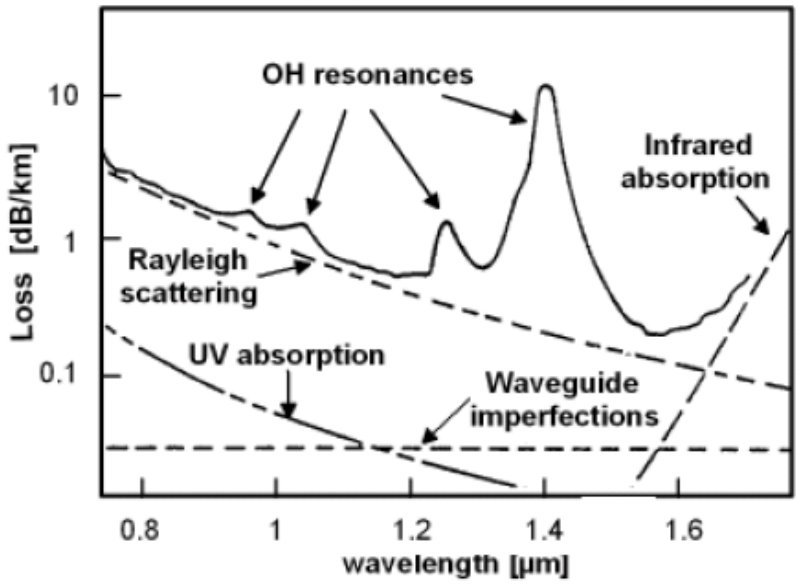

Figure 2-11: Typical loss spectrum of an optical fiber [7]

It can be observed that the loss is minimum around λ=1.55μm with a value of 0.2dB/km. The wavelength region near 1.55μm is known as third transmission window. Another loss minimum is situated at 1.3μm, these wavelength band is called second transmission window.

The loss spectrum shown in Fig 2-11 is the result of several attenuation mechanisms that can be classified in two big groups:

- **Intrinsic mechanisms**: Produced due to the nature of the material employed in the manufacture of the optical fiber. They are not avoidable. In the previous figure these mechanisms are: Material absorption (infrared and ultraviolet) and Rayleigh scattering.

- **Extrinsic mechanisms**: The consequence of external factors such as the presence of impurities in the core introduced in the manufacture process. They are avoidable. In the figure 3 they are: OH ion absorption and waveguide imperfections (imperfection of the core and the cladding, curvatures and microcurvatures).

2.2.2 Chromatic Dispersion

The chromatic dispersion is caused because of different wavelengths traveling along an optical fiber at different speeds. The different wavelengths reach the end of the fiber at different times, causing the light pulse to spread. This happens because the propagation constant β depends, among other things, on the optical frequency ω, the refractive index of the core $n_1(\omega)$ and the refractive index of the cladding $n_2(\omega)$.

Mathematically, the effects of fiber dispersion are accounted for by expanding the mode-propagation constant β in a Taylor series about the center frequency ω_0 [5][6].

$$\beta(\omega)=n(\omega)\frac{\omega}{c}=\beta_0+\beta_1(\omega-\omega_0)+\frac{1}{2}\beta_2(\omega-\omega_0)^2+\frac{1}{6}\beta_3(\omega-\omega_0)^3+L \tag{2.17}$$

where $\beta_m=\left[\frac{d^m\beta}{d\omega^m}\right]_{\omega=\omega_0}$ m=0,1,2, … (2.18)

- The **zero-order** term (β_0) describes a common phase shift.
- The **first-order** term (β_1) contains the inverse group velocity (v_g) and describes an overall time delay without any effect on the pulse shape.

$$\beta_1=\frac{1}{c}\left[n+\omega\frac{dn}{d\omega}\right]=\frac{n_g}{c}=\frac{1}{v_g} \tag{2.19}$$

- The **second-order** term (β_2) contains the second-order dispersion parameter D.

$$D=\frac{d\beta_1}{d\lambda}=\frac{d}{d\lambda}\frac{1}{v_g}=\frac{1}{L}\frac{d\tau}{d\lambda}=-\frac{2\pi c}{\lambda^2}\beta_2 \qquad \tau\text{: Group delay} \tag{2.20}$$

The parameter D is used to be expressed in ps/km/nm. The typical value of D in single-mode fibers (SMF) is 16.9 ps/(km·nm). For example, considering an optical system that consists of an optical source with a 3dB bandwidth of 1nm, SMF 1km long and an ideal receiver at the output of the fiber, optical pulses at the beginning of the fiber will be 16.9 ps broader at the receiver.

- The **third-order** term (β_3) contains the third-order dispersion parameter S (expressed in $ps/km/nm^2$), also called dispersion slope and given by

$$S=\frac{dD}{d\lambda}=\left(\frac{2\pi c}{\lambda^2}\right)^2\beta_3 \tag{2.21}$$

The chromatic dispersion can be divided in two terms, the material and waveguide dispersion:

- **Material dispersion** (D_{mat}) occurs due to the changes of the refractive index of optical fiber [$n_1(\omega)$,$n_2(\omega)$] with optical frequency. This effect can be understood as the interaction between the propagating optical field and the electrons and molecules of the fiber material resulting in a frequency dependent change of the refractive index.
- **Waveguide dispersion** (D_{wg}) is the consequence of the frequency dependent mode propagation constant $\beta(\omega)$ at the core-cladding interface.

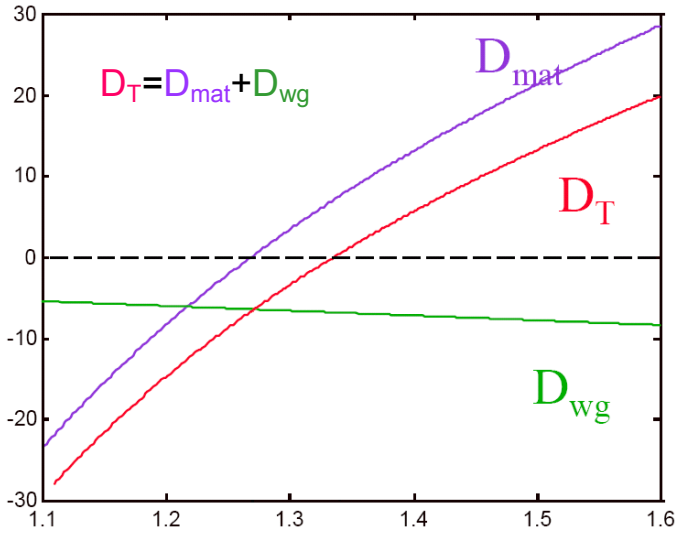

Figure 2-12: Typical Behavior of the Chromatic Dispersion in a Single-Mode

2.2.3 Fiber Nonlinearities

Even though fiber nonlinearities represent a fundamental limiting mechanism to the amount of data that can be transmitted on an optical fiber, if they are used with the proper values of the parameters in the appropriate range, nonlinearities become useful to deal with signal impairments. In this section the nature of the main nonlinear effects will be explained, giving special attention to SPM.

The response of any dielectric to light becomes nonlinear for intense electromagnetic fields, and optical fibers are no exception. On a fundamental level, the origin of nonlinear response is related to an inharmonic movement of bound electrons under the influence of an applied field. Due to that, the induced polarization P from the electric dipoles is not linear with the electric field E, but satisfies the more general relation [5].

$$P=\varepsilon_0\left(\chi^{(1)}\cdot E+\chi^{(2)}:EE+\chi^{(3)}\vdots EEE\right) \qquad (2.24)$$

ε_0: Vacuum permitivity
$\chi(j)$: jth order susceptibility

$\chi^{(1)}$ Represents the dominant contribution to P and its effects are included through the refractive index n and the attenuation constant α. It does not contribute to nonlinear interactions.

$\chi^{(2)}$ Can be neglected since SiO_2 (material used in the manufacture of the optical fibers) is a symmetric molecule.

$\chi^{(3)}$ Is responsible for the nonlinear phenomena. Two basic mechanisms can be distinguished. The real part of $\chi^{(3)}$ is responsible of the most harmful mechanism, explained more in detail afterwards. It arises from the refractive index of the fiber that depends on the optical power propagating through the medium due to the Kerr effect. The general equation for the refractive index in an optical fiber is:

$$\bar{n}(\omega,I)=n(\omega)+n_2 \cdot I \qquad \begin{array}{l} n(\omega) : \text{Linear part of the refractive index} \\ n_2 : \text{Nonlinear refractive index coefficient} \\ I : \text{The optical intensity} \end{array} \qquad (2.25)$$

The imaginary part of $\chi^{(3)}$ is responsible of the second mechanism that causes nonlinearities, the scattering phenomena. It products Stimulated Brillouin Scattering (SBS) and Stimulated Raman Scattering (SRS): SBS sets an upper limit on the amount of optical power that can be usefully launched into an optical fiber. When the SBS threshold for optical power is exceeded, a significant amount of the transmitted light is redirected back to the transmitter. SRS is similar to SBS but with a much higher threshold and it can also cause power to be robbed from shorter wavelength signals and provide gain to longer wavelength signals.

More important and harmful than scattering phenomena are the nonlinear interactions caused by the dependence on the optical power of the refractive index of the fiber, these nonlinear interactions can be discomposed into more basic nonlinear interactions, Fig. 2-14 [8].
A single channel is used for all schemes, as well as for the simulations. Therefore, the predominant nonlinear effects in this thesis are the single-channel nonlinear effects, and more specifically, Self phase modulation (SPM).

The intra-channel nonlinear effects (IXPM and IFWM) have the same behavior than the typical XPM and FWM but interchanging several channels in frequency with several pulses in time (in one channel). The source of the intra-channel nonlinear effects is the chromatic dispersion. Due to the chromatic dispersion, the pulses get broader in time when they are propagating along an optical fiber and they overlap each other. It is in this temporal overlap when the nonlinear interactions occur.

As a RZ signal is used to perform all the simulations, these inter-symbolic interferences are negligible in front of other nonlinear effects; hence they will not be taken into account.

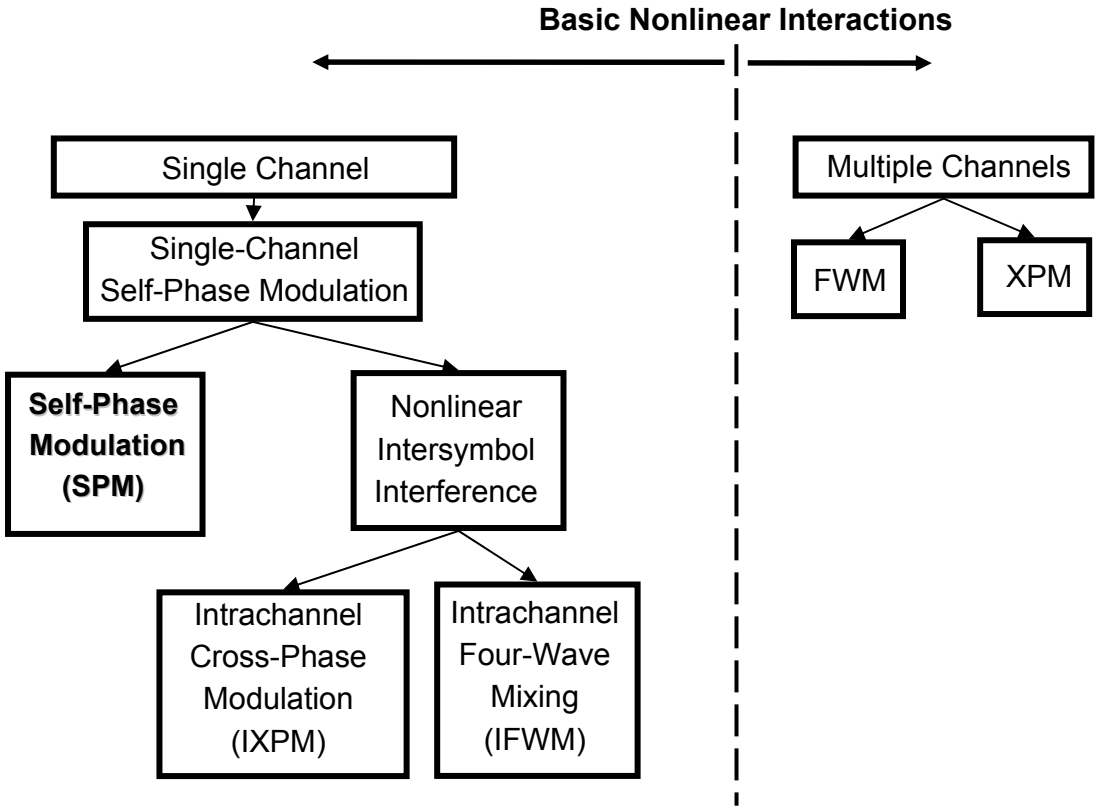

Figure 2-13: Basic nonlinear interactions

2.2.3.1 Self-Phase Modulation

A pulse of light, when traveling in a medium, induces a varying refractive index of the medium due to the optical Kerr effect. This variation in refractive index will produce a phase shift in the pulse, leading to a change of the pulse's frequency spectrum. This manifestation of the intensity, depending on the refractive index in nonlinear optical media due to self-phase modulation, is the temporal analog of self-focusing [5][21].

A general description of SPM in optical fibers requires numerical solutions of the pulse-propagation equation (2.9), in which has been considered a pulse-width larger than 5 ps, and normalized amplitude pulses (2.12). Assuming no dispersion in the fiber, in another words when $\beta_2=0$, the pulse-propagation equation becomes

$$\frac{\partial U}{\partial z} = \frac{j e^{-\alpha z}}{L_{NL}} |U|^2 U \tag{2.26}$$

where α accounts for fiber losses, and L_{NL} for the nonlinear length (2.13)

The Eq. (2.26) can be solved substituting $U=V\exp(j\varphi_{NL})$ and equating the real and imaginary parts so that

$$\frac{\partial V}{\partial z} = 0 \qquad \frac{\partial \varphi_{NL}}{\partial x} = \frac{e^{-\alpha z}}{L_{NL}} V^2 \tag{2.27}$$

As the amplitude V does not change along the fiber length L, the phase equation can be integrated analytically to obtain the general solution

$$U(L,T) = U(0,T)e^{-(j\varphi_{NL}(L,T))} \tag{2.28}$$

where U(T,0) is the field amplitude at z=0 and

$$\varphi_{NL}(L,T) = \left|U(0,T)\right|^2 (L_{eff} / L_{NL}) \qquad L_{eff} = \frac{1-e^{-\alpha L}}{\alpha} \tag{2.29}$$

Equation (2.28) shows that SPM gives rise to an intensity-dependent phase shift but the pulse shape remains unaffected. The nonlinear phase shift φ_{NL} increases with fiber length L. The quantity L_{eff} plays the role of an effective length that is smaller than L because of fiber losses. In the absence of fiber losses, $\alpha = 0$, and $L_{eff} = L$. The maximum phase shift φ_{max} occurs at the pulse center located at T = 0. With U normalized such that |U(0,0)| = 1, it is given by

$$\varphi_{max} = L_{eff} / L_{NL} = \gamma P_0 L_{eff} \tag{2.30}$$

The physical meaning of the nonlinear length is the effective propagation distance at which $\varphi_{max}=1$. The SPM-induced spectral broadening is a consequence of the time dependence of φ_{NL}, This can be understood by noting that a temporally varying phase implies that the instantaneous optical frequency differs across the pulse from its central value ω_o.
The difference $\delta\omega$ is given by

$$\delta\omega(T) = \frac{\partial \varphi_{NL}}{\partial T} = -\frac{L_{eff}}{L_{NL}} \frac{\partial}{\partial T} \left|U(0,T)\right|^2 \tag{2.31}$$

The time dependence of $\delta\omega$ is referred to as frequency chirping. The chirp induced by SPM increases in magnitude with the propagated distance. In other words, new frequency components are generated continuously as the pulse propagates down the fiber. These SPM-generated frequency components broaden the spectrum over its initial width at z 0.
An important aspect to consider is the pulse shape, as the extend of the spectral broadening depends on it; All the simulations have been performed using Gaussian pulses as input signal into the fiber, so taking Gaussian-pulse equations the SPM-induced chirp is

$$\delta\omega(T) = \frac{2m}{T_0} \frac{L_{eff}}{L_{NL}} \left(\frac{T}{T_0}\right)^{2m-1} e^{-\left(\frac{T}{T_0}\right)^2} \tag{2.32}$$

where m=1 for a Gaussian pulse, for larger values of m, the incident pulse becomes nearly rectangular with increasingly steeper leading and trailing edges.

Fig. 7 shows variation of the nonlinear phase shift and the induced frequency chirp across the pulse at $L_{eff} = L_{NL}$.

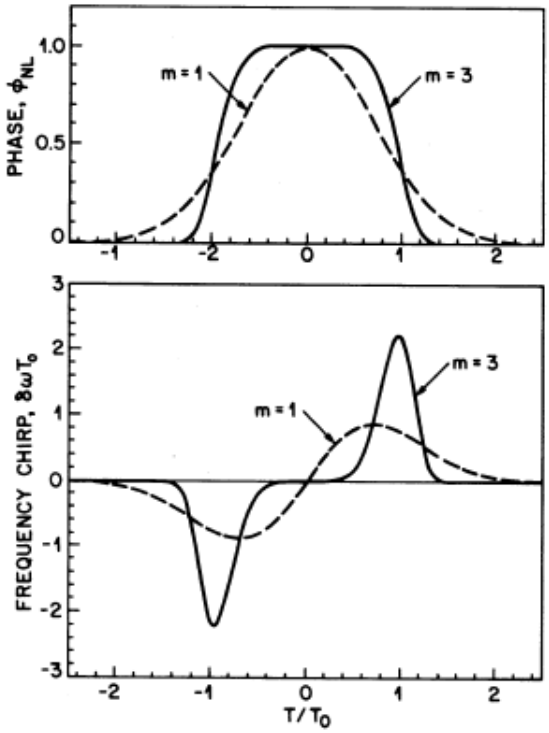

Figure 2-14: Temporal variation of SPM-induced phased shift φ_{NL} and frequency chirp δω.

As φ_{NL} is directly proportional to $|U(0,T)|^2$, its temporal variation is identical to that of the pulse intensity.Referring to δω, note it is negative near the leading edge (red shift) and becomes positive near the trailing edge (blue shift) of the pulse. Second, the chirp is linear and positive (up-chirp) over a large central region of the Gaussian pulse. Third, the chirp is considerably larger for pulses with steeper leading and trailing edges. Fourth, super-Gaussian pulses behave differently than Gaussian pulses because the chirp occurs only near pulse edges and does not vary in a linear fashion.In general, the spectrum depends not only on the pulse shape but also on the initial chirp imposed on the pulse. Fig. 82.16 shows the spectra of an unchirped Gaussian pulse for several values of the maximum phase shift φ_{max}, for a given fiber length.

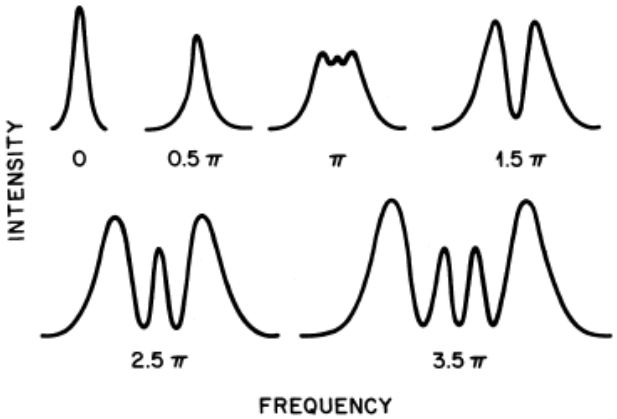

Figure 2-15: SPM-broadened spectra for an unchirped Gaussian pulse. Spectra are labeled by the maximum nonlinear phase shift φ max.

The most remarkable feature of Fig.82-16 is that SPM-induced spectral broadening is accompanied by an oscillatory structure covering the entire frequency range. In general, the spectrum consists of many peaks, and the outermost peaks are the most intense. The number of peaks depends on φ_{max} and increases linearly with it.
The origin of the oscillatory structure can be understood by referring to Fig.9 where the time dependence of the SPM-induced frequency chirp is shown. In general, the same chirp occurs at two values of *T*, showing that the pulse has the same instantaneous frequency at two distinct points. Qualitatively speaking, these two points represent two waves of the same frequency but different phases that can interfere constructively or destructively depending on their relative phase difference. The multipeak structure in the pulse spectrum is a result of such interference

Considering that, in the case of considering both SPM and GVD, the combination of both phenomena can develop new qualitative features, which depend on the fiber parameters. In the anomalous-dispersion regime of an optical fiber, the two phenomena can cooperate in such a way that the pulse propagates as an optical soliton. In the normal-dispersion regime, the combined effects of GVD and SPM can be used for pulse compression [20].

All the schemes and simulations performed are focused on studding of Kerr medium effect, and the subsequent analysis of different techniques to take advantage of its regenerative possibilities. Therefore, only the SPM effects will be taken into account.

3 Regeneration schemes based on Kerr medium

In this section two schemes, previously proposed in literature, are presented based on fiber self phase modulation nonlinearity. We perform detailed analysis of the scheme by examining all the physical mechanisms that take place at each component. By measuring the output signal quality we assess its regenerative properties. Finally, a novel scheme is also proposed and a detailed design analysis is carried out. We prove through numerical simulations that our proposal outperforms the all previous schemes that have been presented in literature.

3.1 NOLM-based DPSK signal regeneration

A first regeneration technique, based on interference using a Nonlinear Optical Loop Mirror (NOLM) is described [9]. It will be shown in the following paragraphs this scheme on its own cannot provide efficient phase regeneration. However, through a proper modification of its structure we can overcome this issure.

3.1.1 Conventional NOLM

NOLM regenerator uses a simple setup, consisting of an amplifier, a coupler, and a highly nonlinear fiber, Fig. 3.1. To upgrade the NOLM to regeneration of optical signals using phase encoding modulation formats, the phase information must be taken into account.

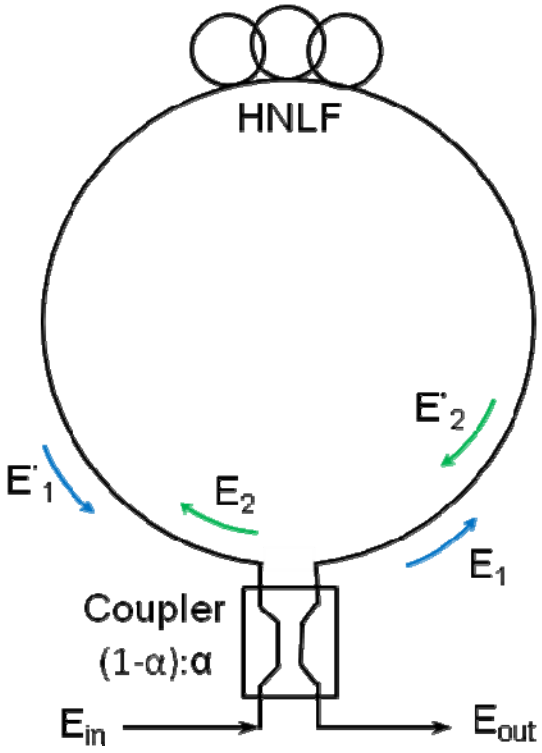

Signal regeneration by a NOLM is based on constructive and destructive interference [10].

The setup in Fig. 3.1 shows that an incoming pulse is split by a coupler with the splitting ratio [(1-α):α] into two counter propagating pulses with different power levels, which propagate through a fiber loop[17].

According to their power levels, the pulses gather different nonlinear phase shifts induced by self-phase modulation (SPM) before they interfere at the coupler.

Therefore, this interference is power dependent and leads to a nonlinear power transfer characteristic curve.

Figure 3-1: NOLM setup, where the colored arrows show the different ways the signals take.

In such loop mirrors, both component pulses which propagate around the loop in opposite directions, and which are transmitted and/or reflected by the loop mirror, depending upon the phases with which the component pulses return to the coupler.
If a coupler divides an input pulse into two equal component pulses, and if the loop affects these component pulses in the same way, i.e., symmetrically, the component pulses will interfere constructively on their return to the coupler and, consequently, will be reflected back through the coupler port through which they entered.
If the pulses are divided into unequal component pulses, or the loop affects the component pulses differently, i.e., asymmetrically, the pulses may interfere either constructively, destructively or partly constructively and partly destructively. In such cases the pulses returning to the coupler may be reflected, transmitted or partly reflected and partly transmitted.

In order to get this transfer function, the pulse peak power of an optical 40-Gb/s signal is analyzed, assuming an optimized coupling ratio of 90:10, and modeled by the equation

$$\begin{pmatrix} E_{out1} \\ E_{out2} \end{pmatrix} = \frac{1}{2}\begin{pmatrix} \sqrt{1-\alpha} & j\sqrt{\alpha} \\ j\sqrt{\alpha} & \sqrt{1-\alpha} \end{pmatrix}\begin{pmatrix} E_{in1} \\ E_{in2} \end{pmatrix} \tag{3.1}$$

And taking as a fiber transfer function the eq. (2.29) governed by SPM, the Output signal in function of the input is as follows

$$E_{out} = E_{in}\left[(1-\alpha)e^{-(j(1-\alpha)\varphi_{NL})} - \alpha e^{-(j\alpha\varphi_{NL})}\right] \tag{3.2}$$

And developing the power and phase we get

$$P_{out} = |E_{out}|^2 = |E_{in}|^2\left[1+(\alpha^2-\alpha)4\cos^2(\varphi_{NL}(\alpha-1/2)\right] \tag{3.3}$$

$$\theta = \tan^{-1}\frac{(1-\alpha)\sin(\varphi_{NL}(1-\alpha)) - \alpha\sin(\varphi_{NL}\alpha)}{(1-\alpha)\cos(\varphi_{NL}(1-\alpha)) - \alpha\cos(\varphi_{NL}\alpha)} \tag{3.4}$$

Assuming a 1 km highly nonlinear fiber (HNLF) without dispersion, an attenuation of 0.6 dB/km , and a nonlinear coefficient of $\gamma = 3\pi$ $(W\cdot km)^{-1}$.

The graph that can be observed in Fig.3-2(a), shows a flattened region, where amplitude fluctuations are suppressed effectively so that $|\Delta E_{out}|^2 < |\Delta E_{in}|^2$. As well as power, it is investigated the influence of the NOLM on the phase Fig.3-2(b). It shows that the phase shift can be approximated by a straight line ~ $-L\gamma|E'_2|^2$, as E'_2 ($|E'_2|^2 > |E'_1|^2$) dominates the phase of E_{out} and is responsible for the induced strong nonlinear phase shift. Hence, amplitude jitter is converted into additional phase fluctuations $\Delta\Phi_{out}$.

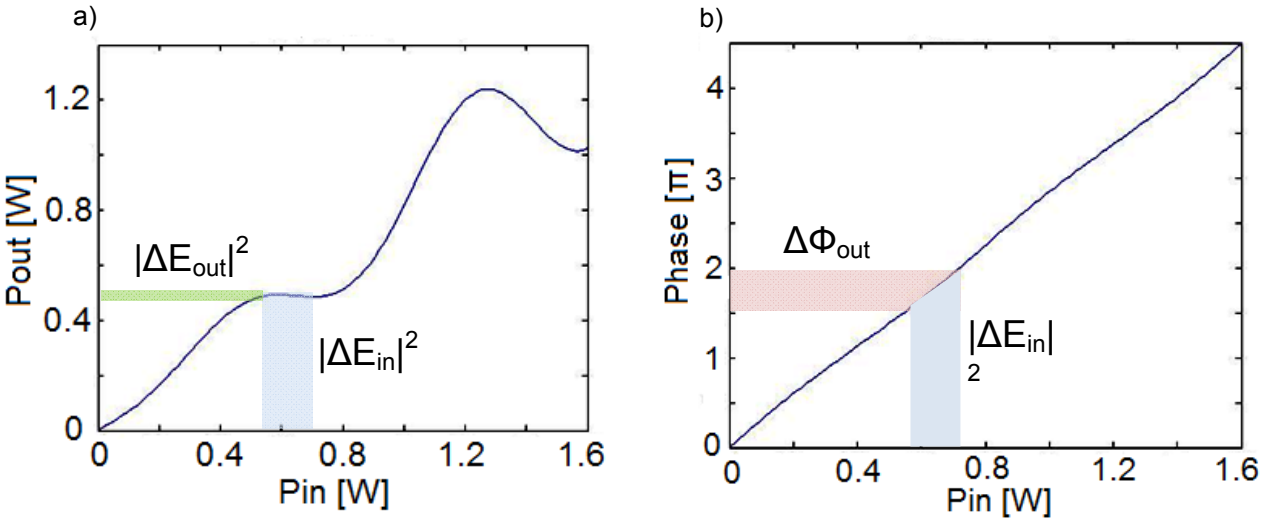

Figure 3-2: Power (a) and phase (b) characteristic of the NOLM. Fluctuations of the amplitude are suppressed in the flattened region.

To check the regenerative properties of the setup out, an impaired NRZ-DSPK signal is introduced as an E_{in}, with power amplitude of 0.7 W. So, white noise is added before the signal goes through the coupler. Note it is introduced enough noise to have a Q^2-factor around 13 dB. In order to take measurements of the Q-factor parameter, a balanced DPSK receiver demodulates the signal, hence we have again amplitude data pulses, as the information in the DPSK is transmitted in the phase, and we can calculate the Q-factor Appendix A.

In Fig. 3-3, the amplitude and phase are plotted in polar coordinate, thus the effect of the phase shift can be clearly observed. In Fig. 3-3 (a), which is the entrance of the regenerator, is plotted in blue the module/phase, in which one can notice the effect of noise, introducing jitter into both the phase and amplitude; whereas in Fig. 3-3 (b) is showed after having passed through the loop. The parameters under study from both graphs, such as the relative amplitude jitter, phase shift fluctuation, etc; are gathered in Table 1.

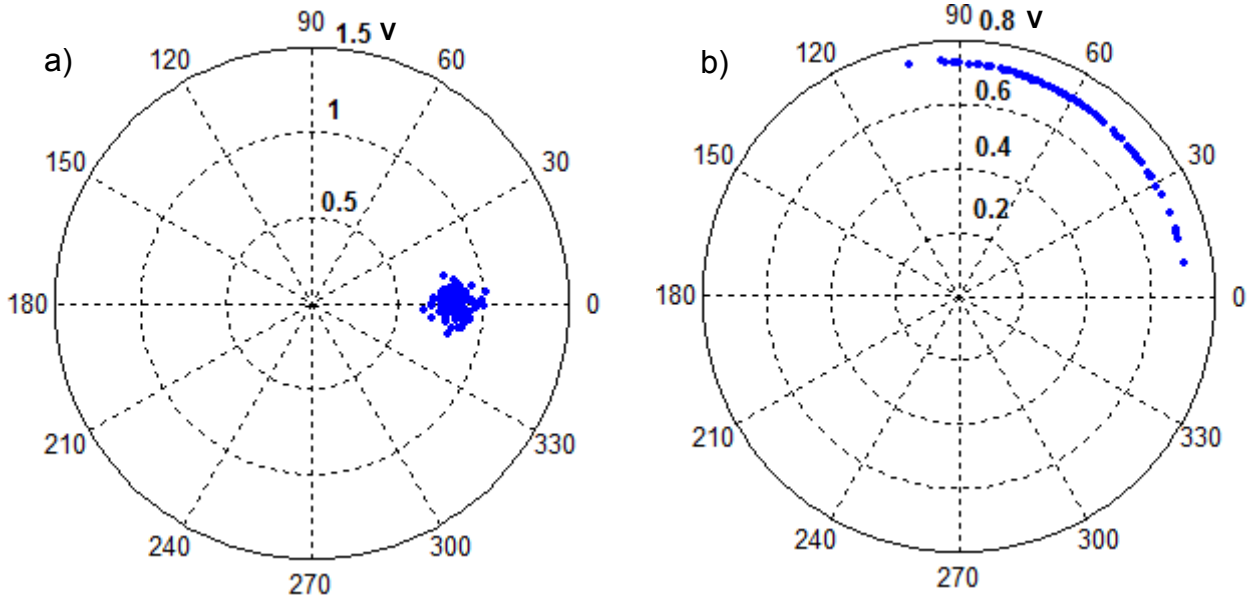

Figure 3-3: Characteristic diagrams, using polar coordinate system, of the NRZ-DPSK module/phase before (a), and after (b) the regenerator.

Input: fig 3(a)	Output: Fig 3(b)	Out/In (rate)
$\mu_{in} \approx 0.8$	$\mu_{out} \approx 0.7$	**0.9**
$\lvert\Delta E_{in}\rvert/\mu_{in} \approx 0.31$	$\lvert\Delta E_{out}\rvert/\mu_{out} \approx 0.1$	**0.32**
$\lvert\Delta\Phi_{in}\rvert \approx 20°$	$\lvert\Delta\Phi_{out}\rvert \approx 90°$	**4.5**

Table 1: Mean, amplitude and phase jitter performance comparison for marks.

Note that Amplitude jitter $|\Delta E|/\mu$ is reduced by the NOLM, but converted into phase jitter according to phase-P_{in} transfer function Fig. 3-2 (b). Therefore, once we demodulate the DPSK signal, all the noise accumulated in the phase is translated to amplitude fluctuations. Because of this, even though before demodulate the signal an amplitude regeneration is achieved, after the DPSK receiver ghost pulses and amplitude jitter will appear since the phase difference of the pulses is no longer exactly 0 or π.

Consequently, for DPSK signal regeneration, apart from a flat region in the output power versus input power characteristic graph, a constant phase flattened plain region of NOLM power characteristic curve is needed. Regarding this, a second scheme with some modifications is studied next.

3.1.2 Modified NOLM

To achieve suppression of the phase noise the scheme is slightly changed Fig. 3-4(a); a directional attenuator (DA) is added [9], which can be realized with a couple of circulators in order to separate both directions, Fig. 3-4(b).

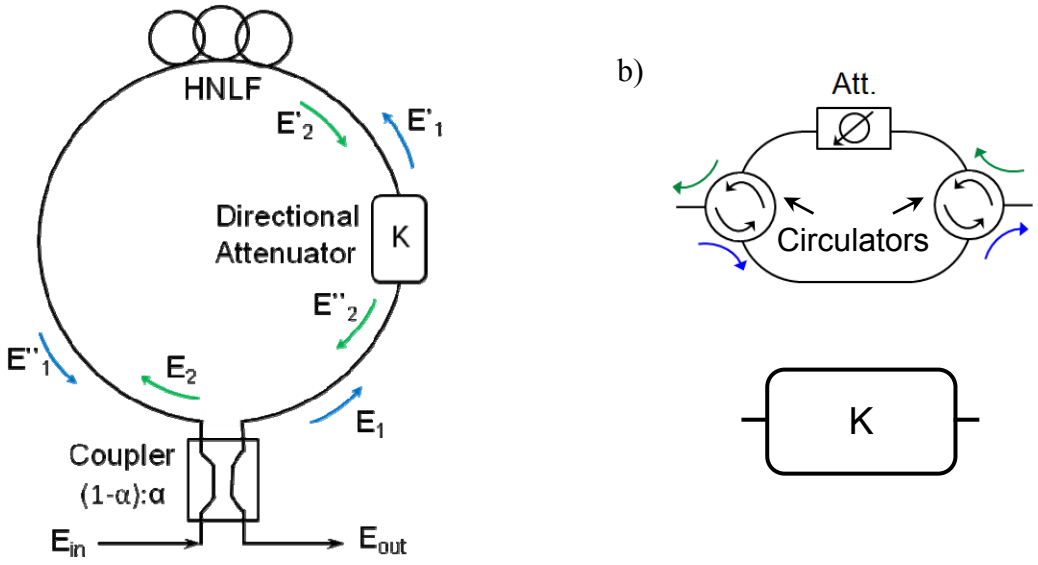

Figure 3-4: (a) New NOLM scheme setup, in which a directional attenuatoris added. (b) General inner view for the DA.

By introducing the attenuator the equation obtained at the output of the regenerator is

$$E_{out} = E_{in}\left[K(1-\alpha)e^{-(j(1-\alpha)\varphi_{NL})} - \alpha e^{-(j\alpha\varphi_{NL})}\right] \tag{3.5}$$

And its subsequent power, and phase

$$P_{out} = |E_{out}|^2 = |E_{in}|^2\left[\alpha^2 + K^2(\alpha^2-\alpha) - 2K\alpha(1-\alpha)\cos^2(\varphi_{NL}(\alpha-1/2)\right] \tag{3.6}$$

$$\theta = \tan^{-1}\frac{K(1-\alpha)\sin(\varphi_{NL}(1-\alpha)) - \alpha\sin(\varphi_{NL}\alpha)}{K(1-\alpha)\cos(\varphi_{NL}(1-\alpha)) - \alpha\cos(\varphi_{NL}\alpha)} \tag{3.7}$$

As in previous case we consider here a coupling factor of 90:10, a piece of fiber of 1 Km, but now with typical nonlinear coefficient values γ $(W\cdot Km)^{-1}$ of 2π, 3π, and 4π in order to see what effect γ has on the scheme, Fig 3-5. In addition, several characteristic curves are displayed for different attenuation constant (K) for each graph.

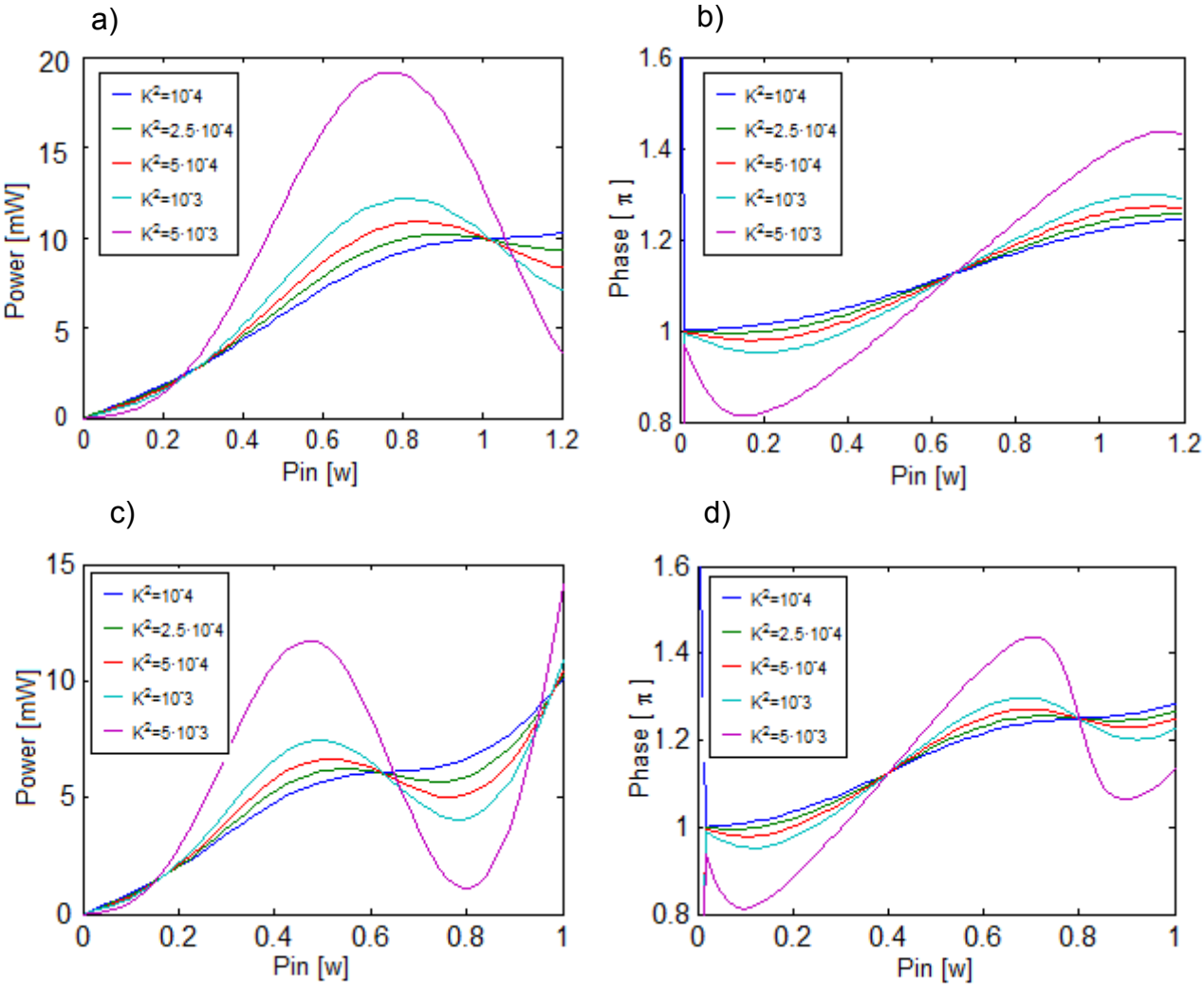

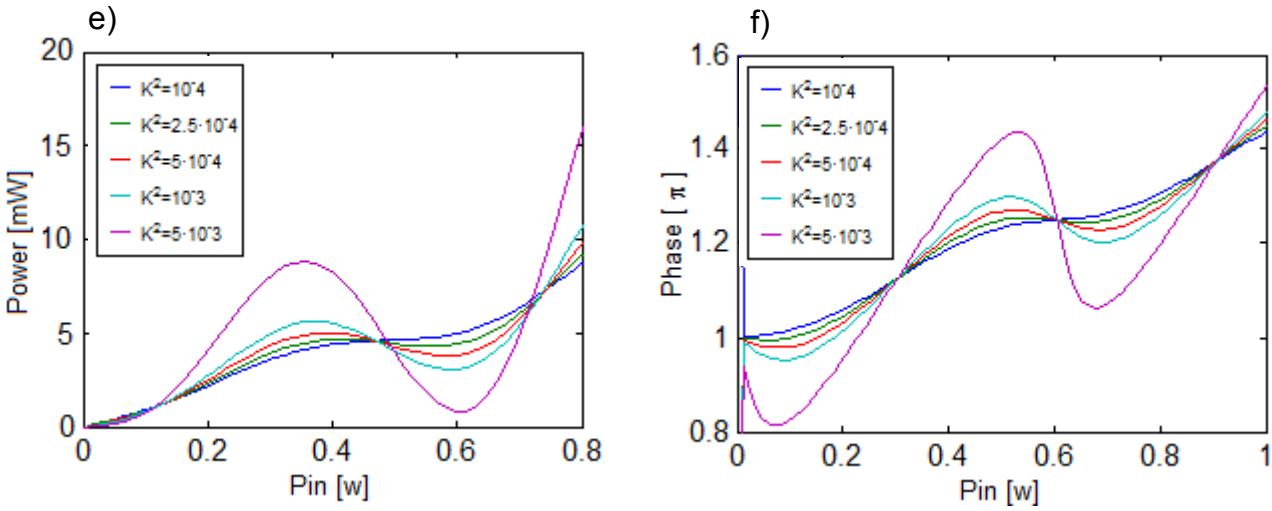

Figure 3-5: Power and phase shift characteristic of the DA-NOLM for γ = 2π (a) (b), γ = 3π (c) (d), γ =4π (e) (f)

Modyfying the value of the attenuator, the curves obtained present a flat region both on the phase and power. Indeed, what differs from the previous scheme is the flattened behavior experimented by the phase shift, this means that a suppression of amplitude jitter can be reached whereas the phase will remain almost constant.
One can notice also, that there is an optimum K value in between 10^{-4} and $2.5 \cdot 10^{-4}$, blue and green curves respectively, since there is a compromise between the flat region in the phase and the power. Furthermore, a general trend can be observed, when the nonlinear coefficient increases, the plain region is shifted to lower values. This is mainly caused by the fact that the phase induced due to the kerr medium (2.29) is proportional to $P \cdot \gamma$, as the length is kept constant. Therefore, if a larger nonlinear coefficient is used, a lower input power is required to provoke a similar response. In addition, for lower values of γ, so larger values of power, the output shows a higher level, this comes from fact that the output is proportional to the input (3.5).

The reason of this power and phase characteristic falls on the interference between a high-powered signal E_1'' with low SPM-induced phase shift, and a low-powered signal E_2'' with a strong phase shift; the signal E_2', since $|E_2'| > |E_1'|$, gathers more phase shift than E_1' while passing through the NOLM fiber. Afterwards, E_2' is attenuated by the directional attenuator which leads to the required condition $|E_2''| < |E_1''|$. The overall low phase shift results from the dominating signal with low phase shift. The flattened regions of the power and phase characteristics are achieved by compensating out the variation of phase and amplitude of E_1'' by E_2'' simultaneously.
Note that existing phase jitter at the entrance of the NOLM is not reduced by this setup but not increased either. In addition this new setup attenuates the NOLM input power as expected from the assumption $|E_{out}|^2 \sim \alpha\ |E_{in}|^2$, since the power of E_2'' is negligible due to strong attenuation.

In order to evaluate the response of the setup, as well as what was seen in the previous scheme, an impaired NRZ-DPSK signal is used as input, so before the signal gets into the coupler is degraded with white noise and then suitably filtered, all these steps are described more in detail in Appendix A.

Considering that, NRZ_DPSK signal with a measured Q^2-factor around 13 dB is inserted into the NOLM, Fig. 3-6 (a). All the setup values are kept equal to the previous scheme, that is a $\gamma=3\pi$, length= 1Km, coupler with 90:10 ratio, and $2.5\cdot10^{-4}$ (-36dB) as an attenuation K^2. In Fig. 3-6 (b) is shown the signal after the regenerator.

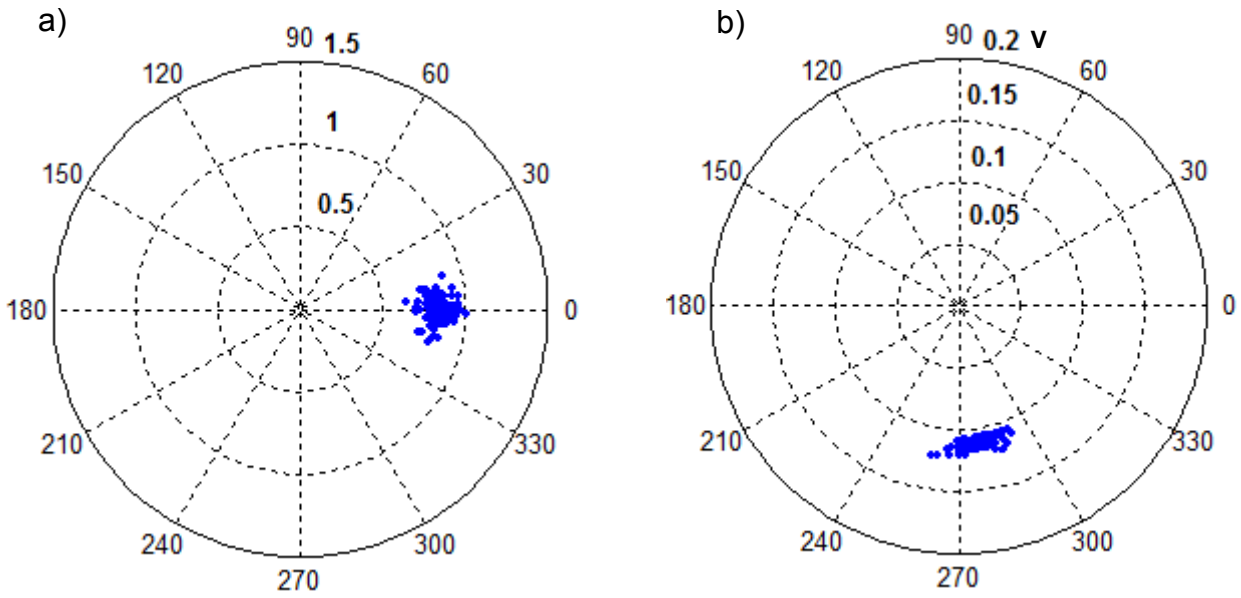

Figure 3-6: Module/phase characteristic polar-coordinate-diagrams of the NRZ-DPSK before (a), and after (b) the modified NOLM regenerator.

According to the preceding results, and consequently quantified in Table 2, many conclusions can be noted. The most remarkable one, and unlike the previous regenerator setup, is the fact that phase shift is not increased, as its $\Delta\Phi_{out}$ practically remains the same as $\Delta\Phi_{in}$, thus after being demodulated the phase noise induced by the Self Phase Modulation is almost negligible. This means that amplitude fluctuations are suppressed at the same time as no phase jitter punishment is accomplished. Therefore, amplitude regeneration can be performed.

Input: fig 6(a)	Output: Fig 6(b)	Out/In (rate)
$\mu_{in} \approx 0.8$	$\mu_{out} \approx 0.12$	**0.13**
$\lvert\Delta E_{in}\rvert/\mu_{in} \approx 0.3$	$\lvert\Delta E_{out}\rvert/\mu_{out} \approx 0.2$	**0.67**
$\lvert\Delta\Phi_{in}\rvert \approx 30°$	$\lvert\Delta\Phi_{out}\rvert \approx 30°$	**1**

Table 2: Mean, amplitude and phase jitter performance comparison for marks.

However, note that at the output the power is reduced considerably, due to both the constructive/destructive effect of the coupler and the strong attenuation (36 dB) induced by the attenuator. Different alternatives can be implemented, such as using amplifiers instead of attenuators, thus the output signal would present a power level comparable to the input one. Nevertheless, an extra source of noise would degrade the signal, since an amplifier itself is not ideal and produces various types of noise.

To have a more "visual" and clearer idea of how the quality of the signal is improved, in Fig.3-7 is showed the comparison between the demodulated input NRZ-DPSK signal and the same signal once passed through the DA-NOLM.

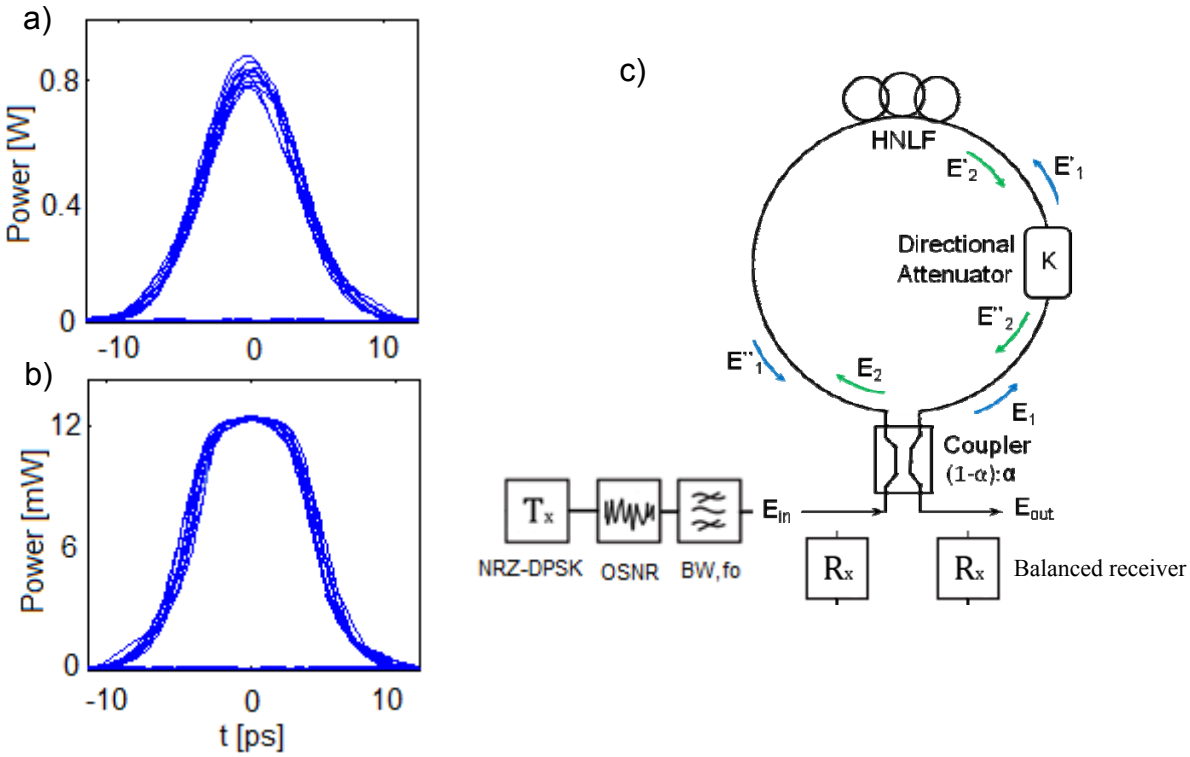

Figure 3-7: Eyediagram before (a) and after (b) the regenerator. (c) Setup to perform the measurements

As seen, the pulses present amplitude jitter regeneration, mainly on the peak power; this is achieved mainly thanks to the flat region above mentioned. On the other hand, the fluctuations of "spaces" (when a zero is transmitted, so that the signal is nearly 0 W) due to noise are not cancelled by this scheme.

The reduction of amplitude variance is translated to an improvement of the Q-factor. So the next step is to measure the quality of the signal by means of the Q-factor parameter, in order either to quantify it or compare this scheme with other regenerators. Regarding this, a new "block" is added after each receiver in which following function is implemented the

$$Q = \frac{\mu_1 - \mu_0}{\sigma_1 + \sigma_0} \tag{3.8}$$

where μ_1 is the amplitude mean level for "marks" whereas μ_0 is for "spaces"; σ_1 and σ_0 is the variance of "ones" and "zeros" respectively. Note that the Q-factor is often given in logarithmic scale, so that it will be defined as

$$Q_{dB} = 10\log Q^2 = 20\log Q \tag{3.9}$$

Once defined the Q-factor parameter, in order to have a more exhaustive analysis of the scheme, output Q_{dB} is depictured for different values of nonlinear maximum phase shift φ_{max} (2.29), and assuming a Q_{dB} at the input around 13 dB, Fig. 3-8 (blue). The measurement is taken for two different phase amplitude depths, the green and red curves appearing in Fig. 3-8.

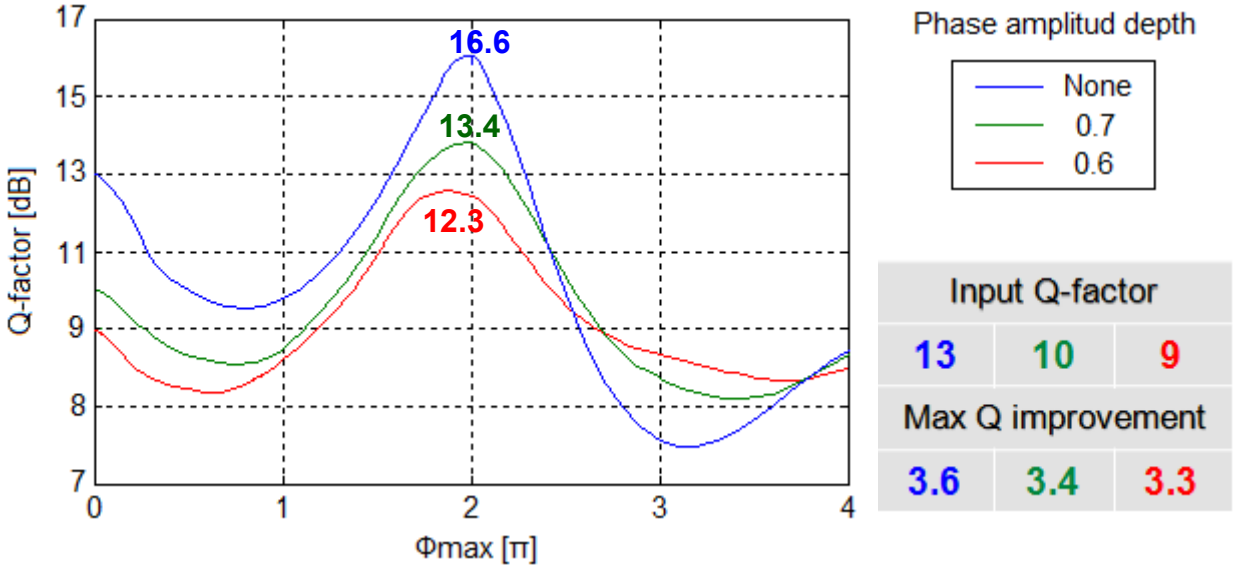

Figure 3-8: Output Q-factor in function of maximum nonlinear phase shift, for

According to preceding results, there are some conclusions to point out. First of all, an improvement is clearly achieved since a maximum gain of 3.6 dB is observed, needless to say, this gain is only accomplished around the peak of each curve, so that 2π.

The reason why the maximum gain is reached for the same range of phase-shift values can be understood by analyzing the graphs obtained in Fig. 3-5. As the regenerative performance occurs in the flat region, if we take the first case, Fig. 3-5(a) (b), it takes place having around 1W of input power, a nonlinear coefficient of 2π, and 1Km of length, which means that $\varphi_{max} \approx 2\pi$. The same can be said about the other two cases in which the flattened region is observed approximately when $\varphi_{max} \approx 2\pi$ as well. Therefore if we want to have a maximum regeneration at the output, a φ_{max} close to 2π is needed, ergo a compromise among the signal peak power value, length, and nonlinear coefficient.

Note that the effect of the phase amplitude depth is a reduction in the Q-factor gain, looking at the table next to the graph in Fig.3-8, we can observe that the bigger the phase depth is, the lower the Q-factor improvement achieved.

3.2 SPM-filtering based DPSK signal regeneration

The main idea behind this section is focused on achieving not only amplitude regeneration as in the previous chapter, but also phase noise suppression. Thus, measure the quality parameters at the output and carry out a comparison with the setup in which only amplitude regeneration is performed.

First, the basic principle used to fulfill the all-optical regeneration is presented, summarizing and explaining the most important steps that take part through the scheme. Note that one of these steps will be the amplitude regeneration process, so before the whole explanation of the setup performance itself, the "Mamyshev" regenerative concept [11] will be introduced and detailed, in order to have a proper background to understand how the amplitude noise jitter is suppressed.

Then, after describing the procedure, a regeneration existing scheme in the literature [12] is examined. Taking the background concepts of this implementation, a novel proposal is presented, and consequently analyzed.

3.2.1 Amplitude-phase regeneration principle

The principal goal is achieving both amplitude and phase noise suppression; regarding that, the following schemes are all based on the principle described next, which bases the phase noise regeneration on the amplitude jitter reduction.
So the performance can be divided into three principal steps, basically the first and the last one a format conversion is done, whereas in the other one amplitude jitter suppression is carried out, Fig. 3-9.
Next, a more detailed explanation of what is inside each block is given in order to know what devices and components are used to accomplish the general function. A DPSK signal is assumed at the input of the regenerator. The first block is used to demodulate the demodulate differential phase-encoded signal. This achieved by a delay interferometer, which makes the conversion from phase to amplitude modulation.

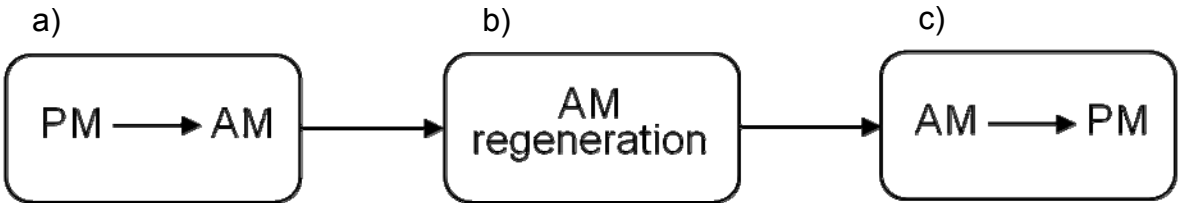

Figure 3-9: Block diagram of main tasks performed. (a) Conversion from phase to amplitude modulation. (b) Amplitude regeneration performance. (c) Reconversion to phase modulation.

3.2.1.1 Phase to amplitude format conversion

As mentioned, a DPSK, specifically a NRZ-DPSK signal is used as incoming signal (Ein), so the information is in the phase while the power remains constant. Then the signal passes through a delay interferometer, Fig. 3-10, in which two couplers modeled by (3.1) and having the same value of $\alpha = 0.5$ split it, as can be seen in the following matrix

$$\begin{pmatrix} E_{out1} \\ E_{out2} \end{pmatrix} = \frac{1}{\sqrt{2}} \begin{pmatrix} 1 & j \\ j & 1 \end{pmatrix} \begin{pmatrix} E_{in1} \\ E_{in2} \end{pmatrix} \tag{3.10}$$

where E_{in1}, E_{in2} are the up-arm and down-arm inputs respectively, and E_{out1}, E_{out2} the outputs. After the first coupler one of two signals is delayed one bit, or what is the same 1/bitrate, whereas the other one is not. Once after the second coupler, at the output of the DI the equations are

$$E_{01} = \frac{1}{2}(-E_i(t) + E_i(t-T)) \tag{3.11}$$

$$E_{02} = \frac{j}{2}(E_i(t) + E_i(t-T)) \tag{3.12}$$

In order to analyzing the signals, we introduce a NRZ-DPSK signal with the following specifications: carrier central wavelength λo= 1550 nm, Bit rate= 40 Gbps, Gaussian pulses as input data (in the phase) with a Duty cycle= 33%, which means T_o=8.3 ps, and Max($|E_{in}|^2$) = P_o= 1W. Considering this, after the DI we obtain a constructive (3.12) and destructive (3.11) ports, specifically the formats attained correspond to a duobinary and AMI respectively,

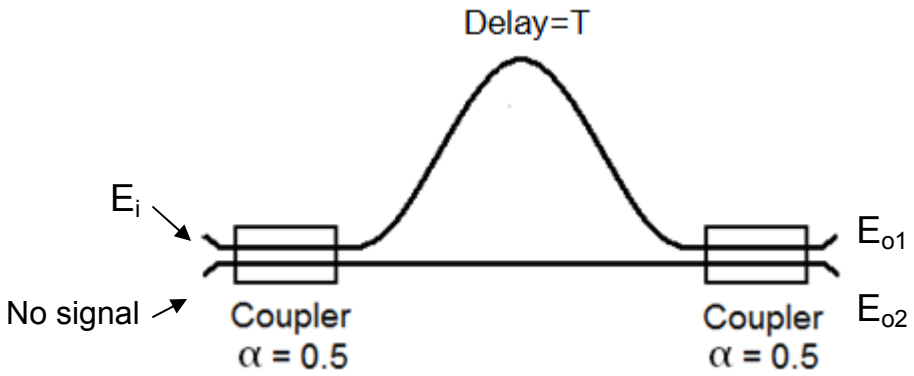

Figure 3-10: Delay interferometer. Signal E_i is the input whereas E_{o1} and E_{o2} are the output ones. A delay equals to the bit period duration is applied to one on two arms.

To have a visual idea of how the two signals perform after passing through the DI, power is depicted in Fig. 3-11. Note that the information before carried in the phase is now in both cases transferred to amplitude, as the power does not remain constant and Gaussian pulses are clearly appreciable. Note as well that both differ from the fact that one is inverted compared

to the other one. Indeed, since the duobinay signal describes inverted Gaussian pulses in contrast to the AMI, which are not inverted.

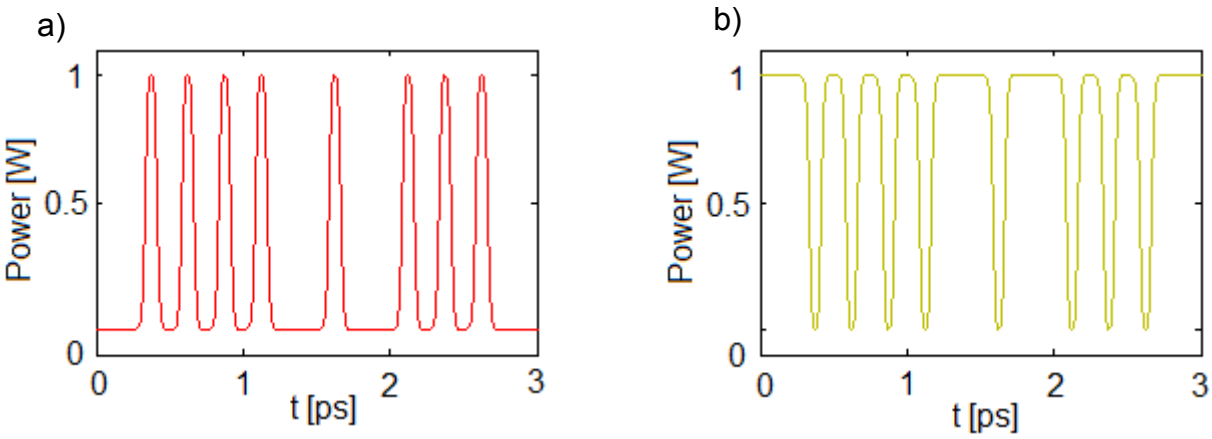

Figure 3-11: Power graphs of (a) E_{01} (AMI) and (b) E_{02} (duobanary) signals

3.2.1.2 Amplitude jitter suppression

This second step describes the 2R regeneration process which improves the amplitude signal quality. Normally there are two basic regeneration techniques based on spectrum broadening (SPM) and subsequent filtering :

- those relying on soliton-like pulse compression in an anomalous-dispersion fiber and subsequent band-pass filtering, tuned at the carrier wavelength of the input signal [13].
- those relying on spectrum broadening and subsequent spectrum slicing by a narrow-band filter at a shifted wavelength [11, 14].

In the specific thesis we have concentrated on the latter one regeneration technique, becauses it is able to provide suppression also in phase apart from the amplitude. However, a brief description of first type regeneration is also given in order to have a general idea of how it works.

First-type Regenerator, the regenerator based on soliton-like pulse compression and filtering has the configuration and is based on the principle presented in Fig. 3-12. It consists of an optical amplifier, an HNLF with anomalous-dispersion and an optical band-pass filter, tuned at the carrier wavelength. The pulse fed into the HNLF experiences pulse compression or broadening, depending on whether its amplitude is larger or smaller than that of the fundamental soliton. If the pulse compression and broadening are adiabatic, the spectrum width of the pulse is broadened and narrowed, accordingly.
Filtering after the HNLF thus gives larger (smaller) loss to the pulse when the incoming pulse has larger (smaller) amplitude than the fundamental soliton. By this mechanism, the pulse amplitude is automatically stabilized. In Fig. 3-12 the specific case of pulse compression and spectral broadening is illustrated, through the successive processing stages. Parameters of this regenerator are the shape and the pulse width T_0 of the input signal, the output power of the

optical amplifier that defines the peak power P_0 of the pulses launched in the HNLF, the length L, the attenuation α, the dispersion D and the nonlinear parameter γ of the HNLF, and finally the shape and the bandwidth BW of the subsequent OBPF.

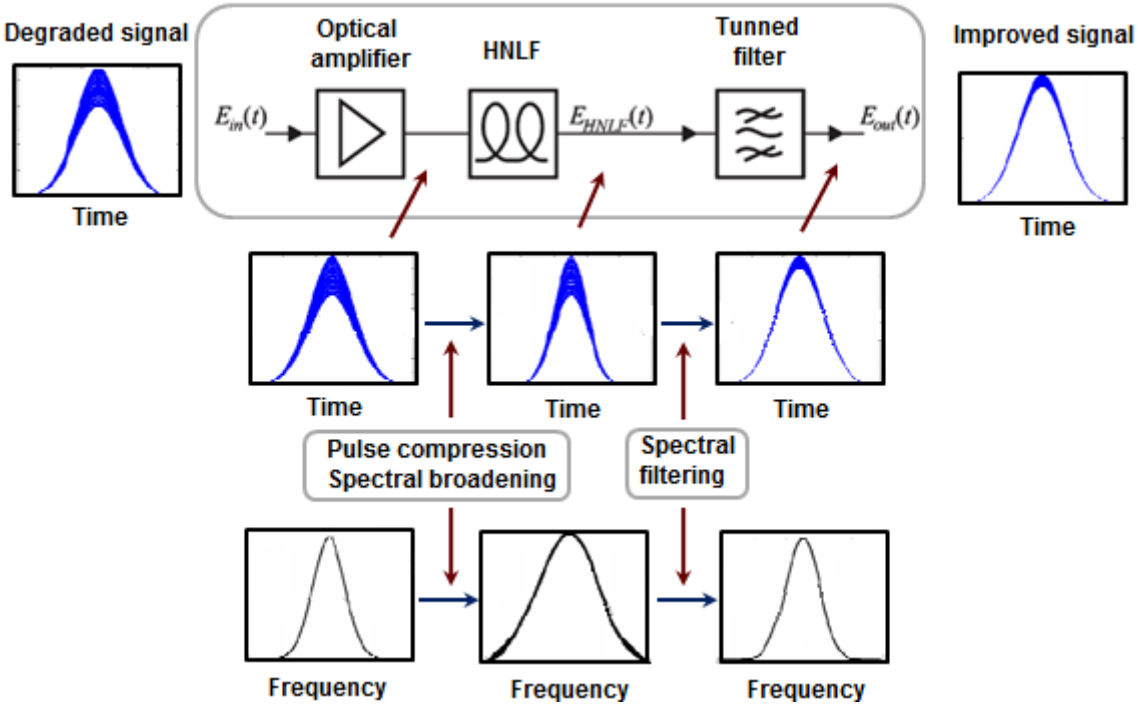

Figure 3-12: Configuration and operating principle of the first-type regenerator.

This type of regenerator provides an efficient mechanism to stabilize the peak power of the signal's pulses acting as an optical limiter, but cannot efficiently suppress the low-intensity fluctuations in the space bit slots. The transfer function between the input and the output peak power of the pulses that characterizes the first-type regenerator is quite linear for low input peak power, and is saturated around the operating point of the regenerator.

Second-type regenerator, the regenerator that is based on Mamyshev concept [11], which is a simple all-optical regeneration technique which suppresses the noise in "zeros" and the amplitude fluctuations in "ones" of return-to-zero (RZ) optical data streams. It is based on the effect of self phase modulation (2.29) of the data signal in a nonlinear medium with a subsequent optical filtering at a frequency which is shifted with respect to the input data carrier frequency f_o. It consists of the same components as the first-type regenerator, i.e. an optical amplifier, an HNLF and an OBPF. Its main difference is that the HNLF has the central frequency of the OBPF is shifted from the input signal's carrier frequency.
During the propagation of the input signal in the HNLF having normal dispersion, its spectrum is broadened under the combined action of the SPM and the group velocity dispersion. Fig 3-13 shows a setup to prove this behavior, note that in this specific case the dispersion is not considered, as it simplifies the scheme, and the characteristic performance observed is close enough to the case when it is considered. Then a portion of the broadened spectrum is sliced by the detuned OBPF, as is illustrated in Fig. 3-14.

The second-type regenerator has inherently the potential of two functions:

- suppressing the noise and eliminating the ghost pulses in the space level
- suppressing the power fluctuations in the mark level.

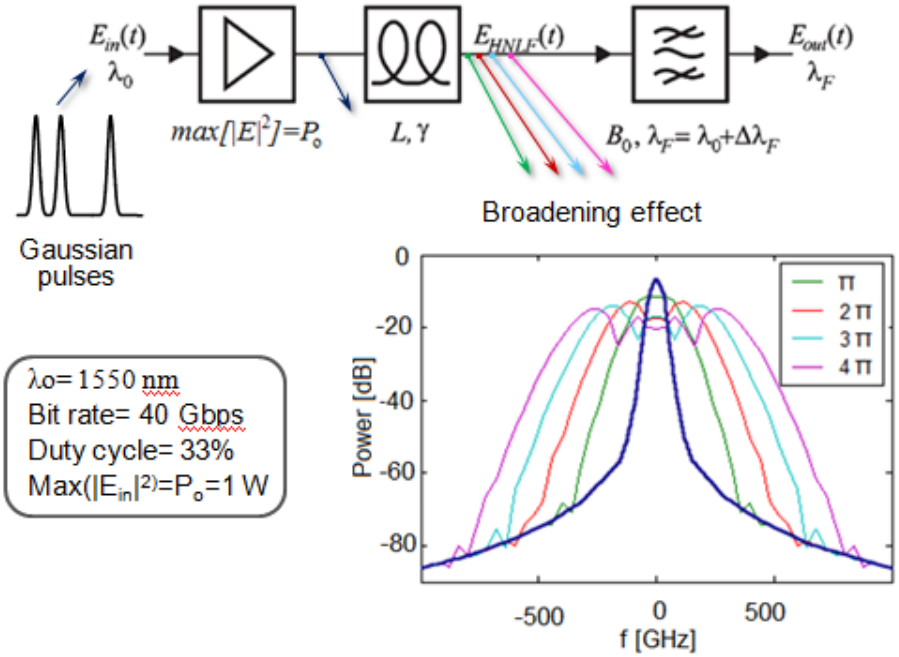

Figure 3-13: Spectral broadening for several max phase-shift (2.23) assuming the values inside the box

Thus, the full 2R functionality can be provided including pahse amplitude depth improvement and optical power limiting [19]. The first function is obtained because the low-power pulses experience small spectral broadening and cannot pass through the filter. Indeed, as the spectral broadening by SPM depends on the pulse peak power P_0 (2.32), it is negligible for a pulse with low pulse peak power such as noise, Fig. 3-14 (a).

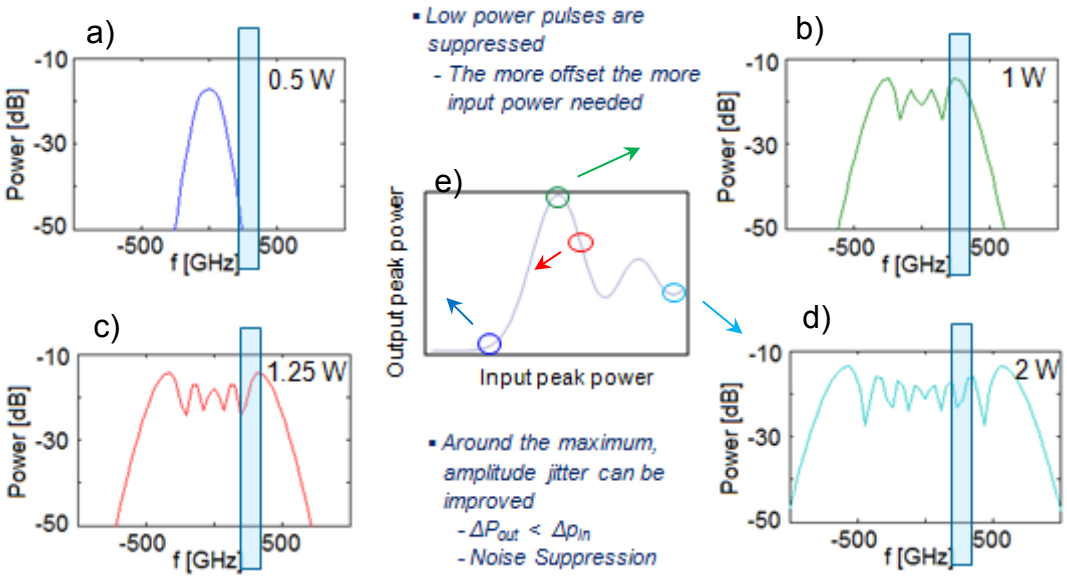

Figure 3-14: In order to understand the power transfer function response (e), spectrums corresponding to different input power are depictured, maintaining L·γ=4π, offset=300GHz, bandwidth=1/T_o=150GHz.

The second function is obtained because the density of the broadened spectrum of high-power pulses inside the filter's pass-band depends only slightly on their peak power, and thus the power fluctuation is absorbed [11]. The input-output peak power transfer function that characterizes the second-type regenerator is a step-like transfer function indicating the existence of a threshold that is defined mainly by the frequency shift Δf of the OBPF with respect to the signal's carrier frequency. Maintaining the same parameters than the previous figure but for the offset, which is analyzed by varying the offset shift respect from the central carrier frequency, we obtain the graph seen on Fig. 3-15.

First of all, remark the two main functions achieved with this method, cancellation of low power pulses (orange mark). Not to mention that the more offset, the higher noise level can be suppressed, to the detriment of increasing either the input power or changing the parameters of the fiber; then, reduction of amplitude jitter around the maximum of each curve, as $\Delta P_{out}<\Delta P_{in}$ due to the power density inside the filter band-pass seen in the previous figure.

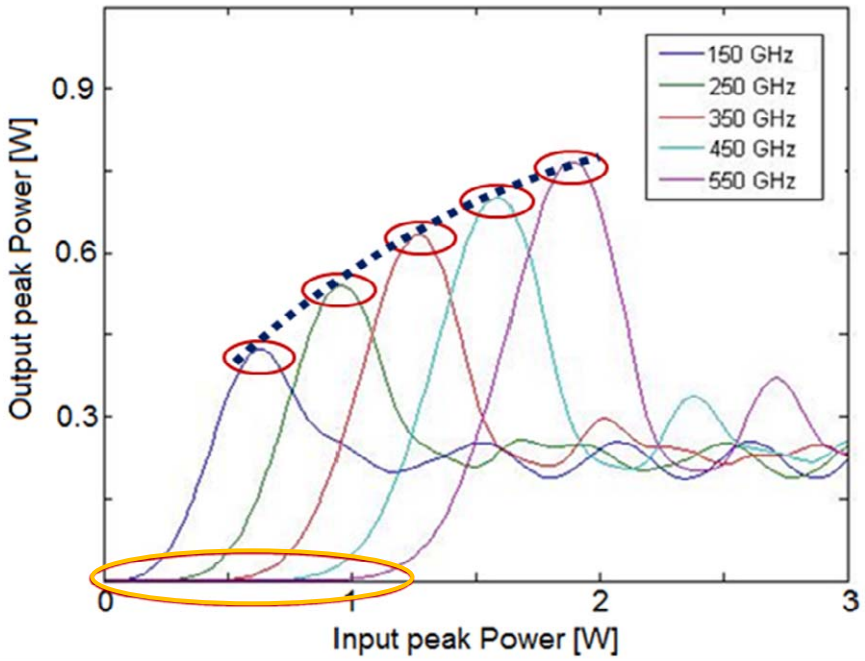

Figure 3-15: Peak power transfer function using different offsets relative to central carrier frequency ($f_f=f_0+f_{offset}$) in the bandpass filter after the HNLF.

Note that an increasing and almost linear trend in the maximums is observed, the reason of this growing comes from the equation (2.29) as the output $\propto$ input$\cdot e^x$, so the more input level we introduce the higher the peak is. Nevertheless, the not linear behavior comes mainly from the fact that once the spectrum is broadened by having passed through the fiber, as larger the phase shift is, the same as saying that the input power is bigger, the lower values the spectral power reaches. In Fig. 13, if we focus on the pink curve and we compared it to the red one, it can be noticed that there is a loss of power in between 1 and 2 dB. So, if the plots in Fig. 3-15 were normalized would be appreciable a decreasing line related to "x" axe that would be approximately like the dotted curve traced in dark blue. Point out that depending on the

specifications or constrains required, it will be more suitable to use either one specific offset or another one.
In order to analyze the regenerative capabilities of the scheme, as well as made with the precedent regenerator based on NOLM, an impaired signal is introduced into it, but now an amplitude modulation format is used since this method works with OOK-modulation, then the signal is properly filtered suppressing all the noise out from the useful signal range, which the only thing it would do is to worsen the quality.

So, the signal is evaluated in two different points, one before the fiber and the other after the offset filtering. A Q^2-factor about 13 dB is forced in order to compare this results to the ones from the scenario seen before. All these results are shown in Fig. 3-16.

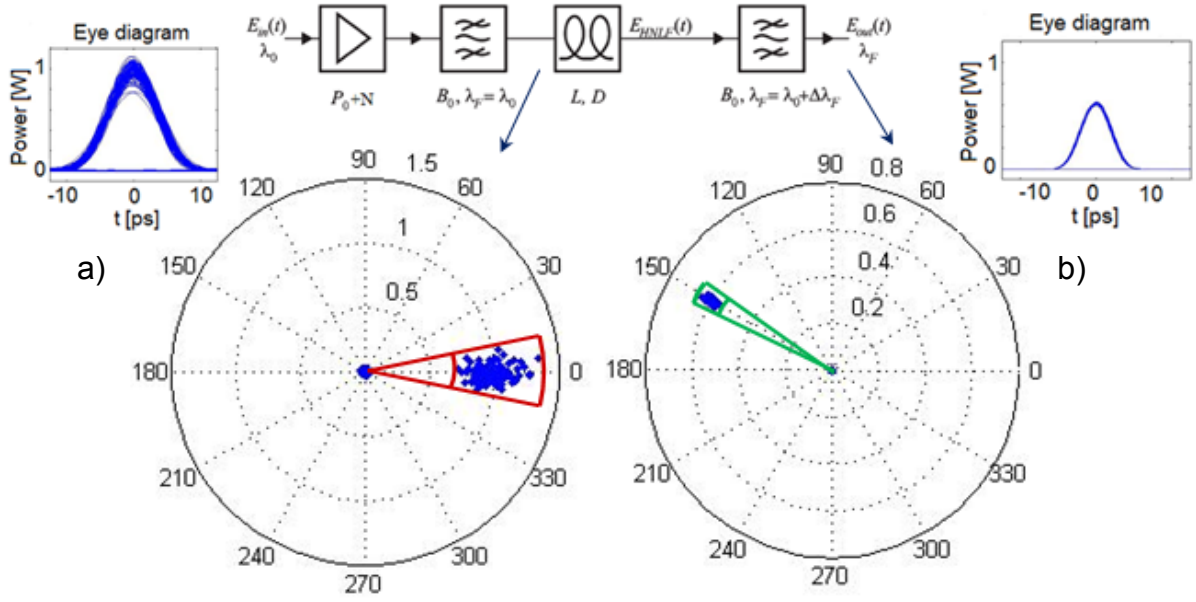

Figure 3-16: Eyediagrams and module/phase polar plots of the signal before (a) and after (b) being regenerated

Both the amplitude and phase parameters are measured and gathered in Table 3. Some conclusions can be taken looking at the 3rd column where the comparison between output in function of input is performed.
An amplitude jitter reduction is accomplished as expected from the application of the Mamyshev concept explained; adding that a higher level of "ones" mean value is achieved compared to the previous setup. Besides a slightly better jitter suppression is fulfilled.

Input: fig 16(a)	Output: Fig 16(b)	Out/In (rate)
$\mu_{in} \approx 1$	$\mu_{out} \approx 0.5$	**0.5**
$\lvert\Delta E_{in}\rvert/\mu_{in} \approx 0.5$	$\lvert\Delta E_{out}\rvert/\mu_{out} \approx 0.2$	**0.4**
$\lvert\Delta\Phi_{in}\rvert \approx 30°$	$\lvert\Delta\Phi_{out}\rvert \approx 10°$	**0.33**

Table 3: Mean, amplitude and phase jitter performance comparison

Note as well, the fact that it is appreciable phase noise suppression; this is not noticeable in the first technique based on NOLM. Nevertheless, next scheme presented does not make use of this, since a reconversion from amplitude to phase is carried out after the offset filter, to achieve a better phase regeneration by means of amplitude jitter suppression, explained in the next section.

3.2.1.3 Amplitude to phase format conversion

In this third and last stage is performed the phase regeneration through transforming the amplitude (already regenerated) pulses back to phase information data. Since the main aim of this thesis is to study the different ways to achieve all-optical noise suppression, all the processes involved in the conversion itself are is not examined in detail, but an overall description of the components and their functions is given. However, a test and measurement of the output signal will give us the achievable quality after having passed right trough the regenerator.

The stabilized data pulses are fed into an all-optical phase modulator (another HNLF) as control pulses, where they modulate the phase of the optical input signal CW. The modulation is based on cross-phase modulation (XPM) between CW and control pulses having different wavelengths with suitable walkoff time between them. Power of the data-bearing control pulses launched into the HNLF is adjusted so that π-phase shift is induced to continuous wave signal. It is noted that the wavelength difference in the phase modulator may be chosen equal to the wavelength shift in the 2R regenerator whereby wavelength- shift free regeneration can be achieved [15][16].
Fig. 3-17 shows the general phase-modulator setup, as it can be seen the main devices used are a coupler, an amplifier, a highly nonlinear fiber, and a bandpass filter.

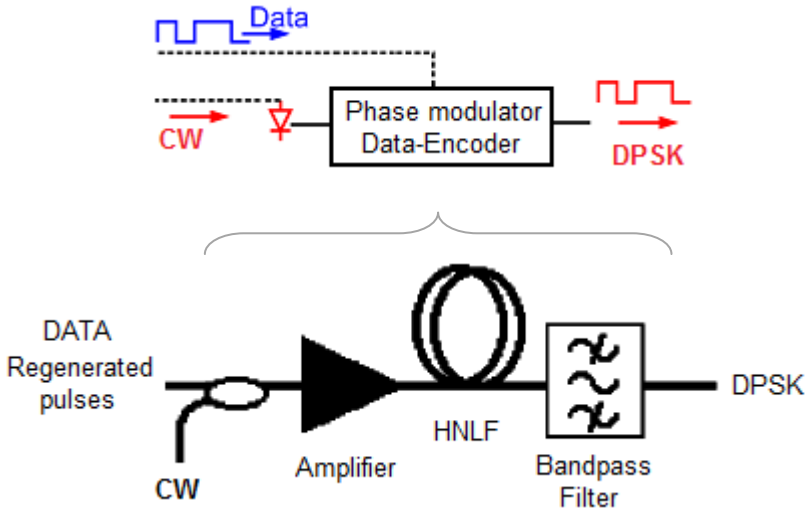

Figure 3-17: Phase modulator setup

3.2.1 Scheme setup performance

Based on the above a detailed description of the subsystem setup is given in Fig. 3-18. Every device is represented as a box with a symbol inside that simplifies and makes more understandable the model, helping to split the main function in basic modules. Note that in Fig. 3-18, two black arrows indicate the two points where the Q-factor measurements will be carried out, because of this a previous demodulation block need to be interposed since an amplitude format is required to measure the man values of "ones" and "zeros", and their respective standard deviation, Appendix A.
Under every block is showed the parameters that take part on the performance of the device in question, and alsothe changeable variable on the scheme. Besides, a brief definition of every block is given in order to know its main function. Remark as well that each block is identified with a number, just to be easier to refer to them.

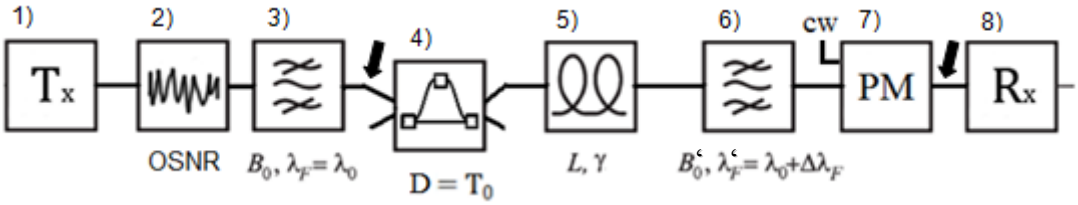

Figure 3-18: Regenerator setup. Each component is represented by one box, from the transmitter to the receiver.

- 1. DPSK signal is sent from the transmitter.
- 2. White noise is added impairing the signal in order to be subsequently analyzed.
- 3. Optical pre-filter eliminates the noise out of the useful signal BW.
- 4. DI turns the phase data into amplitude.
- 5. Kerr medium broaden the spectrum due to SPM.
- 6. Offset optical filter selects the suitable bandwidth.
- 7. Amplitude is modulated into phase once regenerated.
- 8. The receiver demodulates the signal.

Remind that the signal used as an input and subsequently examined is NRZ-DPSK modulated-format signal, as well as the previous schemes presented, with the following specifications:

- Carrier $\lambda_0 = 1550$ nm
- Data – Gaussian pulses
- Duty cycle = 33%
- Bitrate = 40 Gbps
- $T_0 = 8.3$ ps
- Max ($|E_{in}|$) = $P_0 = 1$W

OSNR parameter is referred to the optical signal to noise ratio, so this means that playing with this parameter the difference between the useful signal and noise level is defined. It will be settled to the value that gives at the output of the Q block a Q-factor of 13 dB concerning (3.9). In this case, following the characteristic curve given in Fig. 3-19, the value is around 18dB.

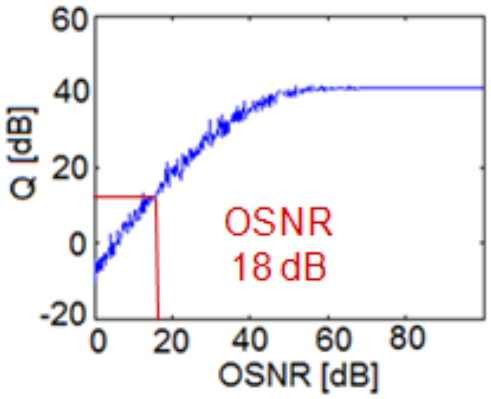

Figure 3-19: Characteristic curve of input Q-factor in function of OSNR.

Observing the shape of the curve, it can be noticed the constant horizontal trend when the OSNR goes over 40 dB. This range can be considered as if there was no noise. The point is shown in which the Q-factor is about 13 dB and it corresponds to an OSNR of 18 dB.

B_0 and **λ_F** make reference to the bandwidth and the central wavelength of the pre-filter respectively. Note that central wavelength λ_0 is set up at the same as the laser, 1550nm. On the other hand the bandwidth is adequately chosen to cancel the noise out of the useful bandwidth but at the same time not to degrade excessively the signal, so there is a compromise choosing the optimum value. A good selection in this case is four times the bitrate, thus 160 GHz.
D alludes to the delay applied to one arm related to the other, as we are interested in adding signals with a delay of one bit in order to convert the phase data to amplitude, hence D=T where T is the bit period, 25 ps.
L, **γ** refer to the fiber parameters length and nonlinear coefficient respectively, they are analyzed together with P_0 as nonlinear phase shift φ_{NL} induced by the kerr medium.
B_0', **λ_F'**, as well as the pre-filter, are the bandwidth and central wavelength. In this case the first one is set up to 1/T where T is the effective bit period (8.3 ps), hence 120GHz; and the second one is examined in order to figure out which value gives the optimum Q-factor at the output.
CW or constant waveform is a constant amplitude and frequency signal that is used as a carrier in which the data is carved in the phase through the pulses coming from the regenerator.

To see what the signal is like in each step before going into the regenerator, next are plotted the power and the phase in blue and green respectively, Fig. 3-20. Note the data is modulated under RZ-Gaussian pulses which go from 0 to π with a certain fluctuation due to the impairment. On the other hand, the power stays constant since no information is carried in the amplitude, though it is affected by the noise as well, so sort of jitter is observed.
Between both graphs there is a reduction of the amplitude of the noise jitter, this is because of the pre-filtering, Fig 3-18(3).

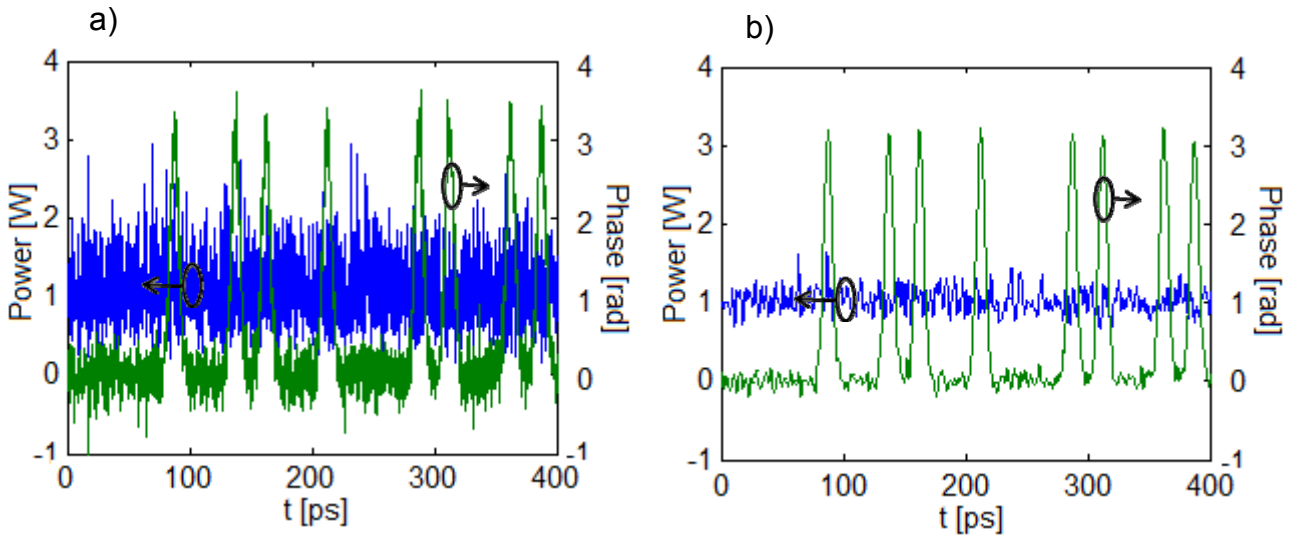

Figure 3-20: Plots of power and phase in time domain (a) before and (b) after noise pre-filtering.

Thereafter, once the signal passed through the delay interferometer shown in Fig. 3-21(a), it can now be observed that the pulses are turned into amplitude. Notice during this process an exclusive-or (xor) operation is performed, so a pulse appears every time there is a change compared to the previous bit. However, this change can be fixed as the function is known, so the undoing processes can be applied. Note the first pulse appearing at the beginning is caused because of the fact that before the initial time (0 ps) the value of the previous adjacent bit is unknown and Matlab considers that there is a change.

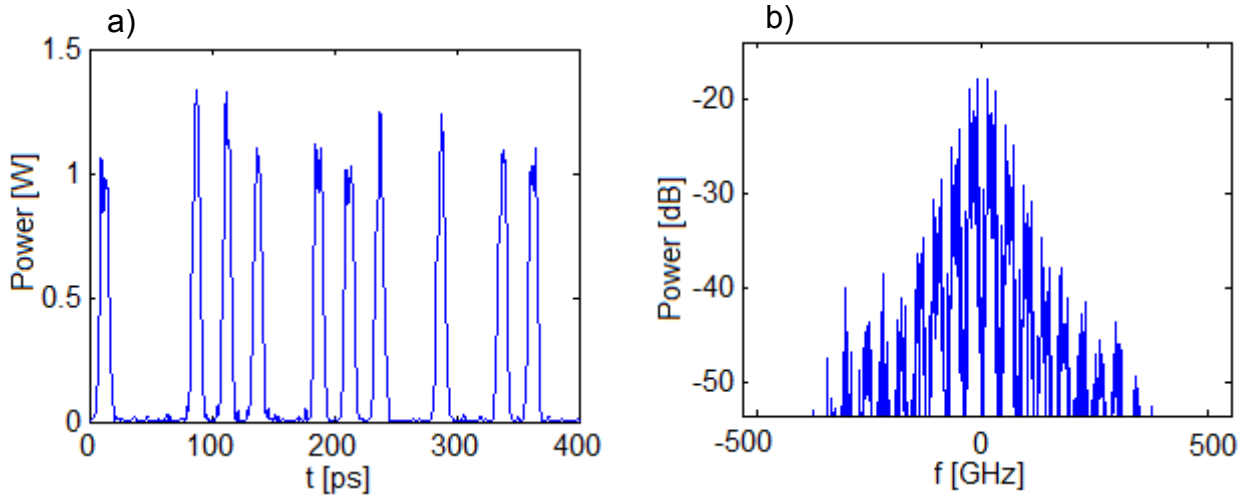

Figure 3-21: **(a) Power graph in function of time. (b) Spectrum of the signal**

Notice that the pulses evidence fluctuations in the peaks, and some jitter in “spaces”, both will be treated by the regenerator as explained above.

In the right graph, Fig. 3-21 (b), it can be seen the spectrum of the signal, it corresponds to an AMI format, which is the destructive arm. At this point the spectrum is not broadened yet, besides the fact that is not totally symmetrical, due to the previously added noise.

Next step is to evaluate the signal after having passed through the fiber, Fig 3-22. It can be noticed that the spectrum has broadened, not only new frequencies are generated but also new peaks appear, which are replicas of the signal; so that by filtering properly one can achieve noise suppression

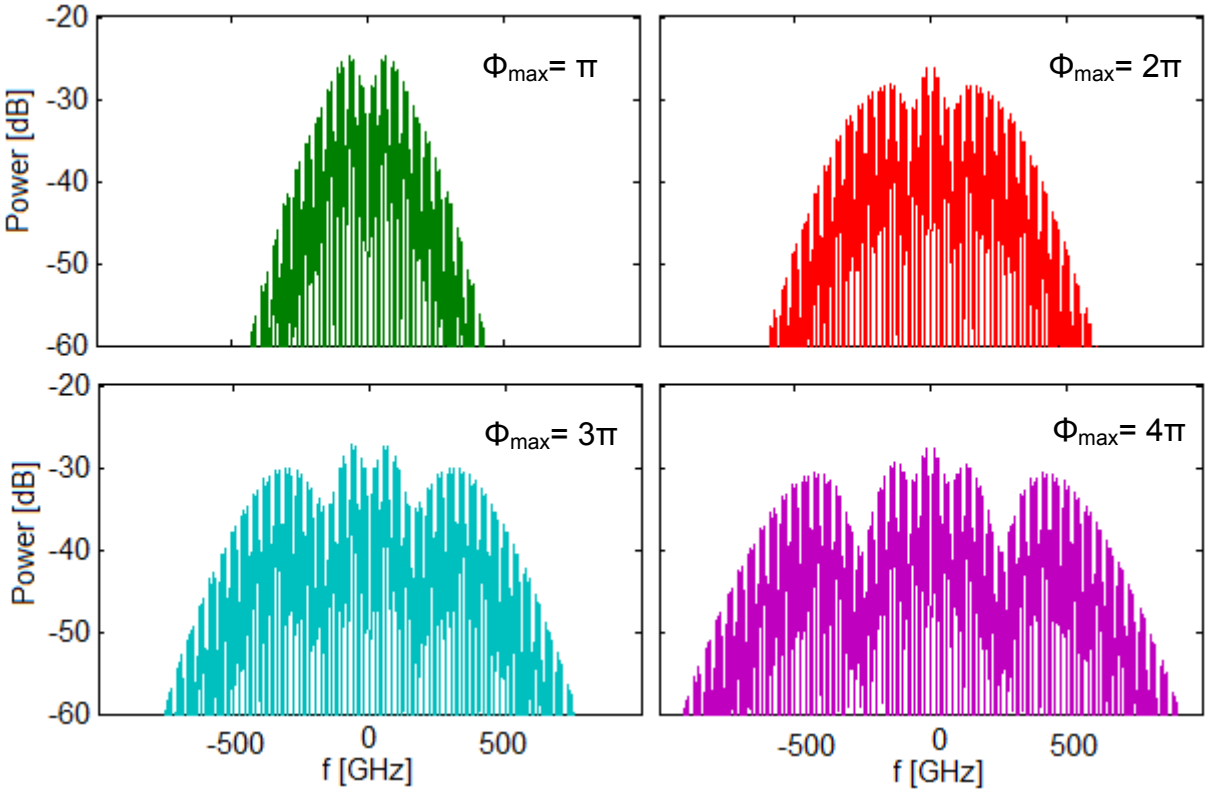

Figure 3-22: Spectrum of the signal after the kerr medium for different values of nonlinear phase shift φ_{MAX}.

We will examine the case in which 4π is taken as a phase shift value, and check out the changes affecting the signal after being filtered. In Fig 3-23 are shown three different values for the offset. The blue one which corresponds to 450 GHz is the one that gives a better response, since the range of frequencies that are inside the bandwidth of the filter are almost the same frequency components than the original signal. Therefore, the pulses are suitably reshaped while important noise suppression is achieved, Fig. 3-24. Moreover, the power peak level of "marks" is less variable. This means that the quality of the signal in terms of Q-factor will be strongly improved, giving higher values.

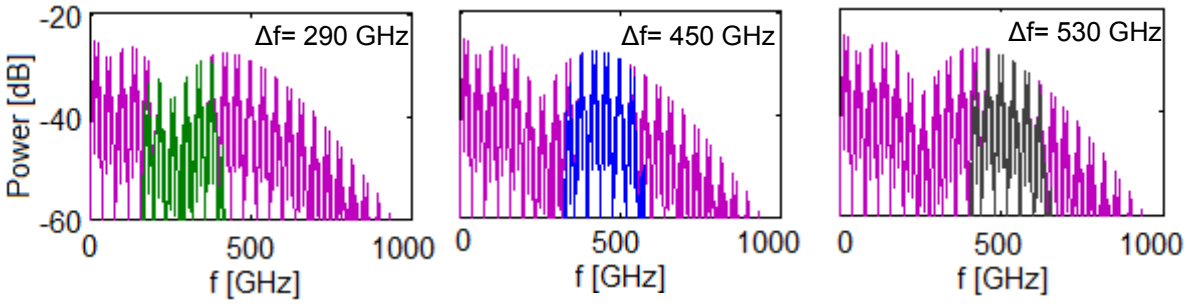

Figure 3-23: Spectrum filtering; in purple the broaden signal due to φ_{NL}, in green, blue, and grey the BW filtered respectively.

So, taking the offsets represented in Fig. 3-23, which are 290, 450, and 530 GHz, the time-domain response is depicted in the following picture, Fig. 3-24. A range of 300 ps is used, as it is enough to observe the difference between the shape of pulses before the signal goes through the fiber, Fig. 3-21(a), and after the post-filtering step.

Now, focusing on the three plots in Fig. 3-24, one can note that both (a) and (c) not only the pulses are incorrectly reshaped, but also the general output power reaches a lower level. This makes sense since the taken frequency components are not the same as the ones at the input, as well as the level of these components is lower. Thus, considering the blue one, in which the only negative point is the loss of power level, the amplitude regeneration is proved

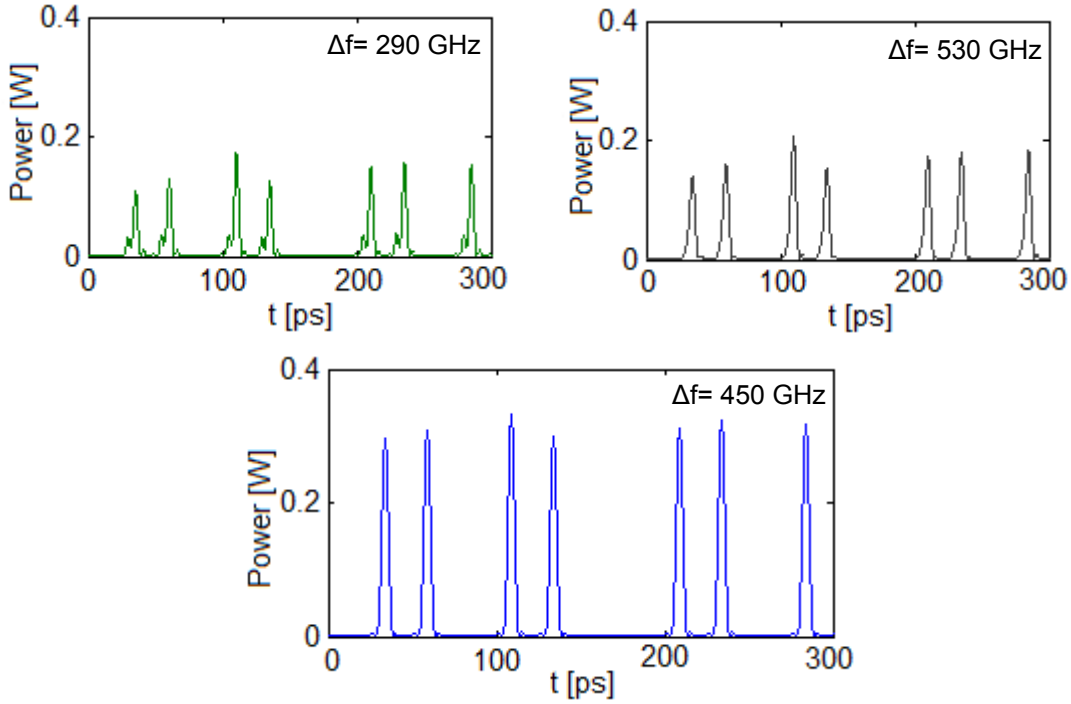

Figure 3-24: Power plots for three different offset filtering.

Once we have seen the amplitude jitter suppression, we will concentrate on measuring the whole regeneration achievable at the output of the scheme. Indeed, this means to evaluate the signal after the phase modulator, where the phase experiments a modulation coming from the pulses. With this in view, now we have again the information on the phase, so that the power of the signal keeps constant while the phase is carved with Gaussian pulses.

To analyze the quality of the signal as made before, the Q-factor is taken into account since it gives us a good and objective judgment of the signal improvement. However, mean amplitude values and its standard deviation are needed, so before measuring them it is required to demodulate the DPSK signal.

Not losing sight of this, Q-factor in function of phase shift φ_{NL} is measured at the output of the regenerator, where the second arrow is placed in Fig. 3-18. Do not forget that it is forced to have an input Q-factor about 13 dB, as made with the former scheme, in order to decide which system gives us a better performance in terms of signal improvement. In addition, in order to have a more exhaustive and complete analysis several offset values are taken; with this an optimum behavior point can be denoted.

Therefore, in the next graph, Fig. 3-25, several curves are depicted showing the trace of the Q-factor (dB), besides a black line indicates the level of the input Q-factor (13 dB) in order to appreciate where an improving related to input is achieved. Observing them some conclusions can be drawn.

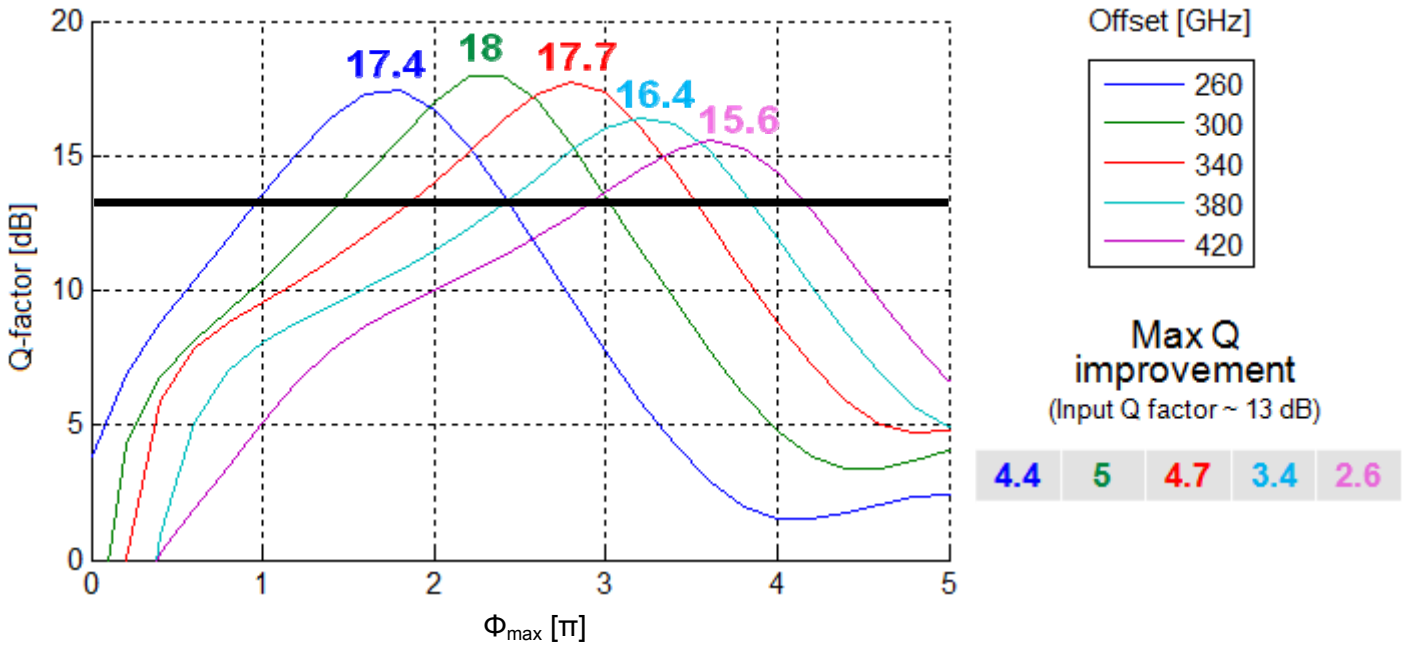

Figure 3-25: Q-factor plot in function of the induced phase shift. Several offsets are considered and depictured in different color.

Taking different offsets to evaluate and characterize the response a maximum for each one is observed, which defines the phase to be taken, in other words the fiber parameters (L, γ). Note that the optimum, or what is the same, the maximum Q-factor gain, is achieved around 300GHz of offset, since there is a gain about 5 dB respect from the input.

On one hand note that from 300 GHz onwards, the larger the offset is, the lower the Q-factor maximums. This is caused mainly by two facts.
Firstly, because a lower power level is inside the offset bandwidth if a higher phase-shift value is chosen, perceivable in Fig. 3-13 where different spectral broadenings are superposed. And secondly, because of the effect of the kerr medium itself, since a higher phase shift implies a larger distortion to the signal, so that a worse quality at the output will be achievable.

On the other hand from 300 GHz down, the smaller the offset is the lower the Q-factor maximums; in this case it is originated by the fact that if an offset closer to 0 is settled some noise, in terms of spectrum, starts to fall inside the filter bandwidth. Therefore, the signal is impaired, so its quality is degraded.
Higher offsets provokes the characteristic curve to be shifted to the right, as a bigger broadening is required, and this is accomplishable by increasing the phase shift, which means increasing either the length or the nonlinear coefficient.

In order to characterize how the signal quality is affected if phase amplitude depth is taken into account, two cases are studied. By phase depth it is understood the loss of amplitude difference between zeros and ones because of zero level increasing. First, in Fig. 3-26(a) is assumed 70%, this means that the mean input power of zeros is increased by a factor of 0.3 compared to the ideal case, while the noise impairment is kept equally. And second in Fig. 3-26 (b) is assumed 60%. Hence, in each case there is a lower input Q-factor, worse as closer to 0.

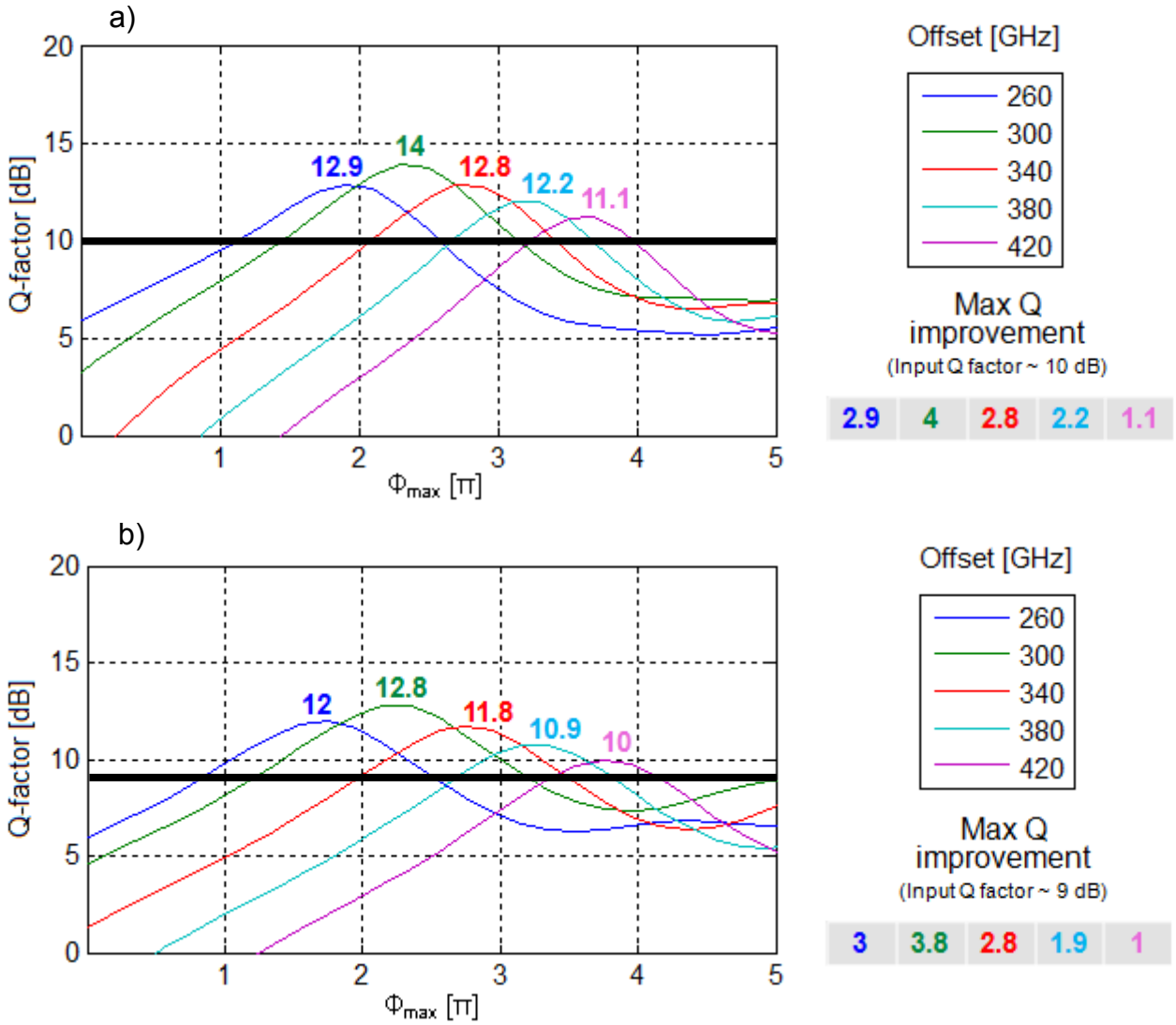

Figure 3-26: Q-factor characteristic curve in function of induced phase shift for (a) an pahse amplitude depth of 0.7, and (b) 0.6.

According to results seen in the figure above, we come to some conclusions. It is observed that the higher the pahse amplitude depth is (closer to 0), the less Q-factor gain is achieved. This is logical provided that there is lower depth power level in the pulses while the noise is not reduced, so that smaller input Q-factor; this is turned into bigger fluctuations relative to signal level in both spaces and marks, which makes more difficult to reach the same gain performance. Once having a general analysis of the whole system, and this implies knowing how the scheme responds either in front of the phase shift or the offset filtering, a novel scheme using the same principles is presented.

3.3 SPM-filtering-loop based DPSK signal regeneration

Up to now we have been analyzing and evaluating the properties of various schemes which base part of its regeneration performance on kerr medium effect, as the study of likely regeneration systems depending on nonlinearities is the main aim of this thesis.
Assuming this, a new proposal is presented partially based on concepts from both former scenarios. First of all the idea of using a loop from the first scheme is going to be taken, and then the regeneration principle from the other one.

This proposal aims at taking advantage of the fact that the half of the signal is wasted, indeed after the delay interferometer one of both arms is no longer used, which means that 3 dB are being misused, Fig.3-27.

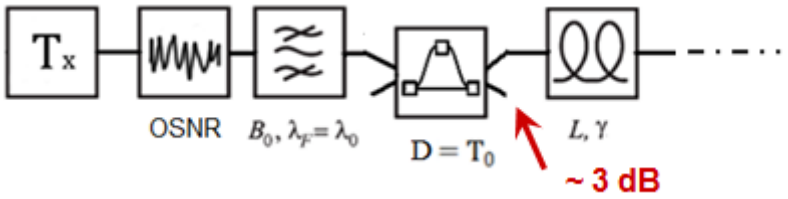

Figure 3-27: Loss of power due to the no use of one arm.

Taking this into account, next it is presented the first proposal using a loop as a main innovation. Note that this first design will not be the definitive one, since several problems will appear and some modifications will have to be performed to solve them.

3.3.1 Scheme setup performance

The new design proposed has some parts that are similar to the previous schemes; all these ones are not deeply explained again, but slightly enumerated and commented. In Fig.3-28, the complete setup is depicted, moreover blue and green arrows are added in order to visualize the two different ways the signals take while going throw the regenerator.

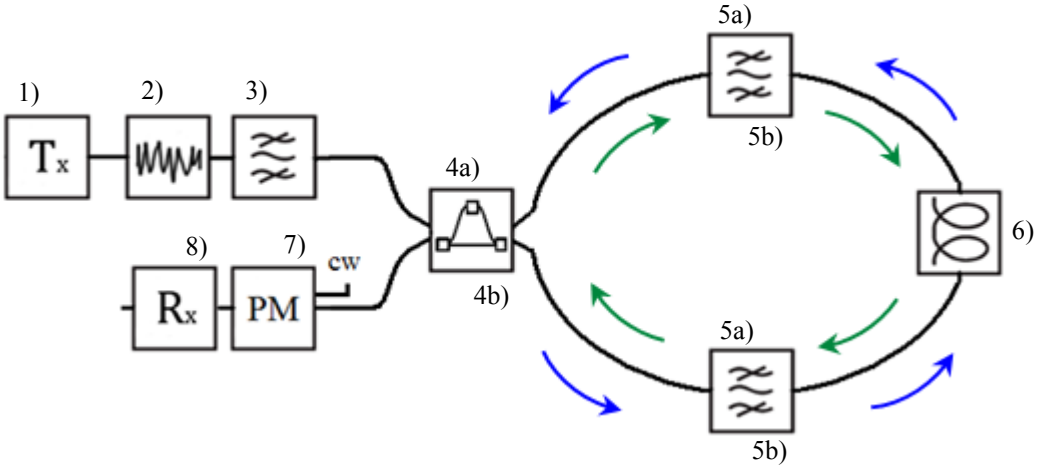

Figure 3-28: Regenerator setup. Block diagram of all its components

- 1, 2, 3. After a white noise channel and filtering, the signal gets into the regenerator.
- 4a. DI turns the phase data to amplitude.
  - Upper arm: Gaussian pulses (AMI).
  - Lower arm: inverted Gaussian pulses (Duobinary).
- 5a. Filters let pass the signal, since a band-pass centered on f_o is used.
- 6. HNLF broads the spectrum due to SPM.
- 5b. Offset optical filters ($f_o+\Delta f$) select the suitable bandwidth.
- 4b. DI recombine both amplitude signals.
- 7. Amplitude is modulated into phase once regenerated
- 8. Receiver demodulates the signal.

In this case we will focus on describing the new features with respect to the former scheme, so it is assumed an impaired NRZ-DPSK as input signal, keeping all the same specifications, see Fig. 3-18 and beyond.
Now both arms are used which means that apart from having an AMI format in the destructive port (3.11), in the upper arm; in other words looking at Fig.3-28 the green path, we have a duobiany signal in the other way. Thus, the signal properties are going to be analyzed after each block changing, and then compared to the other one.

As seen in Fig.3-11, the duobinary signal presents inverted Gaussian pulses, so this means that the spectrum will differ over the AMI one. In the following picture, Fig.3-29, this can be appreciated.

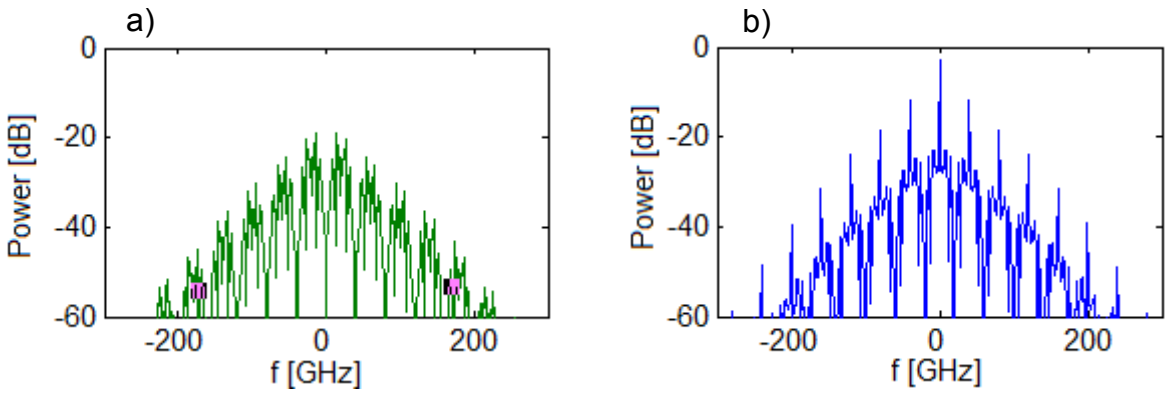

Figure 3-29: Spectrum plots after first passing through the DI. (a) upper arm (AMI, green way), and (b) duobinary (lower arm, blue way).

Note that there is a higher power peak in the duobinary signal; this can be explained by looking at the time domain plot, since most of the time the power remains as a constant around the high level. Hence, frequency components closer to 0 (responsible for constant behavior in time domain) take place with a higher level than AMI spectrum.

Next step the signals "face" with are the filters, unlike the filter seen in the previous scheme now we need a different transfer function. This first time the signal need to remain unchanged, so that unfiltered, but the second time after being broadened a frequency shifting

will be required. Thus, the transfer function now has two different pass bands, in Fig. 3-30 it is clearly depicted and subsequently indicated with two grey rectangles.

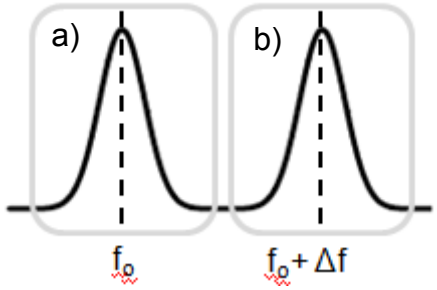

where $\mathbf{f_o}$ is the carrier frequency, in other words the laser central frequency/wavelength and **Δf** is the offset shifting. This last is a variable parameter, which is adapted according to each simulation.

Figure 3-30: Filter transfer function. (a) Spectral band to let the unbroadened signal pass. (b) Spectral band to filter the suitable broadened pass.

As the spectrum has a different power level, after the signal (duobinary) going through the fiber, it experiments a diverse broadening, in terms of power. To examine and evaluate the properties, the same maximum phase shift φ_{max} is chosen (4π). Then different offsets are selected in order to see what happen if it is not taken the correct shifting, Fig 3-31.

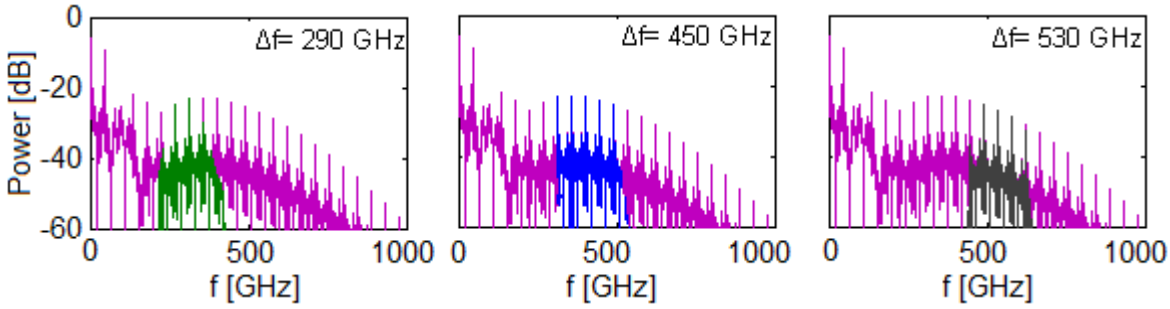

Figure 3-31: Spectrum filtering; in purple the broaden signal due to φ_{NL}, in green, blue, and grey the BW filtered.

Once the signal is been filtered, it loses the previous signal format; note that before the filter we have a duobinary signal, and its power amplitude presents inverted Gaussian pulses Fig. 11(b). However, the effect of filtering causes the inverted pulses turn into normal Gaussian pulses. This is an event that will allow us to recombine the signal from one arm (blue way) with the signal of the other one (green way) in the delay interferometer once having done the complete loop.

Therefore, observing the corresponding amplitude plots in time-domain for each different offset in Fig. 32, and as well as happening in the case of AMI signal, the best pulse reshaping is achieved when the bandwidth of the filter covers the range around a peak. Not only a better reshaping is accomplished but also a higher power level reached, since higher spectral components are inside the range filtered.

So now we have two amplitude-regenerated signals that are going to be recombined in the delay interferometer, with the aim of having the same shape at the output of it. We need to have a similar signal in both input arms, this means that the signals cannot be much delayed between each other, and the power level needs to be similar.

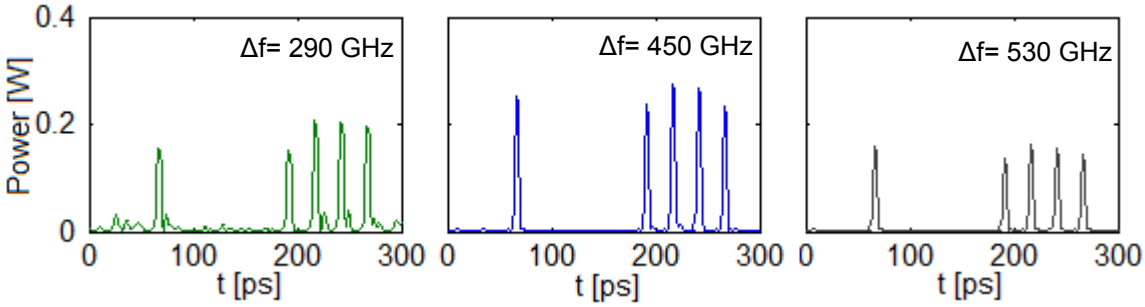

Figure 3-32: Power plots corresponding to the cases depictured in Fig. 31.

According to the plots obtained from both signals, Fig. 3-24 and Fig. 3-32, and taking the case of 450GHz, a difference between the power levels is observed, due to the distinct broadening already commented. In order to see this clearly, in Fig. 3-33 both signals are superposed; apart from observing this differing in amplitude a delay is noticeable as well. Note that both phenomena are indicated in the graph, as well as named with two parameters; **K** which is the variation of power amplitude level, and **D** the delay between both signals.

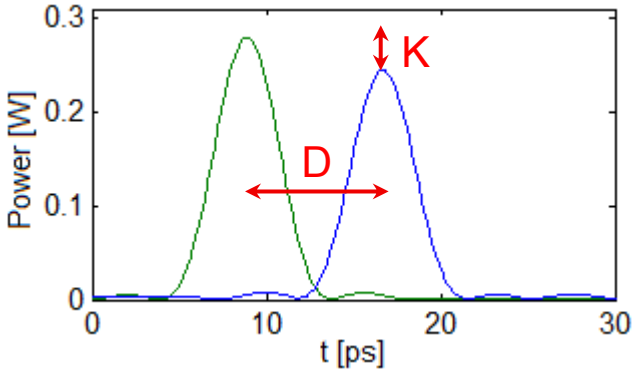

Figure 3-33: Pulse snapshot for clockwise (green) and counterclockwise (blue) signals. Amplitude difference and time delay are marked and labeled.

Notice that the delay observed between both signals is because of filters, specifically it comes from the fact that the filters interact when there is a change in the power, and in particular the pulses start to grow when there is a change from no power to power. Hence, if we have a look in the illustration below, Fig. 3-34, it is shown graphically where this delay is coming from.

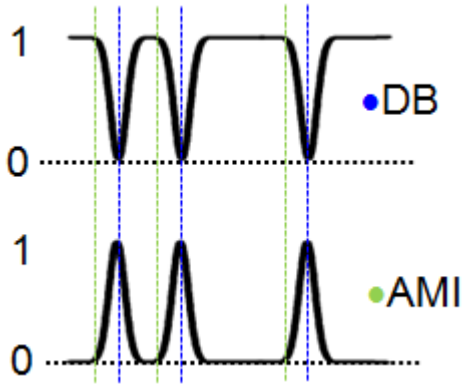

Power graph for an AMI and duobinary format signals, in which the green dotted line denote the instant when the pulses will start to grow in the case of the new filtered signal coming from the AMI. Whereas the blue one is the same but applied to the other way signal DB. The gap between each pair of lines is delay between both signals.

Figure 3-34: Induced delay between signals due to the effect of filtering

In order to solve these two issues, the difference in amplitude and the delay, it is introduced an attenuator, and a delay to counteract these effects. Nonetheless, these new components only have to apply to one signal, so that we need to add two circulators to make the signal go into different ways, depending on which one it is, Fig. 3-35. It is considered 1 dB of loss in each circulator, and both the attenuator and fiber (delay) are considered ideal, with no secondary effects.

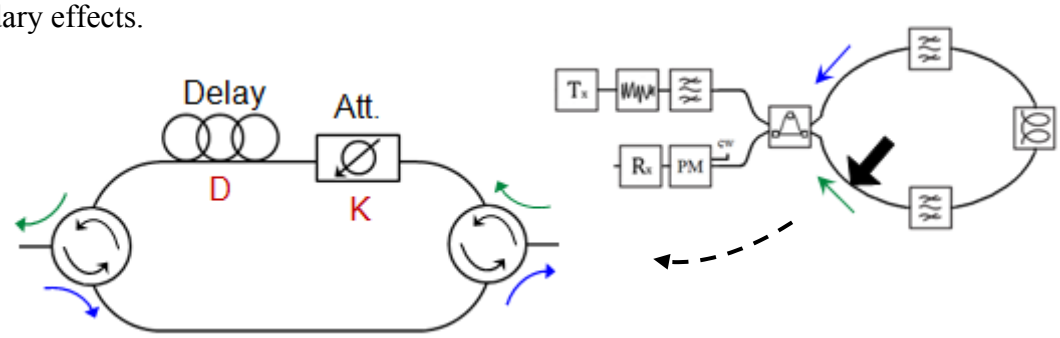

Figure 3-35: Scheme modification to adjust the amplitude and time between both way signals.

Once the two signals are balanced, the next step is to recombine them in order to take advantage of the amplitude regeneration accomplished in both arms. Note that we have two similar signals, which have the information in the amplitude, in other words power-amplitude pulses Thus it is a different scenario compared to the NRZ-DPSK. Now before the delay interferometer a phase shift of π is required in one of both signals in order to avoid having a multilevel amplitude signal at the output port.

After the delay interferometer the signal passes through the phase modulation. Remember that here it is achieved the amplitude-phase regeneration; so at the output of this block we have a regenerated NRZ-DPSK.
Next, as made with the others schemes, the Q-factor parameter is evaluated in order to check out the benefits, as well as to carry out the comparison performance. Note that to calculate this parameter we need to measure the mean of "marks" and "spaces" as well as their standard deviations. Therefore, a DPSK receiver is used to demodulate the signal into amplitude format in the same way as all the others setups; this process is explained more in detail in Appendix A.

Taking as variables the maximum phase shift φ_{max} and the offset, it is depicted the Q-factor in Fig. 3-36. By looking at the characteristic curves, it is denoted a certain different behavior related to the previous scheme, Fig. 3-25. Although the general trend remains similar, which means that the optimum point is achieved with the same phase shift and offset, a flattened shape on the peaks of each curve is observed. In addition, note that in general higher Q-factor values are accomplished, giving a better regenerative performance. Not only this feature is relevant but also the fact that for lower values of phase shift using the same offset, higher Q values are reached. In other words better noise suppression, better performance.

In short, the main improvements in this new setup which uses a loop are remarked in Fig.3-36, and can be summarized in two points:

- Lower phase values can be used to obtain the same or better Q-factor improvement keeping the same values of the components (blue circle in Fig.3-36)
- A higher, wider, and flatter maximum behavior is achieved (red circle in Fig. 36)

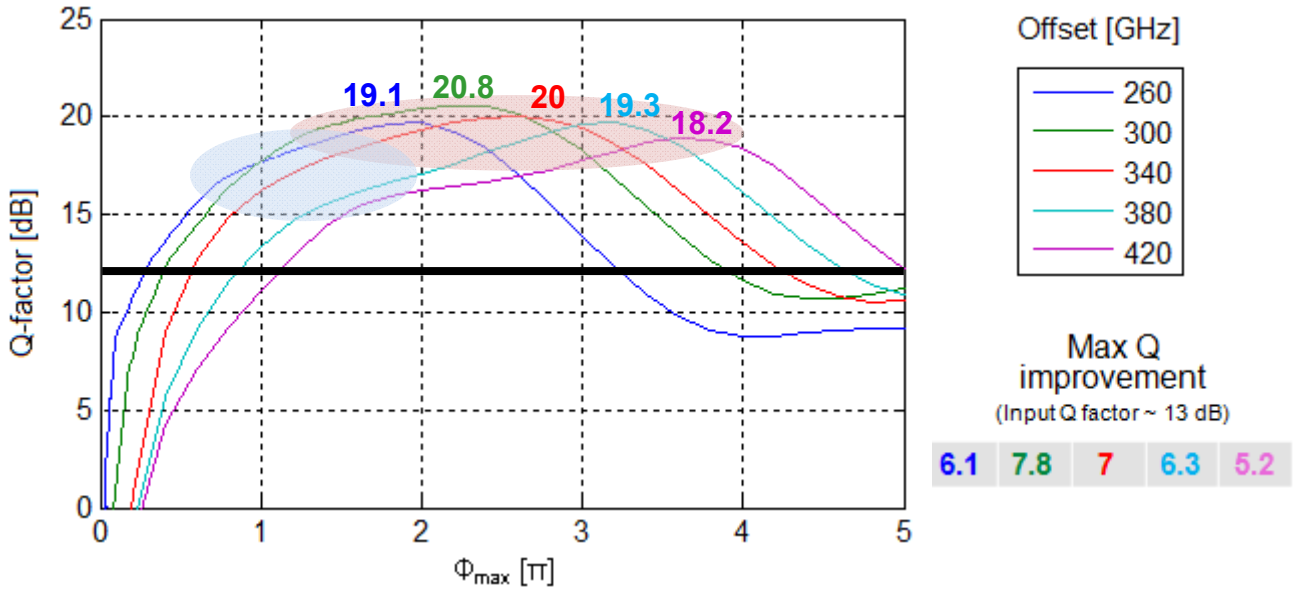

Figure 3-36: Q-factor plot in function of the induced phase shift for different filter offsets.

The main advantage of first point (blue area) is that being able to go to lower phase shift values while keeping the same conditions and the quality not being reduced, implies that minor values either for fiber length **L** or nonlinear coefficient **γ** or input power $\mathbf{P_o}$.

Second point indicates the importance of higher Q-factor gain in function of input, this can be seen as a general rising, and it is mainly caused by the fact that both ways are simultaneously regenerated which directly implies using two signals, so double power compared to the previous case.
Note also that a more relaxing behavior is accomplished, implying that all the characteristic curves for each offset are over 13 dB (input Q-factor) for a wider range of phase shift values, which means that regeneration would be achieved. This feature can provide great advantages to our scheme; take the case in which is more convenient to use a specific value of offset filtering, so in this situation one has a more loose margin for choosing the most suitable parameters, and this also has to be considered as a positive attainment.

Comparing the maximum reached Q-factor values between the former scheme and this one, (max Q improvement tables), it is observed a difference around 3 dB in favor of the new one, this shows an enhancing that makes the second setup more suitable, in terms of maximum all-optical signal regeneration achievement.

In order to check how the phase amplitude depth affects to our scheme, it is performed the same two cases as before, 0.7 and 0.6, Fig 3-37. So that, the input Q-factor is the same as the former setup 10 and 9 dB respectively, and it is indicated in both plots with a black line to make it visually clearer.

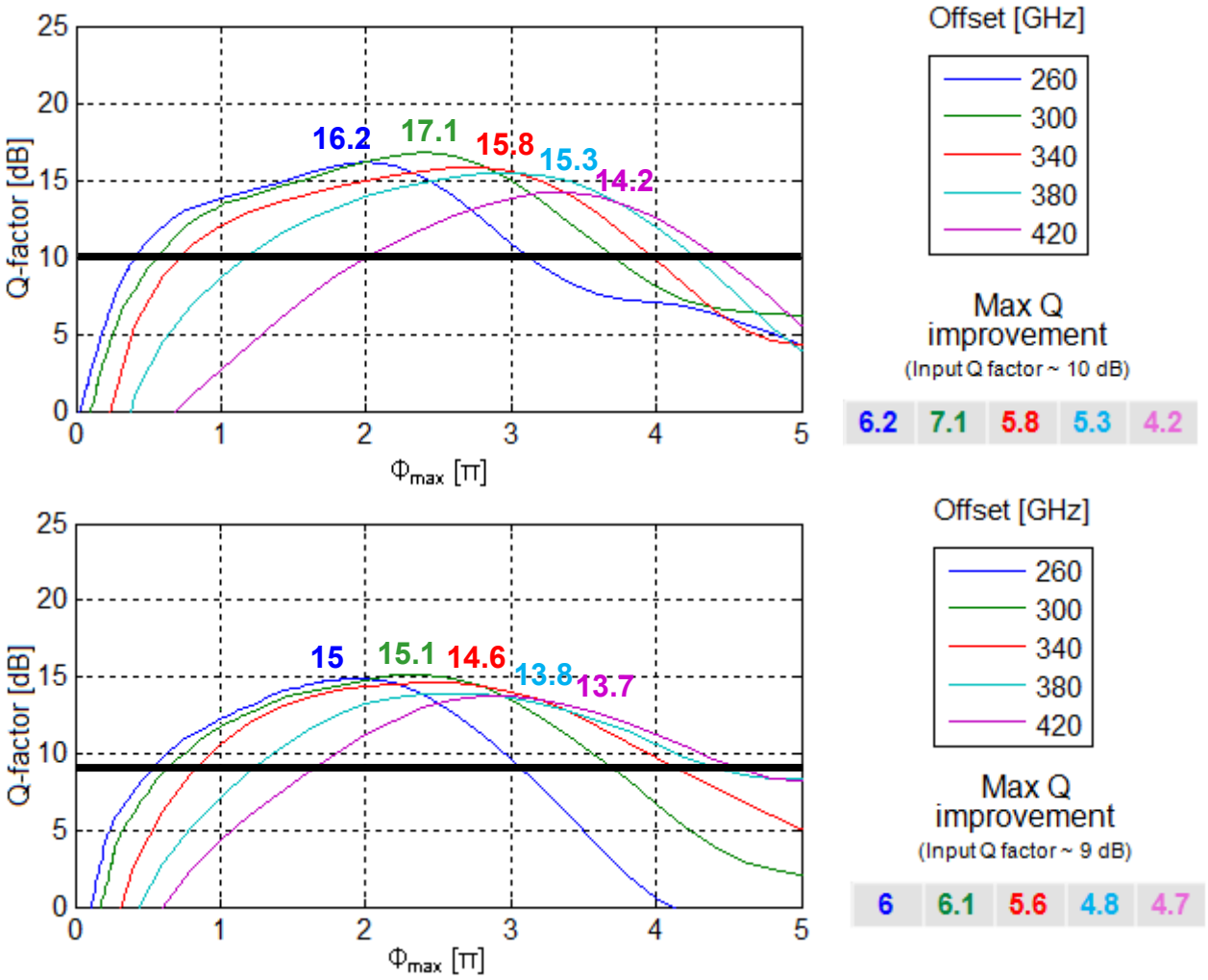

Figure 3-37: Q-factor characteristic curve in function of induced phase shift for (a) an pahse amplitude depth of 0.7, and (b) 0.6.

Similar to the previous scheme the lower the input Q-factor, so that closer the phase depth to 0, the smaller the gain is. The reason of this is that if the noise standard deviation is larger related to the depth level, which is the same than keeping the noise level and reducing the power depth level. Thus it is more difficult to compensate and suppress the jitter, especially in "marks". And this is reflected directly to the Q-factor.

Although there is a decrease on the capacity of regeneration if the phase amplitude depth is considered, the general average level of Q-factor curves is kept over the value of the former scheme. The general conclusion one comes to, it is that a decreasing trend is performed as bigger phase amplitude depth is, but on the other hand it follows the same pattern as the case without using the loop. Hence, it can be considered that a similar behavior is experimented by both schemes in front of the phase amplitude depth, slightly better for the new proposal though.

In order to check if there is any modification that could improve the regeneration performance, it is shown how the response changes when a different offset is applied in each filter. To analyze it, it is taken the same input signal specifications; this means a NRZ-DPSK signal with the same parameters used so far (see end of page 44).
The maximum phase shift φ_{max} is kept equal, 4π; whereas the central frequency of one of the filters is shifted related to the other one, see Fig. 3-38.

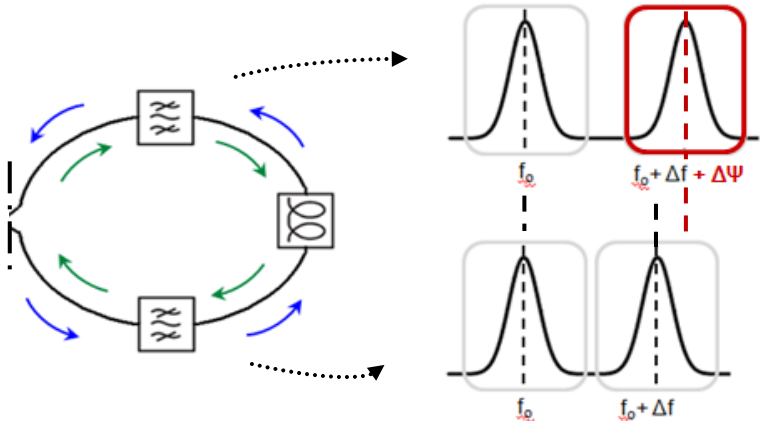

Figure 3-38: Filter shifting modification. ΔΨ is the difference between the offset central frequencies.

To examine if this variation is able to improve the general performance, both signals are examined just after being filtered. With this, we will see what effect is developed by checking out the shape of the pulses, the delay between them, and the power level. Therefore, in Fig. 3-39 it is depicted the same bit for both signals, the green one is referring to the clockwise signal which remains unchanged since the filter readjustment does not affect it, and the blue one is the counterclockwise signal for different ΔΨ.
As one can observe the bigger the shifted (ΔΨ) is, the lower the observed power at the output. The reason comes from the fact that moving the center frequency of the filter causes spectral components inside the bandwidth not to be the optimum ones.

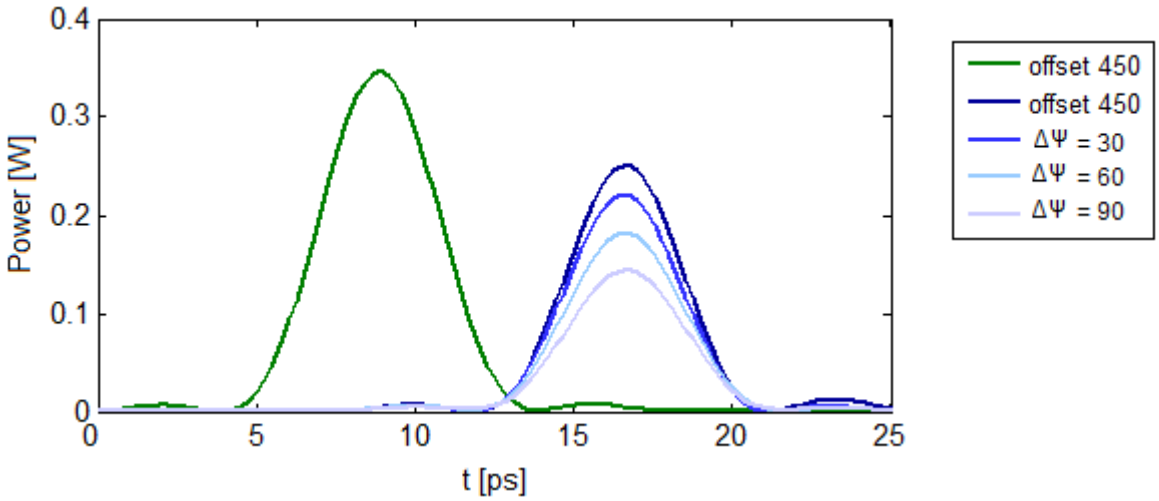

Figure 3-39: Pulse snapshot for clockwise (green) and counterclockwise (blue) signals. Different ΔΨ are applied and depictured as well.

Note

that the delay is kept equal; this is because the signals just before the filters, or in other words the pulses, are still the same. Thus the power change from 0s to 1s (Fig.3-34) remains unchanged. It is proved that the best performance is fulfilled when both filters have the same central frequency, since the highest power level is achieved. Hence a worse Q-factor would be reached if a difference between both filters existed.

3.3.1.1 RZ-DPSK. Push-pull mode.

In the chapter we shall explore if the proposed regeneration scheme can also work for the RZ-DPSK format. There are basically two techniques to perform this type of signal; using a stright phase modulator, and using a MZI modulator in push-pull mode, see section 2.1.2.1; we will focus on the latter; a process of RZ-DPSK generation using a MZI is visually summarized on the next Fig. 3-40.

To be consistent with all the results of the former schemes that have been analyzed, the same specifications will be considered as input signal, but for the fact that now we have a RZ format, which means that the optical power is not kept constant.

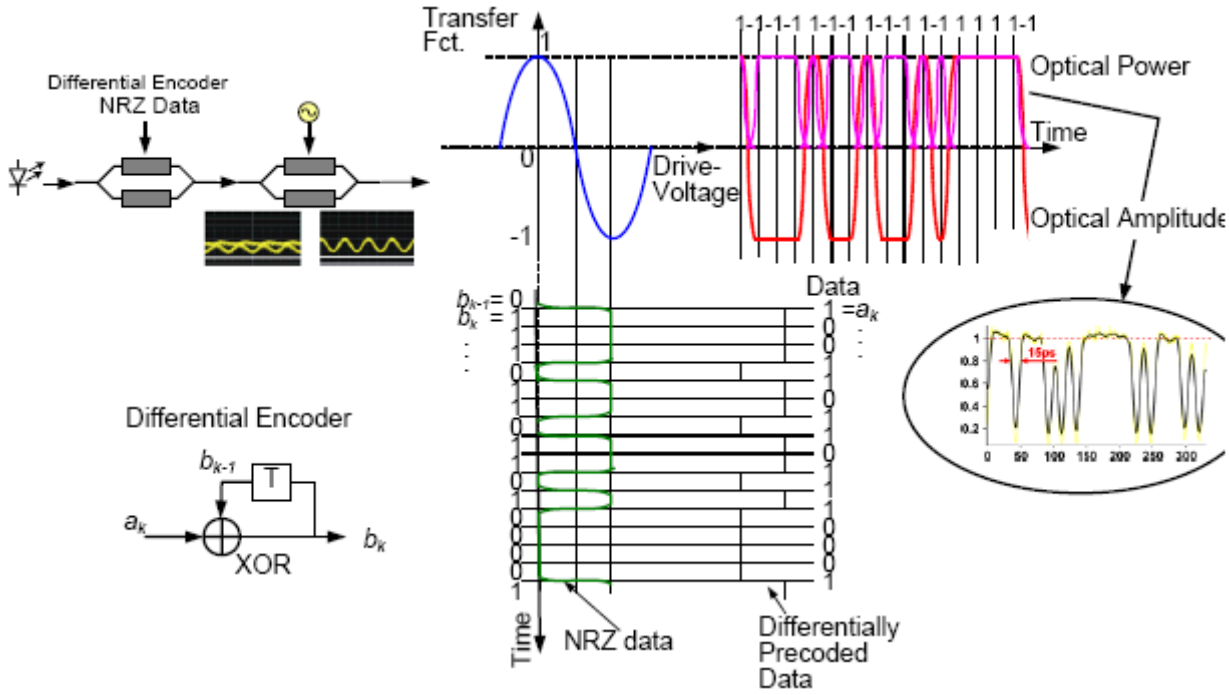

Figure 3-40: RZ-DPSK performance using a Mach-Zehnder Interferomter modulator for data encoding

Now the input signal is carved by a continuous and periodic signal, thus the resulting input signal is depicted in Fig. 3-41, in which power and phase characteristic curves are plotted before the signal being impaired.

Next, when the signal goes through the DI, suffers a different behavior in both output arms, besides compared to the previous scheme now the constructive port performs in a different

way. Indeed, this is caused by the fact that in the former case the optical power was kept constant on top when there was absence of change, in other words “spaces”; whereas in this case this does not happen as the power follows a carved-pulse pattern.

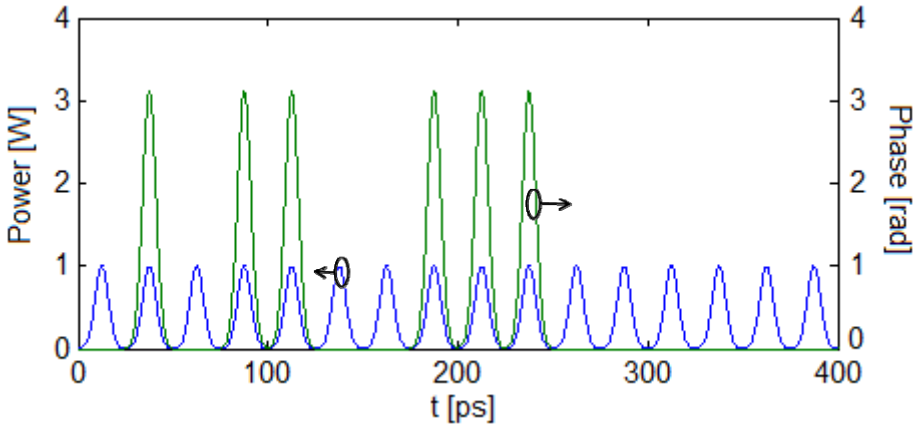

Figure 3-41: Power and phase for a RZ-DPSK signal

Because of this, now the inverted pulses obtained before, Fig 3-42 (a), in terms of optical power, are no longer observable. Instead a different pattern of pulses it appears, depicted in Fig. 3-42 (b); in these two graphs noise is not considered in order to clearly appreciate the shape of the pulses. In both sides the units for each plot is indicated.

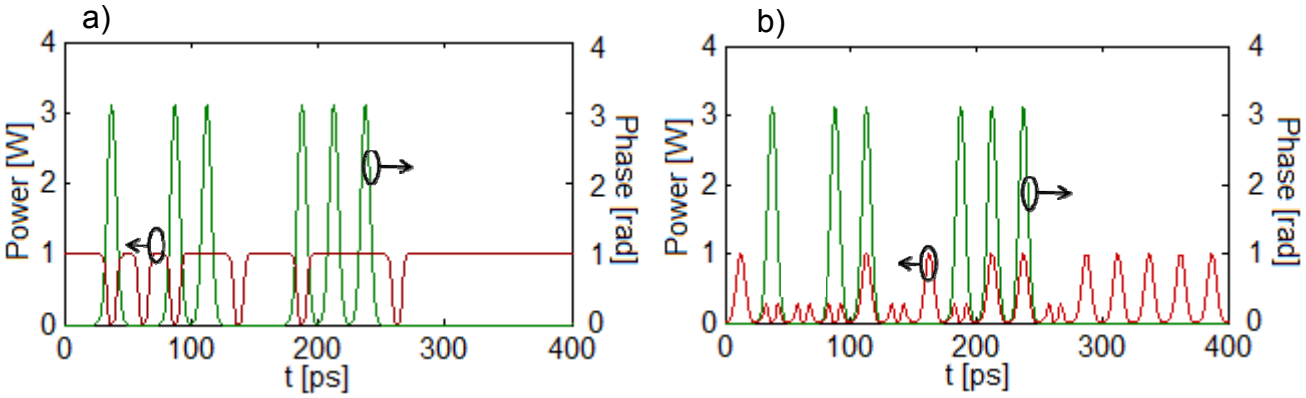

Figure 3-42: In green the phase of the signal before being demodulated to amplitude by the DI, and in red the constructive-arm signal power once gone through the DI. Using (a) NRZ-DPSK and (b) RZ-DPSK formats.

Note that now the pattern is different, where before there was a constant now there are pulses, owing to RZ amplitude input pulses. However the destructive port is kept equal either if it is a NRZ or ZR. Next stage is to examine how the signal is after being filtered, whether the pattern is the same as the other arm, in order to recombine both signals in the DI again. It is assumed the case of having a maximum phase shift φ_{max} of 4π and an offset filtering of 450 GHz, the same values used in previous cases. In Fig.3-43, the amplitude plots are represented for both arms after the signal has been filtered. This means just before the delay interferometer. Notice that the graphs are not the same. There are two important factors that produce this mismatching.

- Different pulse sequence in time, in other words distinct bitwords.
- Multilevel pulses, power amplitude is not kept equal for all the pulses.

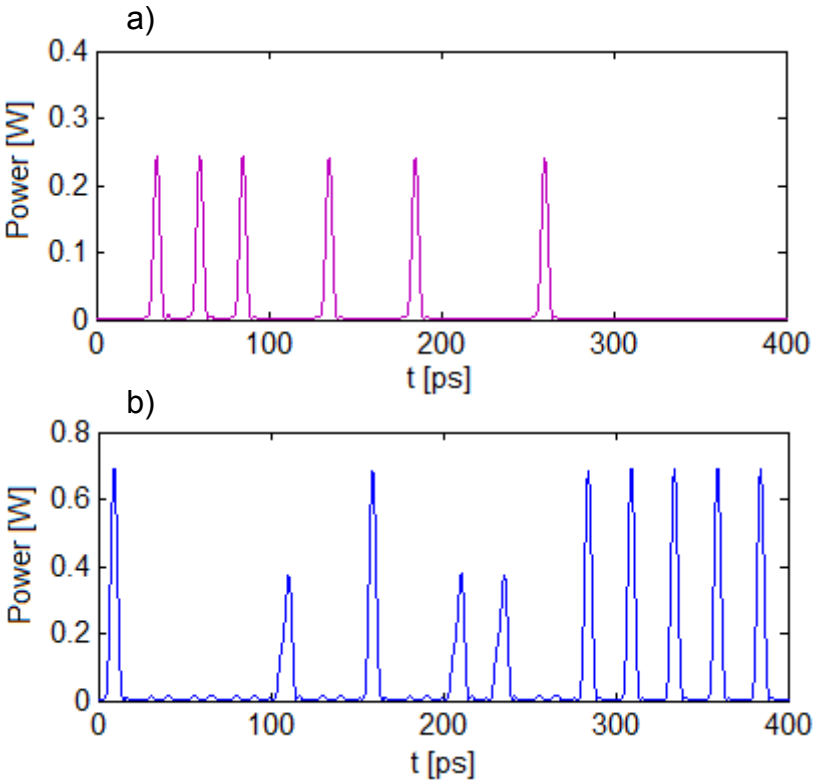

Figure 3-43: Power plots of (a) clockwise and (b) counterclockwise signals after being filtered.

Due to these differences it is not possible to use both signals and recombine them through the DI to achieve proper signal regeneration. If we do so, the signal at the output port is nothing like the input one. In other words, even though some jitter could be suppressed, it would be impossible to recover the same shape and sequence.
However, it does not mean that RZ-DPSK is not compatible with the Mamyshev principle of regeneration, since the destructive (AMI) keeps the same response than the case in which a NRZ-DPSK is used. Therefore, the existing scheme using only one of both arms is able to regenerate NRZ as well as RZ.

In short, we can affirm that this new scheme gives a satisfactory performance dealing with NRZ-DPSK signals; indeed, it has shown an improvement in the quality factor parameter (Q), so that a better regeneration capability compared to the formers setups.
But on the other hand it is not suitable to regenerate return to zero DPSK signals, because of the existing differences between both arms already commented above.

4 Summary

Nowadays communications are essential in our lives. We live in a society based on the transmission of data, and it has grown significantly with the appearance and development of new technologies. There are countless reasons for sending information, but two fundamental issues immediately come to mind. Firstly, one always hopes that what has been sent reaches its destination, despite the distance involved, and of course not only that but, one expects the receiver to get the message, unadulterated and error-free. On the other hand, when there is a great amount of data to be delivered at the same time, the necessity to use high bitrates arises, hence the use of optical fibers, since higher capacities are available.

The transmission of signals through a fiber is irremediably degraded by several factors coming from either the fiber itself or external causes. Regarding this, DPSK-format signal has shown both promising long-haul records and transfer capacities. So in order to deal with these impairments, different systems and schemes need to be developed to minimize the damaging or even to regenerate the signal by suppressing the noise.

This thesis presents the study of various scenarios aiming to suppress the undesired noise. Since there are many ways to face the problem of noise, we have focused on schemes that take advantage of fiber nonlinearities, specifically self phase modulation produced principally by the Gordon-Mollenauer effect. The analysis of each scheme is made by measuring either the time or frequency domain, and taking the Q-factor as the parameter by which to compare objectively the regenerative capabilities of every scheme. As the DPSK signal is sensitive to both the phase and the amplitude, the followed path in this thesis has been from schemes achieving amplitude regeneration, to setups reaching phase and amplitude jitter suppression, which is directly reflected on the Q-factor parameter.

First, a NOLM-based all-optical regenerator has been examined, which fulfills amplitude jitter reduction by means of nonlinear transfer function, where a flat region appears for a specific input power range. However, this behavior is not observed with phase. Concerning this a modified implementation adding a directional attenuator has been examined; giving maximum values of Q improvement around 3.6 dB. Playing with the pahse amplitude depth, it is observed a good response, as the gain is practically kept equal. Only a loss of 0.3 dB in the gain is experimented when the pahse amplitude depth is 0.6. Despite these positive results, it has been seen that the other analyzed schemes can present a better performance.

Next a new method of noise suppression it has been introduced which shows a better performance in terms of amplitude noise cancelation. It is based on the Mamyshev concept, which basically consists of filtering the broadened signal with an offset respect to the carrier central frequency, in such a way that noise, with low power compared to the signal, is not broadened enough to get into the bandpass filter. Considering this, the second setup examined and already existing in the literature, bases its capabilities on strong amplitude jitter

suppression. That is to say, first the phase information is turned into amplitude. It is at this point is when jitter is reduced. And finally once improved it is modulated back to phase-encoding achieving both phase and amplitude all-optical regeneration. Then the Q-factor graphs has been analyzed for different filtering offsets, in which a maximum Q improvement of 5 dB can appreciated, about 1.5 dB more than the previous one. Nevertheless, when the pahse amplitude depth is introduced a reduction of gain is noted as well; it does not follow the same trend seen in the former scheme, as it is more noticeable, now there is a loss of 1.2 dB between the case in which is considered and the one it is not. In short, similar response to pahse amplitude depth is performed but higher Q-factor values are achieved.

A novel scheme which takes concepts from both former setups has been proposed, it gathers the phase-amplitude principle of regeneration from the second system presented, and the idea of using a loop from the first one. It takes advantage of the fact that now the two output ports of the DI are used. Some modifications have been introduced in order to have a proper regenerated signal at the output port of the DI. Once again, the Q-factor has been measured in function with induced phase shift for various offsets. In this case the maximum gain achieved is around 7.8 dB, almost 3 dB more than the best result so far. Furthermore, the shaping on peaks is performed more relaxed, in other words a good response is held for a wider range of phase shift permitting a looser choice of parameters without losing too much signal quality. Thus, this is also an issue to be considered as an advantage of this new scheme in front of the two other ones. Regarding the pahse amplitude depth, in this case it is slightly more noticeable, since a loss of 1.7 dB is reached for 1.2 dB in the previous one; it is a difference of about half dB which is not significant at all. To sum up we can consider thet this scheme improves the former one not only because the same response, or even a little better, is given in front of the pahse amplitude depth, but also better Q characteristic curves.

Moreover, the response of the setup has been studied when a difference between the central frequency of filters exists. It has been observed that the greater the gap the lower the efficiency achieved. This means that it should be used the same central frequency, but if this is not feasible, should be as closer as possible. Also the bandwidth of both filters plays an important role; it has been considered a bandwidth of about the inverted bit period duration, which covers suitably the spectral components of the original signal.

Concerning all the mentioned results, an NRZ input signal has been used, specifically a NRZ-DPSK. So the last step is changing the input signal format to RZ, and checking out how the performance proceeds. Analyzing the signals once inside the regenerator, we observe that the same method used so far is not applicable, since different bit patterns appear in each direction. This causes the signal at the output to lose its initial bit sequence, in other words, a different bit word referred to the input one would appear.

As a general conclusion, in this thesis the phase and amplitude regeneration of DPSK by means of several scenarios has been studied and analyzed, introducing a new scheme showing significant improvement in terms of noise suppression.

Appendix A: DPSK Demodulation

The followed method to demodulate DPSK signal, in which a balanced receiver is assumed, for all the schemes presented in this thesis is the following one:

Basic DPSK characteristics:

- Bit set {0, 1} -- symbol set {-1, 1} i.e. $\{e^{j\pi}, e^{j0}\}$
- One symbol transfers one bit information
- Bit 0: leave phase alone, bit 1: introduce a pi - phase change

Transmission

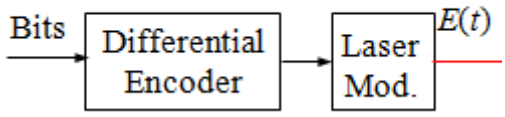

Reception

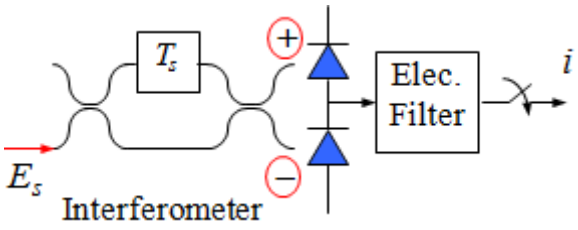

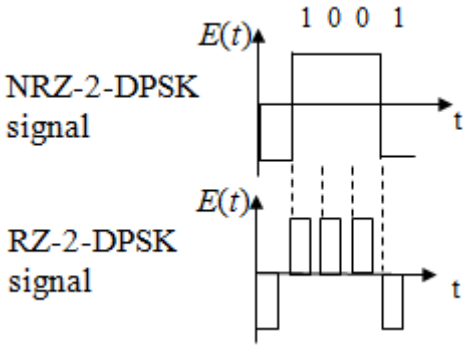

$$i = \left| \frac{E_s(t) + E_s(t - T_s)}{2} \right|^2 - \left| \frac{E_s(t) - E_s(t - T_s)}{2} \right|^2$$

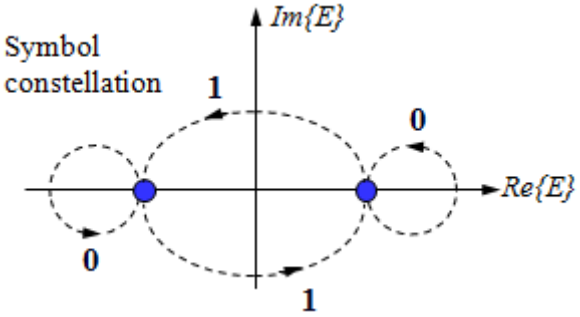

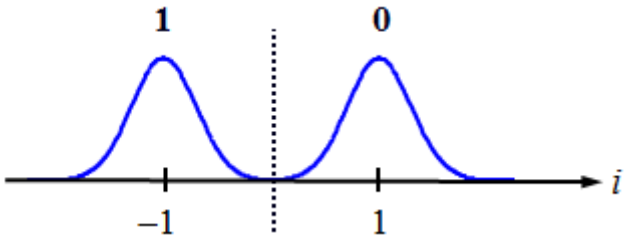

The equation in the box allows us to calculate the Q-factor, since it can be measured the amplitude mean for both “ones” and “zeros”, as well as the standard deviation.

Appendix B: References

[1] Prof. Dr. J. Leuthold, "Optical Communication Systems",Institute of High-Frequency and Quantum Electronics (IHQ), SS 2008

[2] X. Wei, J. Leuthold, Ch. Dorrer, D.M. Gill, and X. Liu,"Chirp Reduction of π/2 Alternate-Phase Pulses by Optical Filtering",Proc. OFC'2005, Anaheim (USA), paper JWA42, March 2005

[3] A.H. Gnauck, and P.J. Winzer, "Optical Phase-Shift-Keyed Transmission", Journal of Lightwave Technol. vol. 23, no. 1, pp.115-130, Jan. 2005

[4] J. H. Sinsky, A. Adamiecki, A. Gnauck, C. Burrus, J. Leuthold, O. Wohlgemuth, "42-7-Gb/s integrated balanced optical front end with record sensitivity", Proc. OFC 2003, Atlanta, GA, 2003, Postdeadline paper PD39

[5] Govind P. Agraval, "Nonlinear Fiber Optics", Second Edition, Academic Press, San Diego California, 1989

[6] José Capmany, F.Javier Fraile, Javier Martí, "Optical Communications Basics", Sintesis. September 2001

[7] Anes Hodzic, "High bitrate optical transmission systems employing a 40 Gb/s channel data rate",University of Berlin, PhD Thesis. 2004

[8] René-Jean Essiambre, Gergory Raybon, Benny Mikkelsen,"Pseudo-Linear, Transmission of High-Speed TDM Signals: 40 and 160 Gbps" Optical Fiber Telecommunications IVB chapter 6 Academic Press 2002

[9] K. Cvecek, G. Onishchukov, K. Sponsel, A. G. Striegler, B. Schmauss, and G. Leuchs "Experimental Investigation of a Modified NOLM for Phase Signal Regeneration", IEEE Photonics technology letters, vol 18, no 17, September 1, 2006

[10] M. Meissner, K. Sponsel, K. Cvecek, A. Benz, S.Weisser, B. Schmauss, "3.9-dB SNR gain by an NOLM-based 2-R regenerator" IEEE Photon. Technol. Lett., vol. 16, no. 9, pp. 2105–2107, Sep.2004

[11] G. P. V. Mamyshev, "All-optical data regeneration based on self-phase modulation effect", Proc. ECOC, 1998, pp. 475–476.

[12] Masayuki Matsumoto, "A Fiber-Based All-Optical 3R Regenerator for DPSK Signals" IEEE Photonics technology letters, vol 19, no 5, March 1, 2007,

[13] B. Dany, P. Brindel, O. Leclerc, and E. Desurvire, "Transoceanic 4x40 Gbit/s system combining dispersion-managed soliton transmission and new 'black-box' in-line optical regeneration", Electron. Lett., vol. 35, pp. 418–419, Mar. 1999.

[14] S. Taccheo and K. Ennser, "Investigation of amplitude noise and timing jitter of spectrum-sliced pulses", IEEE Photon.Technol. Lett., vol. 14, pp. 1100–1102, Aug. 2002.

[15] I. Kang, C. Dorrer, L. Zhang, M. Rasras, L. Buhl, A. Bhardwaj, S. Cabot, M. Dinu, X, "Regenerative all optical wavelength conversion of 40-Gb/s DPSK signals using a semiconductor optical amplifier mach-zehnder interferometer", ECOC 2005, Glasgow, U.K., 2005, Paper Th 4.3.3.

[16] P. Vorreau, A. Marculescu, J.Wang, G. Böttger, B. Sartorius, C. Bornholdt, J. Slovak, M. Schlak, C. Schmidt, S. Tsadka, W. Freude, and J. Leuthold, "Cascadability and regenerative properties of SOA all-optical DPSK wavelength converters", IEEE Photon. Technol. Lett., vol.18, no. 18, pp. 1970–1972, Sep. 15, 2006.

[17] A. G. Striegler, M. Meissner, K. Cvecek, K. Sponsel, G. Leuchs, and B. Schmauss, "NOLM-based RZ-DPSK signal regeneration", IEEE Photon. Technol. Lett., vol. 17, no. 3, pp. 639–641, Mar. 2005.

[18] A. H. Gnauck and P. J. Winzer, "Optical phase-shift-keyed transmission", J. Lightw. Technol., vol. 23, no. 1, pp. 115–130, Jan. 2005

[19] T.-H. Her and G. Raybon, "Optimization of pulse regeneration at 40 Gb/s based on spectral filtering of self-phase modulation in fiber", IEEE Photon Technol. Lett., vol. 16, no. 1, pp. 200–202, Jan. 2004

[20] R. H. Stolen and C. Lin, "Self-phase-modulation in silica optical fibers", Phys. Rev. A, Gen. Phys., vol. 17, no. 4, pp. 1448–1453 Apr. 1978

[21] J. P. Gordon and L. F. Mollenauer, "Phase noise in photonic communications systems using linear amplifiers", Opt. Lett., vol. 15, no. 23, pp. 1351–1353, Dec. 1990.